Rep. Prog. Phys. **59** (1996) 131–234. Printed in the UK

Powder diffraction

J Ian Langford† and Daniel Louër‡

† School of Physics and Space Research, University of Birmingham, Birmingham B15 2TT, UK
‡ Laboratoire de Chimie du Solide et Inorganique Moléculaire (URA CNRS 1495), Groupe de Cristallochimie, Université de Rennes I, Avenue du Général Leclerc, 35042 Rennes Cedex, France

Abstract

The powder diffraction method, by using conventional X-ray sources, was devised independently in 1916 by Debye and Scherrer in Germany and in 1917 by Hull in the United States. The technique developed steadily and, half a century later, the 'traditional' applications, such as phase identification, the determination of accurate unit-cell dimensions and the analysis of structural imperfections, were well established. There was then a dramatic increase of interest in powder methods during the 1970s, following the introduction by Rietveld in 1967 of his powerful method for refining crystal structures from powder data. This has since been used extensively, initially by using neutron data and later with X-rays, and it was an important step towards extracting 3-dimensional structural information from 1-dimensional powder diffraction patterns, in order to study the structure of crystalline materials. Similarly, techniques which do not involve structural data have been introduced for modelling powder diffraction patterns, to extract various parameters (position, breadth, shape, etc.) which define the individual reflections. These are used in most applications of powder diffraction and are the basis of new procedures for characterizing the microstructural properties of materials. Many subsequent advances have been based on this concept and powder diffraction is now one of the most widely used techniques available to materials scientists for studying the structure and microstructure of crystalline solids. It is thus timely to review progress during the past twenty years or so.

Powder data have been used for the identification of unknown materials or mixtures of phases since the late 1930s. This is achieved by comparison of experimental data with standard data in crystallographic databases. The technique has benefited substantially from the revolution in the development of storage media during the last decade and from the introduction of fast search/match algorithms. Phase identification sometimes precedes a quantitative analysis of compounds present in a sample and powder diffraction is frequently the only approach available to the analyst for this purpose. A new development in quantitative analysis is the use of the Rietveld method with multi-phase refinement.

A major advance in recent years has occurred in the determination of crystal structures *ab initio* from powder diffraction data, in cases where suitable single crystals are not available. This is a consequence of progress made in the successive stages involved in structure solution, e.g. the development of computer-based methods for determining the crystal system, cell dimensions and symmetry (indexing) and for extracting the intensities of Bragg reflections, the introduction of high resolution instruments and the treatment of

0034-4885/96/020131+104$59.50 © 1996 IOP Publishing Ltd

line-profile overlap by means of the Rietveld method. However, the intensities obtained, and hence the moduli of the observed structure factors, are affected by the overlap problem, which can seriously frustrate the determination of an unknown crystal structure. Although numerous structures have been solved from powder data by using direct or Patterson methods, the systematic or accidental total overlap of reflections continues to focus the attention of a number of crystallographers. New approaches for the treatment of powder data have been devised, based on maximum entropy methods and 'simulated annealing', for example, to generate structural models. Additionally, resonant diffraction (anomalous scattering) is used as an aid to structure solution.

There has been spectacular progress in characterizing the microstructural properties which arise from various types of structural imperfection. The principal advance has been the 3-dimensional reconstruction of 'anisotropic' (direction- or *hkl*-dependent) features or properties of polycrystalline materials. These include the shape of diffracting domains and the distribution of the size, structural 'mistakes' induced during the formation or subsequent treatment of a sample and dislocations or other forms of lattice distortion. The main innovation here has been a comparison of experimental data with those derived from a physical model based on data from other techniques or from prior knowledge of the behaviour of the material.

Most aspects of powder diffraction are brought together in analysing data from experiments carried out under non-ambient conditions, a field that continues to expand as more intense sources of radiation become available. Such experiments can be carried out over a wide range of temperature and at ever increasing pressures. Chemical or solid-state reactions and other processes, such as phase transformations, can be followed *in situ* by means of time-resolved diffraction.

For the benefit of the reader who is unfamiliar with powder diffraction, a résumé of the basic principles underlying the various techniques and applications is included. Sources of radiation, modern instrumentation and detectors are also considered, since these have played a major ro le in the progress of powder diffraction during the past two decades. Numerous examples are discussed throughout the review, in order to illustrate the main applications and procedures. Powder diffraction is interdisciplinary and these are inevitably drawn from various branches of science. However, it should be remembered that, in the main, the use of powder diffraction is frequently a 'means to an end', albeit an important stage in a study of polycrystalline materials.

This review was received in August 1995.

The review is respectfully dedicated to the memory of

Professor A J C Wilson, FRS
1914–1995

Contents

	Page
1. Introduction	135
2. Basic principles	137
2.1. Characteristics of powder diffraction patterns	137
2.2. Diffraction line profiles	139
2.3. Convolution and deconvolution	140
2.4. Structural imperfections	142
3. Modelling of powder diffraction data	145
3.1. General considerations	145
3.2. Line-profile functions	146
3.3. Total pattern fitting	148
3.4. Reliability, precision and accuracy	152
4. Instrumentation and experimental considerations	154
4.1. Sources of radiation	154
4.2. Diffractometers and cameras	159
4.3. Detectors	160
4.4. Non-ambient diffraction	163
4.5. Sample preparation and experimental strategy	165
4.6. Instrument characterization and Standard Reference Materials	166
5. Databases and phase identification	169
5.1. Databases	169
5.2. Phase identification (Search/Match)	172
6. Crystal structure refinement from powder data	177
6.1. Factors affecting precision and accuracy	177
6.2. Current practices with the Rietveld method	182
6.3. Some applications of the Rietveld method	182
6.4. Pattern decomposition and structure refinement	188
7. *Ab initio* structure determination	188
7.1. Historical overview	188
7.2. Powder pattern indexing	189
7.3. Extraction of integrated intensities	192
7.4. Structure solution	193
7.5. Combined X-ray and neutron diffraction	196
7.6. Noteworthy examples of *ab initio* structure determination	197
7.7. Integrated software	197
8. Resonant diffraction (anomalous dispersion)	198
9. Quantitative phase analysis	199
9.1. Introduction	199
9.2. The internal-standard and the reference-intensity-ratio methods	200
9.3. Quantitative phase analysis by the Rietveld method	201
10. Line-profile analysis and microstructural properties	202

10.1.Microstructure of materials 202
10.2.Analysis of microstructure based on Fourier series 202
10.3.Integral-breadth methods 209
11. Dynamic and non-ambient diffraction 211
11.1.Time- and temperature-dependent powder diffraction 211
11.2.High pressure diffraction 216
11.3.Magnetic X-ray powder diffraction 219
12. Concluding remarks 220
Appendix. Analytical functions commonly used to model powder diffraction line profiles 221
References 223

1. Introduction

Diffraction of X-rays or neutrons by polycrystalline samples is one of the most important, powerful and widely used analytical techniques available to materials scientists. For most crystalline substances of technological importance, the bulk properties of a powder or a polycrystalline solid, averaged throughout the sample, are required; in general a single-crystal data, even if they can be obtained, are usually of little interest except for determination of the crystal structure or for studying some other fundamental physical property. In the main, powder diffraction is a means to an end, in that it frequently forms part of a wider investigation of physical, chemical or mechanical properties of materials. It is also interdisciplinary in nature, a technique which is equally applicable to a study of the behaviour of semiconductors and superconductors, for example, as to alloys, catalysts, minerals, pharmaceutical substances or polymers. Indeed, as will be evident from this review, powder diffraction transcends the traditional, and increasingly artificial, subject areas of science.

The basic difference between coherent scattering from planes of atoms of spacing d in a single crystal and a random powder is that diffracted beams from individual crystallites in the latter generate cones with semi-angle 2θ, where

$$2\theta = \sin^{-1}(\lambda/2d) \tag{1.1}$$

λ being the wavelength of the radiation used. In the reciprocal-space representation, the lattices associated with individual crystallites are oriented randomly and points given by the position vector

$$\boldsymbol{d}^* = h\boldsymbol{a}^* + k\boldsymbol{b}^* + l\boldsymbol{c}^* \tag{1.2}$$

in the single-crystal case become spheres of radius $|\boldsymbol{d}^*|(= 1/d)$ for a random powder, where $\boldsymbol{a}^*$, $\boldsymbol{b}^*$, $\boldsymbol{c}^*$ are vectors defining the reciprocal unit-cell and hkl are the Miller indices, which are proportional to the direction cosines of the planes in question. Thus:

$$d^* = 2\lambda^{-1}\sin\theta. \tag{1.3}$$

(It should be noted that the quantity Q $(= 2\pi d^*)$ is often used in other areas of materials science to denote the magnitude of the scattering vector.) In a powder-diffraction experiment, a 1-dimensional representation of diffracted intensity as a function of the radial distance d^* is normally obtained. Two types of experiment are possible, angle dispersive, in which monochromatic radiation is used, and energy dispersive for which the scattering angle is fixed. In some applications, the variation of intensity as a function of d^* is all that is required. In others, it is necessary to reconstruct the 3-dimensional lattice.

The aim of this review is to give a résumé of the principal techniques of modern powder diffraction and, through examples, an account of the information which can be obtained on the character and properties of crystalline materials. A section on basic concepts (section 2) is followed by the modelling of powder diffraction patterns (section 3) and a discussion of instrumentation and experimental strategy (section 4). An admirable account of the basic principles of powder diffraction, and of the sources of radiation, instruments and detectors used, is given in volume *C* of the *International Tables for Crystallography* (Wilson 1992). A

valuable source for further information on practical considerations is *Methods and Practices in Powder Diffraction* (Jenkins 1989a). The remainder of the review is concerned with applications to materials science.

By far the most widely used application of powder diffraction is the identification of unknown materials (section 5). This has undergone a revolution in recent years, with the introduction of compact disks to store standard data and the development of greatly improved software for accessing and searching databases. Phase identification was introduced early in the history of powder methods, with the classic paper by Hanawalt, Rinn and Frevel (1938) which contains powder data for 1000 substances. This was the forerunner of the Powder Diffraction File (PDF), which is now administered and distributed by the International Centre for Diffraction Data (ICDD). The PDF currently (1995) contains data for over 70 000 substances.

The second application to be considered is the refinement of crystal structures by means of powder data (section 6). This was made possible by significant advances in instrumentation and improvements to digital computers during the 1960s and was pioneered by Rietveld (1967, 1969), whose name has since been associated with the method. Indeed, the introduction of the Rietveld method for structure refinement was one of the main factors which gave rise to the veritable renaissance of powder methods which took place during the 1970s (Langford 1981). Significant progress has also been made in the procedure known as *pattern decomposition*, whereby a non-structural model is fitted to a complete diffraction pattern to obtain parameters defining the individual Bragg reflections. This technique, which is also discussed in section 6, is now applied routinely in modern powder diffraction and the resulting diffraction line-profile parameters are used in a variety of applications.

In recent years, the ultimate stage in structural studies was achieved by the *ab initio* solution of moderately complex structures from powder data (section 7) and it is a field where significant progress continues to be made. This remarkable development has benefited from greatly improved instrument resolution and advances in the methods used at each stage in the analysis. These include the development of powerful indexing procedures, whereby a 3-dimensional reciprocal lattice can be reconstructed from 1-dimensional powder diffraction data, the extraction of integrated intensities of overlapping Bragg reflections by improved modelling techniques and the possibility of refining atomic co-ordinates by the Rietveld method. Associated with structure solution is the exploitation of resonant diffraction (anomalous scattering) from selected atoms, by selecting an appropriate wavelength or energy (section 8). Although this technique is not new, it has only been possible to apply it routinely with the advent of dedicated synchrotron-radiation facilities.

Traditional applications of powder diffraction, such as the quantitative analysis of samples containing a mixture of phases (section 9) and studies of microstructural properties (section 10) have also benefited from improved instrumentation and computing facilities. The former profited from the introduction of the Rietveld method and the latter from pattern-decomposition techniques. A wealth of information can now be obtained on the microstructural properties of materials with low symmetry, whereas previously structural imperfections could only be studied in detail for high-symmetry structures and diffraction patterns with minimal peak overlap.

Finally, an exciting development of powder diffraction, made possible by advances in the performance of detectors and other ancillary equipment, has occurred in the field of non-ambient diffraction (section 11). Data can be obtained over a wide range of temperature or pressure and dynamic experiments can be carried out while the sample environment is changed. Thus ‘real-time’ studies can be made of changes in structure or microstructure when a sample is subjected to some external perturbation. This has application in studying

phase transformations or in following solid-state reactions.

All branches of science have benefited from the dramatic developments in computing facilities in recent years and powder diffraction is no exception. In general, computing requirements in this field are not unduly demanding and analysis can usually be carried out by means of a Personal Computer (PC). Inevitably, software development has been considerable and many earlier programs have been adapted for PC use. Some 650 programs which are currently available are listed in the *World Directory of Powder Diffraction Programs* (Gorter and Smith 1995), compiled under the auspices of the Commission on Powder Diffraction of the International Union of Crystallographty (IUCr) and updated regularly. Brief details of each program are given, together with information on where it can be obtained. Many public domain programs are in fact obtainable through the Program Exchange Bank†. Reference to the appropriate section of the World Directory is made throughout this review and the directory is indispensable to anyone newly involved in powder diffraction. Additionally, a Collaborative Computational Project in Powder Diffraction (CCP14), sponsored by the Engineering and Physical Sciences Research Council (EPSRC), was initiated in 1994 at the Daresbury Laboratory with a view to collecting together a suit of core programs for analysing powder data. This is freely available to academic users and it can be accessed via electronic mail.

Although all the main uses of powder diffraction have been covered in this review, some applications have, due to space restrictions, necessarily been omitted or only treated briefly. These are largely concerned with samples which are intermediate between being truly polycrystalline and single crystals and include the important techniques of glancing-angle and grazing-incidence diffraction, used to characterize thin films and multi-layers, the study of texture and the measurement of residual stress. These have, however, been reviewed elsewhere.

Of the many applications of powder diffraction, the most significant advance in recent years has been the determination of crystal structures from powder data. The contribution to our understanding of the behaviour of high-T_c superconductors and zeolites, for example, or to elucidating the complexities of semiconductor structures at ultra-high pressures, has been incalculable. Other important advances during the last decade or so have been the 3-dimensional modelling of structural imperfections and in dynamic studies of non-equilibrium phenomena, and a very recent development is the detection, by using a synchrotron source, of the magnetic scattering of X-rays by a powder sample (Collins *et al* 1995). These are all areas where further progress is likely to be made in future, as intense sources of radiation and high resolution instruments become more widely available, but perhaps the most radical development will be in analysing the structure and microstructure of individual particles or grains in a polycrystalline sample.

2. Basic principles

2.1. Characteristics of powder diffraction patterns

The radial distribution in reciprocal space of the intensity scattered coherently from a given set of planes within a powder sample, a *Bragg reflection*, can be characterized by parameters defining its position, maximum intensity, area (integrated intensity), dispersion, shape and

† Details of the Program Exchange Bank and copies of the program can be obtained from Dr S Gorter, Department of Chemistry, University of Leiden, NL-2333 CC Leiden, The Netherlands. E-mail: GORTER_S@rulgca.LeidenUniv.nl

asymmetry. Powder diffraction techniques are based on the measurement of one or more of these parameters for as many reflections as are required (or can be measured) in a particular application. The Bragg reflections are superimposed on a slowly varying background due to incoherent scattering, which mainly arises from thermal diffuse scattering (TDS), Compton scattering and, if the energy of the incident radiation is sufficiently high, fluorescence from the sample. Additionally, there is a small coherent TDS contribution associated with each Bragg reflection. (See, for example, Suortti 1995.)

The number, disposition and intensity of reflections in a diffraction pattern depend primarily on the symmetry and size of the unit cell and the arrangement of atoms within it, but are also influenced by the nature and wavelength of the radiation used (section 4.1). The basic equation for the integrated intensity I of the reflection hkl for a random powder sample illuminated by a primary beam of intensity I_p is

$$I = I_p K \lambda^3 V^{-2} m_{hkl} P L F_{hkl}^2 v \tag{2.1}$$

where K depends on whether X-rays or neutrons are used to collect the data, V is the volume of the unit cell, m_{hkl} is the multiplicity of the hkl reflection, P is the polarization factor, L the so-called Lorentz factor, F_{hkl} is the structure factor, taking into account thermal effects, and v is the effective diffracting volume of the sample, including the effects of absorption. P is of the form $(1 + C\cos^2\theta)/(1 + C)$, where $C = 1$ for an unpolarized beam and $C = cos^2\theta_m$ if an incident-beam monochromator is used, θ_m being the Bragg angle of the monochromator. The Lorentz factor for a random powder, in reflection mode, is of the form $(\cos\theta\sin^2\theta)^{-1}$. The factor $\cos\theta$ arises from the fact that spherical shells of diffracted intensity in reciprocal space intersect the Ewald sphere at an angle which depends on θ. Also, the surface area of the spherical shells increases as d^{*2}, which is embodied in the factor $\sin^2\theta$. F_{hkl} is a function of the atomic scattering factor f which, in the X-ray case, depends on the atomic number Z and decreases rapidly with increasing $\sin\theta/\lambda$. Neutrons, on the other hand, are scattered by nuclei and the scattering lengths b in general are of similar magnitude for all $\sin\theta/\lambda$. There are, however, measurable differences in b for different elements and for isotopes of the same element. For example, b is -0.38×10^{-14} m for hydrogen and is $+0.65 \times 10^{-14}$ m for deuterium. The neutron also has a magnetic moment and magnetic structures can be studied by means of neutron-magnetic scattering. Further information on the various factors in equation 2.1 is given in volume C (section 6.2) of the *International Tables for Crystallography* (Wilson, 1992).

In general the degree of overlap of reflections becomes increasingly severe as d^* increases and, especially in the X-ray case, the intensity decreases. These factors limit the scope of powder methods, particularly for materials of intermediate or low symmetry, and modern methods, such as maximum entropy, are being used to tackle the problem of 'unscrambling' overlapped reflections (e.g. David 1990). The theoretical number of lines N for planes having a spacing greater than d_N is given by the number of possible lattice points in reciprocal space for which d^* is less than d_N^*. This is approximately equal to the volume of a sphere with radius equal to d_N^* divided by the volume V^* of the reciprocal unit cell, or

$$N \sim 4\pi(d_N^*)^3/3V^*. \tag{2.2}$$

In practice, the actual number of observed lines is less, due to multiplicity and systematic absences. For the triclinic system the number is about half that given by (2.2) and the factors for other crystal systems have been evaluated by de Wolff (1961).

The observed intensity $y(x_i)$ at some point x_i in a powder diffraction pattern is the *sum* of the contributions from all neighbouring reflections $h_j(x_i)$, plus the background $b(x_i)$ at that point, or

$$y(x_i) = \sum_j h_j(x_i) + b(x_i). \tag{2.3}$$

In an angle-dispersive experiment x is normally the scattering angle 2θ and in the energy-dispersive case it is usually energy or d. The recovery of individual reflections, as is required in some applications of powder diffraction, is thus a *desummation* operation and this procedure is known as *pattern decomposition* (section 3.3.1). The breadth and shape of individual diffraction lines, on the other hand, depend on the characteristics of the instrument used and on any structural imperfections present in the sample. An observed diffraction line profile $h(x)$ is then the *convolution* of the contribution $f(x)$ from the sample with an instrument function $g(x)$, or

$$h(x) = f(x) * g(x). \tag{2.4}$$

In studies involving the microstructure of a sample, $f(x)$ is obtained by removing $g(x)$ from $h(x)$, *a deconvolution* procedure, or by separating the breadths and other parameters defining the individual convoluted functions.

Instrumental line profiles arise from the distribution of wavelength in the incident beam (section 4.1), convoluted with several functions due to the geometry of the instrument used (size of source, beam divergence, slit widths, residual misalignment, etc.). Both the breadth and shape of instrumental line profiles vary continuously with $\sin\theta/\lambda$ and, for the angle-dispersive X-ray case, tend to be approximately Gaussian at low angles and become progressively more Lorentzian as wavelength dispersion becomes increasingly dominant at high angles (Louër and Langford 1988; Langford, Cernik and Louër 1991). Contributions to $h(x)$ from sample microstructure are considered in section 2.4.

It is always desirable to minimize the instrumental contribution, in so far as is practicable. However, the optimum configuration in a particular application will inevitably be a compromise between resolution and adequate intensity. If the breadth of reflections is dominated by sample imperfections, it may be possible to improve resolution by annealing the sample, provided that the microstructural properties of the specimen are not of interest.

2.2. Diffraction line profiles

The measure of location of a diffraction line profile most widely used in powder diffraction is the position of the maximum intensity $I_0(2\theta_0$ in an angle-dispersive experiment). The simplest measure of dispersion (line breadth) is the full width of the intensity distribution at half the maximum intensity *(FWHM* or $2w$) if the distribution is symmetrical, or $w_1 + w_2$ if it is not, where w_1 and w_2 are the widths, at half maximum intensity, on the left- and right-hand side of the peak ordinate. A more useful measure of dispersion in some applications, which includes all the data for a given line profile, is the *integral breadth*, defined as the width of a rectangle having the same area A and height as the observed line profile, or

$$\beta = A/I_0. \tag{2.5}$$

It is sometimes convenient to characterize the shape of a line profile by assuming that it has the form of some analytical function and those commonly used in powder methods have been reviewed by Young and Wiles (1982) and are listed in the appendix. Alternatively, for some purposes it is sufficient to give an indication of the overall form of an intensity distribution by means of the *shape factor* ϕ, defined as the ratio of the *FWHM* to the integral breadth (Langford 1978, 1992), or

$$\phi = FWHM/\beta. \tag{2.6}$$

ϕ, for which no assumption is made regarding the actual form of the intensity distribution, is always less than unity for diffraction line profiles. Larger values of ϕ indicate a rapid fall-off of intensity in the tails of a line profile and smaller values are indicative of a slower decrease. Asymmetry is frequently modelled by using 'split functions', with different widths and/or shape parameters on each side of the peak ordinate. Simple measures of asymmetry are then given by the ratios $(w_2 - w_1)/(w_1 + w_2)$ or w_2/w_1.

Line profiles can be represented by Fourier series, for the purpose of deconvoluting the contributions which give rise to an observed line profile and for the physical interpretation of diffraction effects. This approach is mainly applicable to relatively simple diffraction patterns, such as occur with high symmetry materials, and is considered below and in section 10. Wilson (1963) applied the standard measures of position and dispersion used in statistical analysis (i.e. the centroid and variance) to powder diffraction, since the central moments of convoluted functions (section 2.3) can readily be separated. This approach has been reviewed recently by Berti (1993).

2.3. Convolution and deconvolution

The convolution integral, implicit in (2.4) and given by

$$h(x) = \int_{-\infty}^{+\infty} f(y)g(x-y)\,\mathrm{d}y \tag{2.7}$$

can readily be evaluated for a given $f(x)$ and $g(x)$, but there is no unique mathematical solution to obtaining $f(x)$ from $g(x)$ and $h(x)$, except for simple analytical functions. Instability of the solution arises from the perturbing nature of the noise associated with experimental data; the problem is ill-posed, in that a small perturbation in $h(x)$ gives rise to an arbitrarily large perturbation in $f(x)$. The problem of errors in deconvolution methods has been considerred by many authors (e.g. Jones and Misell 1970; Price 1982) and various ways for dealing with solution instability have been proposed.

A widely used procedure, first applied to powder diffraction by Stokes (1948), is to express $g(x)$ and $h(x)$ as Fourier *series,* defined in the same interval, and then to use the multiplicative property of the Fourier *transforms* of convoluted functions, or

$$F(t) = H(t)/G(t) \tag{2.8}$$

where $F(t)$, $G(t)$, $H(t)$ are equivalent to the (complex) Fourier coefficients $F(n)$, $G(n)$, $H(n)$at discrete values of t. $f(x)$ can then be obtained from the inverse of $F(n)$. In this

approach, due to random errors in $h(x)$ and $g(x)$, the quotient $H(n)/G(n)$ can become very large at high frequencies and the resulting $f(x)$ can have large oscillations superimposed on the true profile. The uncertainty is considerably less for low harmonic numbers (n small) (see, for example, Louër, Coupé and Le Bail 1984). The corresponding Fourier coefficients $F(n)$ were used by Warren and Averbach (1950, 1952) for characterizing microstructural properties from two or more orders of a reflection (section 10.2.2). A serious limitation of this approach is that experimental line profiles are necessarily truncated at a finite range, which can give rise to appreciable systematic errors (Young, Gerdes and Wilson 1967; Langford *et al* 1988). A correction for truncation can be made by assuming that the line-profile tails have a particular form (Delhez *et al* 1986; Vermeulen *et al* 1991, 1992), but the method is restricted to powder patterns with well resolved lines and thus to high-symmetry materials, in the main. Some practical aspects of Fourier deconvolution are discussed by Cernansky (1983), e.g. the application of digital filters to suppress oscillations. A procedure for obtaining the Fourier coefficients of $f(x)$ directly, based on a truncation of the Fourier series, was used by Le Bail and Louër (1976). This leads to a set of algebraic equations which can be solved by means of a least-squares procedure.

An approach to deconvolution based on regularization algorithms (Phillips 1962; Tikhonov 1963), to correct the observed diffraction line profile $h(x)$ for instrumental contributions, was introduced by Louër, Weigel and Louboutin (1969). From the quadrature approximation to a convolution product, equation 2.7 is transformed to a set of linear equations of the form

$$\boldsymbol{h} = A'\boldsymbol{f} \tag{2.9}$$

where A' is the convolution matrix. The solution having the minimum functional norm is selected by minimizing a regularization scheme, e.g.

$$\min(\|A'\boldsymbol{f} - \boldsymbol{h}\|^2 + \varepsilon\|\boldsymbol{f}\|^2) \tag{2.10}$$

where $\|\boldsymbol{f}\|^2 = \sum_i f(x_i)^2$. The instability is then replaced by a well-posed stable minimization. The procedure incorporates a small and positive parameter ε, related to the noise levels of h and g, which plays a weighting rôle between the smoothness of the solution and the minimization. A procedure based on the minimization of an economical function, based on the sum of the squared relative differences between the observed and calculated line profiles, by using the flexible simplex method, has also been described (Moraweck, de Montgolfier and Renouprez 1977). Wiedemann, Unnam and Clark (1987) devised a method of deconvolution, based on Euler's characteristic equation, which uses a combination of least-squares, background and smoothing criteria to minimize the effect of random counting errors.

The iterative method of van Cittert (1931) was applied by Ergun (1968) to correct the X-ray diffraction patterns of carbon black. This is based on m successive convolutions:

$$f_m = f_{m-1} + (h - f_{m-1} * g) \tag{2.11}$$

where $f_0 = h$. This procedure can be shown to have the same form as the regularization methods, with $1/m$ having a rôle similar to that of ε.

Another class of deconvolution methods, applied to powder diffraction data, uses the principles of information theory. The maximum entropy method (MEM) has been found to be efficient with simulated profiles having various noise levels. For example, the intense diffraction line profiles for an aluminium oxide (corundum) sample were deconvoluted from the instrumental contribution without noticeable oscillations appearing in the tails of the f profiles (Kalceff, Armstrong and Cline 1994).

Croche and Gatineau (1977) give practical rules for applying deconvolution procedures to diffraction line profiles and show that deconvolution can readily be performed when the width of the instrumental function $g(x)$ is smaller than half the width of the observed line profile $h(x)$.

A different approach to deconvolution is to assume that $g(x)$ and $h(x)$ can be modelled by analytical functions whose breadths can be separated. Such a function is the Voigtian, the convolution of one or more Lorentzian and Gaussian functions, which is frequently a good approximation to observed diffraction line profiles (Langford 1978). The corresponding Lorentzian and Gaussian breadths can be obtained for $g(x)$ and $h(x)$, and hence for $f(x)$. This procedure, based on the integral breadth, has been summarized by Langford (1992). Toraya, Yoshimura and Sömiya (1983) devised a procedure based on numerical methods for the deconvolution of Pearson VII functions, as defined in the appendix, and Howard and Snyder (1985) developed a numerical deconvolution procedure for a split Pearson VII function, which models asymmetric line profiles. Since average values of quantities defining the microstructural properties of interest are obtained, information on their variation in the vicinity of a reciprocal-lattice point is lost. Nevertheless, procedures based on the breadths of the constituent profiles can in principle be applied to data from any crystalline material, regardless of structural symmetry or complexity of the diffraction pattern (section 10). The main limitation at present is the inadequacy of pattern-fitting algorithms to model peak clusters with severe overlap.

2.4. Structural imperfections

2.4.1. Analysis of diffraction line broadening. The definition of a crystal lattice is based on the concept that the environment of all points is identical, but only in exceptional circumstances does this occur in practice; 'real' materials contain structural imperfections which give rise to a spread of intensity around each reciprocal-lattice point. There are two categories of structural imperfection which can modify diffraction line profiles $f(x)$ by a measurable amount. The first is the finite size of domains over which diffraction is coherent, measured in the direction $\boldsymbol{d}^*_{hkl}$ for a given reflection. This can be the mean thickness of individual crystallites (or grains, in a polycrystalline sample), but it can also relate to a sub-domain structure, e.g. the mean distance between structural 'mistakes', the separation of regions bounded by low-angle grain boundaries, etc. Here, unless specified otherwise, 'size' or 'crystallite size', will be used to refer to any of these effects. The second category is based on a distortion of the crystal lattice, which amounts to a variation of d spacing within (or possibly between) domains. This can arise from microstrain, due to an applied or residual stress, or from a compositional gradient in the sample. It is not possible to distinguish between these effects from diffraction data, but the distinction is usually evident from the nature of the sample. For convenience, they are known as 'strain' effects. Dislocations contribute to both categories of line broadening; there will be a 'size' contribution due to their mean separation, inversely proportional to the dislocation density, and microstrain arising from internal stress fields. Unlike strain broadening, which increases with the order of a reflection, size broadening is constant in the direction $\boldsymbol{d}^*_{hkl}$ and this is

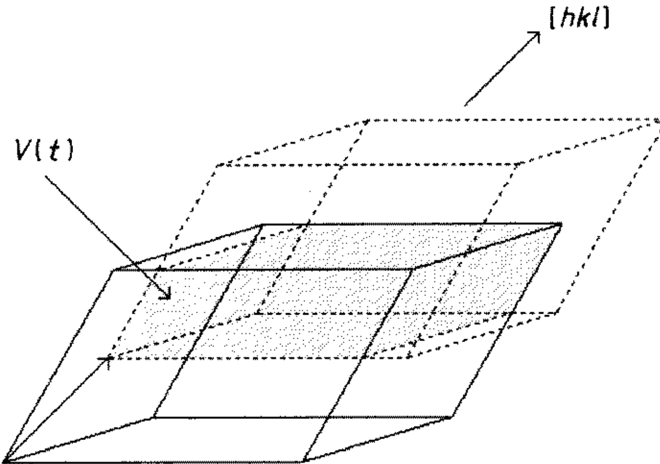

Figure 1. $V(t)$, the volume common to a crystallite and its 'ghost' displaced a distance t in the direction [hkl] of the diffraction vector. $V(t)$ is proportional to the Fourier transform of the diffraction line profile due to crystallite size.

used to separate the two contributions to the overall breadth due to structural imperfections.

If s is the distance from the reciprocal-lattice point hkl at d^*_{hkl} from the origin, measured in the direction of the scattering vector, the line profile due to the combined effects of crystallite size and lattice distortion is, from Wilson (1970, equation 10-68).

$$f(s) = V^{-1} \int_{-\tau}^{+\tau} V(t) Y(t) \exp(-2\pi \mathrm{i} s t)\, \mathrm{d}t \tag{2.12}$$

where $V(t)$ is the volume common to a crystallite and its 'ghost' (or double) displaced a distance t in the direction $\boldsymbol{d}^*_{hkl}$ (figure 1) (see Stokes and Wilson 1942), τ is the value of t for which $V(t) = 0$ and $Y(t)$ is the mean value of the product FF^* of the structure factor and its complex conjugate for unit cells a distance t apart. (See also Guinier 1963.) $f(s)$ is thus the inverse Fourier transform of the product $V(t)Y(t)$, which is the basis of the Warren–Averbach method for microstructural analysis (section 10.2.2).

If there are no lattice distortions (when $Y(t)$ is constant), from (2.12) the integral breadth β^*_S due to size effects is simply

$$\beta^*_S = V(0) \Big/ \int_{-\tau}^{+\tau} V(t)\, \mathrm{d}t \tag{2.13}$$

where $V(0)$ is the mean volume of crystallites. The reciprocal of this quantity has been defined by Wilson (1963) as the *integral breadth apparent size* ε_β, or

$$\varepsilon_\beta = \beta^{*-1}_S. \tag{2.14}$$

ε_β is thus the volume-weighted thickness of crystallites measured in the direction $[hkl]$. Aside from the case of crystallites with parallel faces and reflections from planes parallel

to these surfaces, this is clearly less than the maximum thickness τ. From Wilson (1963, equation 19.26), the quantity $V(0)/V'(0)$, the reciprocal of the initial slope of the Fourier transform of the normalized line profile, is also a measure of size. This is the *Fourier apparent size* ε_F, which can be interpreted as the total area of projection of unit volume of the crystallites on to the reflecting planes. In general, ε_F is also less than τ and is not equal to ε_β. Additionally, an important result derived by Bertaut (1949) is that the second derivative of the Fourier transform $V(t)$ is proportional to the distribution of the thickness, measured in the direction of the diffraction vector, within and between crystallites and may thus be regarded as a size distribution function.

$Y(t)$ depends on the complexity of the model adopted for the variation of the structure factor with position inside the crystal and its interpretation is not so straightforward as that of $V(t)$—for further information, see Wilson (1962a, 1963, 1970). Frequently, some average value of strain, based on the assumption that lattice distortion is independent of t, will suffice. For this purpose, Stokes and Wilson (1944) introduced the concept of an *apparent strain* η_β (see also Wilson 1963, equation 20.10), where, for the integral breadth,

$$\eta_\beta = 2\beta_D^*/d^* \tag{2.15}$$

where β_D^* is the breadth of the line profile due to strain (lattice distortion).

The quantities ε and η, whether derived from integral breadths or Fourier series, are based solely on diffraction theory and in general they give little insight into the nature of the microstructural properties which give rise to $f(x)$. Values of such analytically-determined parameters are, however, widely used in applications where their physical interpretation is unimportant. These include obtaining an indication of changes in diffraction effects due to sample preparation or treatment, or to varying experimental conditions. If physically meaningful results are required to characterize microstructure, then a realistic model must be introduced to account for the observed phenomena. This can sometimes be based on the behaviour of ε and η, if data for a large number of reflections are available, or on information obtained from complementary experiments, such as TEM or SEM.

2.4.2. Interpretation of apparent size and strain The information of interest in any study of domain size by means of powder diffraction is usually an indication of the form of crystallites and an estimate of their mean dimensions. τ must therefore be determined for various directions $[hkl]$, which amounts to generating a 3-dimensional representation of crystallites from 1-dimensional diffraction data. If the domains are other than spherical, ε will depend on the direction of the diffraction vector and the corresponding line breadths are then said to be 'anisotropic', i.e. do not vary monotonically with 2θ or d. In order to obtain τ from ε , a model corresponding to some 'average' shape is ascribed to the diffracting domains, taking into account the approach used in the analysis. For example, for domains which may be regarded as spherical, ε is constant for all $[hkl]$ and the mean diameter $\langle D\rangle$ is $4\varepsilon_\beta/3$ for the integral-breadth method or $3\varepsilon_F/2$ from the Fourier approach. ε, and hence the actual mean dimensions, can be obtained for different domain shapes by evaluating $V(t)$ and its derivatives (Wilson 1962a). ε and τ for cylindrical crystallites have been evaluated by Langford and Louër (1982) and for hexagonal prisms by Vargas, Louër and Langford (1983). These forms are particularly relevant to materials having hexagonal symmetry and the case of parallelepipeds, applicable to other crystal systems, has been considered by Langford (1992). Also, Grébille and Bérar (1985) have evaluated $V(t)$ for the more general case of crystallites having the form of convex polyhedra, by dividing each

crystallite into regions over which the integration is tractable. These models, which include acicular and plate-like crystallites as limiting cases, cover most domain shapes likely to be encountered in practice.

Line broadening due to structural mistakes varies with hkl in a manner which depends on the nature of the mistake (stacking or deformation faults, layer mistakes, twin or growth faults, etc.) and on the crystal system. Additionally, there will be a 'size' contribution arising from their mean separation and mistakes can also displace diffraction lines and introduce asymmetry. Wilson (1962a) and Warren (1969) have discussed the interpretation of these parameters in terms of structural mistakes.

A simple interpretation of η in terms of an actual strain e can be based on an assumed stress model (Stokes and Wilson 1994). For example, if the stress is assumed to be isotropic and the distribution of strain is approximately Gaussian, then

$$\eta_\beta = 2(2\pi)^{1/2}\langle e^2\rangle^{1/2} \tag{2.16}$$

$$\approx 5\langle e^2\rangle^{1/2} \tag{2.17}$$

where $\langle e^2\rangle^{1/2}$ is the r.m.s. strain. Alternatively, if all values of stress between zero and a maximum value $\hat{p}$ are assumed to be equally likely, then

$$\eta_\beta = 4\hat{e} \tag{2.18}$$

where $\hat{e}$ is the corresponding maximum strain. The Warren–Averbach procedure for strain analysis, considered in section 10.2.2, includes provision for a t-dependence of lattice distortion.

The precision of ε and η depends only on the quality of the data and validity of the procedure used for separating the breadths and other parameters of convoluted functions. On the other hand, any derived quantities used to describe microstructural properties are clearly model-dependent. Nevertheless, microstructural information should be meaningful, and even accurate, if independent results from a large number of reflections are found to be self-consistent.

3. Modelling of powder diffraction data

3.1. General considerations

The first step in analysing powder diffraction data is to extract from individual Bragg reflections such information as is required in a particular application. If this is the identification of unknown materials, then only the peak positions and heights are required and these parameters can normally be obtained routinely and with sufficient accuracy by using peak-search programs such as those provided by diffractometer manufacturers. (See, for example, Mallory and Snyder 1979.) However, most other applications require a more comprehensive characterization of individual peaks. A major development in modern powder diffraction is the fitting of a calculated model to the entire, and often complex, observed diffraction pattern, in order to overcome the problem of line overlap and to obtain parameters which define each reflection. In this approach the calculated intensity $y(x)$ may be represented as

$$y_{\mathrm{cal}}(x) = \sum_j h_{\mathrm{jcal}}(x) + b(x) \tag{3.1}$$

where $h_j(x)$ is the contribution at x from the jth peak, $b(x)$ is the background and the summation is again for all reflections which contribute to the intensity at x. The model requires an analytical representation of individual peaks and the background variation. Parameters defining the model are then refined, by the method of least squares or some other procedure, until the quantity

$$S = \sum [y_{\mathrm{obs}}(x) - y_{\mathrm{cal}}(x)]^2 \tag{3.2}$$

or a similar expression with an appropriate weighting factor $w(x)$ [e.g. $w(x) = 1/y(x)$], is a minimum, the summation being over all data points in the diffraction pattern. Maximum-likelihood methods have also been used in powder diffraction refinement procedures and it has been shown that, for low counting statistics, they can be more powerful than ordinary least-squares fitting methods (Antoniadis, Berruyer and Filhol 1990).

3.2. Line-profile functions

A function used to model an individual diffraction line must clearly approximate closely to the observed distribution of intensity. Additionally, it should be capable of deconvolution and interpretation in terms of physical quantities, if information on microstructural properties is required. There are numerous approaches to the modelling of diffraction lines, both analytical and non-analytical (e.g. Young and Wiles 1982), but the functions most commonly used at present are the Pearson VII (Hall *et al* 1977), the Voigt (Langford 1978) and the pseudo-Voigt (Wertheim *et al* 1974). The form of these functions, together with the Lorentzian (Cauchy) (L) and Gaussian (G), are given in the appendix. The Pearson VII is simply $[L]^m$, where m gives an indication of the shape of the profile, particularly the rate of decrease of intensity in the tails. The Pearson VII clearly includes the Lorentzian ($m = 1$) and it tends to a Gaussian as $m \to \infty$. The Voigt function is the convolution of Lorentzian and Gaussian components and can be characterized by the shape parameter ϕ. The limiting values of ϕ are $2/\pi$ ($= 0.6366$) for L and $2(Ln2/\pi)^{1/2}$ ($= 0.9394$) for G. The pseudo-Voigt is the summation of L and G functions in the ratio $\eta/(1-\eta)$, where η is generally termed the pseudo-Voigt mixing parameter or Lorentzian fraction ($\eta = 1$ for L and 0 for G). Wertheim *et al* (1974) have shown that the simpler pseudo-Voigt is a close approximation to a Voigt, but it is of course a summation of its constituent functions, rather than a convolution. It is customary to give equal widths to the L and G components of a pseudo-Voigt, but there is no particular reason why this restriction should be imposed, other than for convenience during refinement. Line profiles for which $\phi < 2/\pi$ are regarded as 'super-Lorentzian' (Wertheim *et al* 1974). The Pearson VII and pseudo-Voigt cannot readily be deconvoluted analytically and, if they are used in line-profile analysis, the equivalent Voigt parameters can be obtained (Delhez, de Keijser and Mittemeijer 1982).

The above functions are symmetrical; line-profiles displaying asymmetry are usually modelled by means of 'split' functions, for which different parameters are refined on each side of the peak ordinate. Brown and Edmonds (1980) introduced the split Pearson VII function to model asymmetric line profiles. Howard and Snyder (1983) evaluated a number of profile shape functions and concluded that this function was the most suitable for modelling asymmetric $g(x)$ profiles in the X-ray case. The numerical convolution of a

symmetric $f(x)$ using this split $g(x)$ model is reviewed by Snyder (1995). This approach to the modelling of skewness is semi-empirical and, for some powder diffraction applications, e.g. the Rietveld method (section 3.3.2), a more precise description of asymmetry due to axial divergence may improve the fit of the pattern. Studies based on diffraction optics which give an accurate representation of diffraction profiles at low angles have been made (Bérar and Baldinozzi 1993; Finger, Cox and Jephcoat 1994). Occasionally, high-resolution data reveal line profiles for which the intensity in the tails decreases more slowly than a Lorentzian (Hastings, Thomlinson and Cox 1984; Young and Sakthivel 1988; Marezio *et al* 1988; Plévert and Louër 1990). Such 'super-Lorentzian' profiles can be modelled by means of a Pearson VII with $m < 1$ or a pseudo-Voigt with $\eta > 1$, but not by a Voigt.

A different approach was adopted by Pyrros and Hubbard (1983), who modelled line profiles with rational functions. These are the ratio of two polynomials and are generalizations of the Lorentzian, approximating well to a Pearson VII for small values of m. Although excellent fits were obtained for single lines and doublets, the number of parameters required to model a complete pattern may be prohibitively large.

A number of non-analytical profile functions have been proposed. These include the use of the Learned Function (Hepp and Baerlocher 1988), whereby parameters 'learned' from well-resolved lines, usually for small d^*, are extrapolated to model overlapped regions. This approach can only be used in cases where the precise shape of individual lines is not required, since no account is taken of any variation in shape with d^* or lattice direction. Toraya (1990) has introduced the Array Profile Function (APF) to describe diffraction lines. This consists of an array of discrete parameters for representing $y_{\mathrm{obs}}(x)$ which are adjusted by the method of least squares until an optimum fit is obtained.

For many years well-resolved lines in powder diffraction patterns have been represented by the 1-dimensional Fourier series

$$y_{\mathrm{obs}}(x) = \sum_{n=-\infty}^{+\infty} \{A_n \cos(2\pi n x) + B_n \sin(2\pi n x)\} \tag{3.3}$$

since deconvolution can readily be carried out in Fourier space. This approach has been used for the separation of $K\alpha_1 - K\alpha_2$ components (Kidron and De Angelis 1971) and extended to the case of overlapping lines (Mortier and Costenoble 1973; Le Bail, Duroy and Fourquet 1988).

Whatever approach to line-profile modelling is used, the observed intensity distribution is necessarily truncated at a finite range, normally defined as $\pm k \times FWHM$ relative to the peak ordinate, whereas theoretical line profiles normally extend to $\pm\infty$, as do the analytical functions used to model them. The maximum theoretical value of k is equivalent to $d^*_{hkl}/2$, but in practice, owing to overlapping line-profile tails, this can only be achieved when the pattern consists of a series of orders of a particular reflection, as can occur in cases of extreme preferred orientation. (See Delhez *et al* 1986.) In general, systematic errors in line-profile parameters due to truncation are inevitable. Toraya (1985) noted that, for a Gaussian function and $k = 3$, more than 99% of the profile area is included, but for a Lorentzian function the corresponding value of k is about 63. The choice of range in a particular application depends on the character of the line-profile tails, but a value k in the range 10 to 20 is normally acceptable for most purposes.

3.3. Total pattern fitting

There are two approaches to the modelling of a complete diffraction pattern. In one, pattern decomposition, the superposition of analytical line-profile functions and a suitable background model are fitted to the observed data and in the other, the Rietveld method, information on crystal structure is included.

A characteristic of diffraction patterns is that the density of lines, and hence the degree of line overlap, increases as $(d^*)^3$ $(= 1/d^3)$ (see equation 2.2). In general a pattern thus becomes increasingly 'scrambled' as the scattering angle or energy increases. Also, the intensity of lines decreases as d^* increases. This is due to the influence of thermal vibrations, which increases as $(d^*)^2$, and, in the X-ray case, the decrease in atomic scattering factor with increasing d^*. Pattern decomposition is concerned with 'unscrambling' overlapped peaks and in general there will be an upper limit of d^* beyond which meaningful line-profile parameters cannot be obtained. However, sufficient data can normally be acquired from lines at low and intermediate values of d^* to predict the behaviour of line profiles at higher values, if this is needed in a particular application. It should be noted that occasionally cases of total overlap occur, i.e. lines have identical values of d^*, and these cannot be resolved by pattern decomposition. Total overlap can be accidental or it can arise from lattice symmetry. For example, the 333 and 511 reflections for cubic lattices have the same d^*.

3.3.1. Pattern decomposition. Many applications of powder diffraction do not require a knowledge of the crystal structure and in such cases a diffraction pattern can be characterized adequately by pattern decomposition, where the aim is to obtain quantities which describe each individual Bragg reflection. The calculated intensity at point x_i is given by

$$y_{\mathrm{cal}}(x_i) = \sum_j A_j \Phi(x_i - x_j) + b(x_i), \tag{3.4}$$

where A_j is the calculated area of the jth peak, Φ is the function used to model the peaks (see appendix), normalized to unit area, and the summation is over all reflections which contribute to the intensity at x_i. The fitting of equation (3.4) is normally restricted to few lines, typically up to 10 reflections, to limit the number of parameters to be refined. Pattern decomposition is normally carried out in two stages; firstly, approximate peak positions are obtained, usually by finding where the second derivative of $y_{\mathrm{obs}}(x_i)$ with respect to x_i changes sign, along with estimates of the peak height and width, and secondly the line-profile parameters are refined for all peaks in a group (e.g. Taupin 1973a; Sonneveld and Visser 1975; Parrish, Huang and Ayers 1976; Hayakawa and Oka 1981; Langford *et al* 1986). If the unit cell is known, the first stage can be avoided by using calculated starting values of the peak positions (Pawley 1981; Toraya 1986; Le Bail, Duroy and Fourquet 1988). Programs for carrying out pattern decomposition are incorporated in software packages marketed by the main diffractometer manufacturers, e.g. the profile fitting PC-program PROFILE from Socabim, in which the available functions include the Pearson VII, pseudo-Voigt and Voigt together with their 'split' versions. Details of currently available programs are given in Table 12 of Gorter and Smith (1995). An example of a Pearson VII function (see appendix) fitted to a single experimental line profile for cold-worked tungsten is shown in figure 2(a). Good agreement between the experimental data and the fitted function in the line-profile tails, as indicated in the lower part of the figure, is essential if a systematic error in the integrated intensity is to be avoided. The fitting of a Pearson VII function to a group of

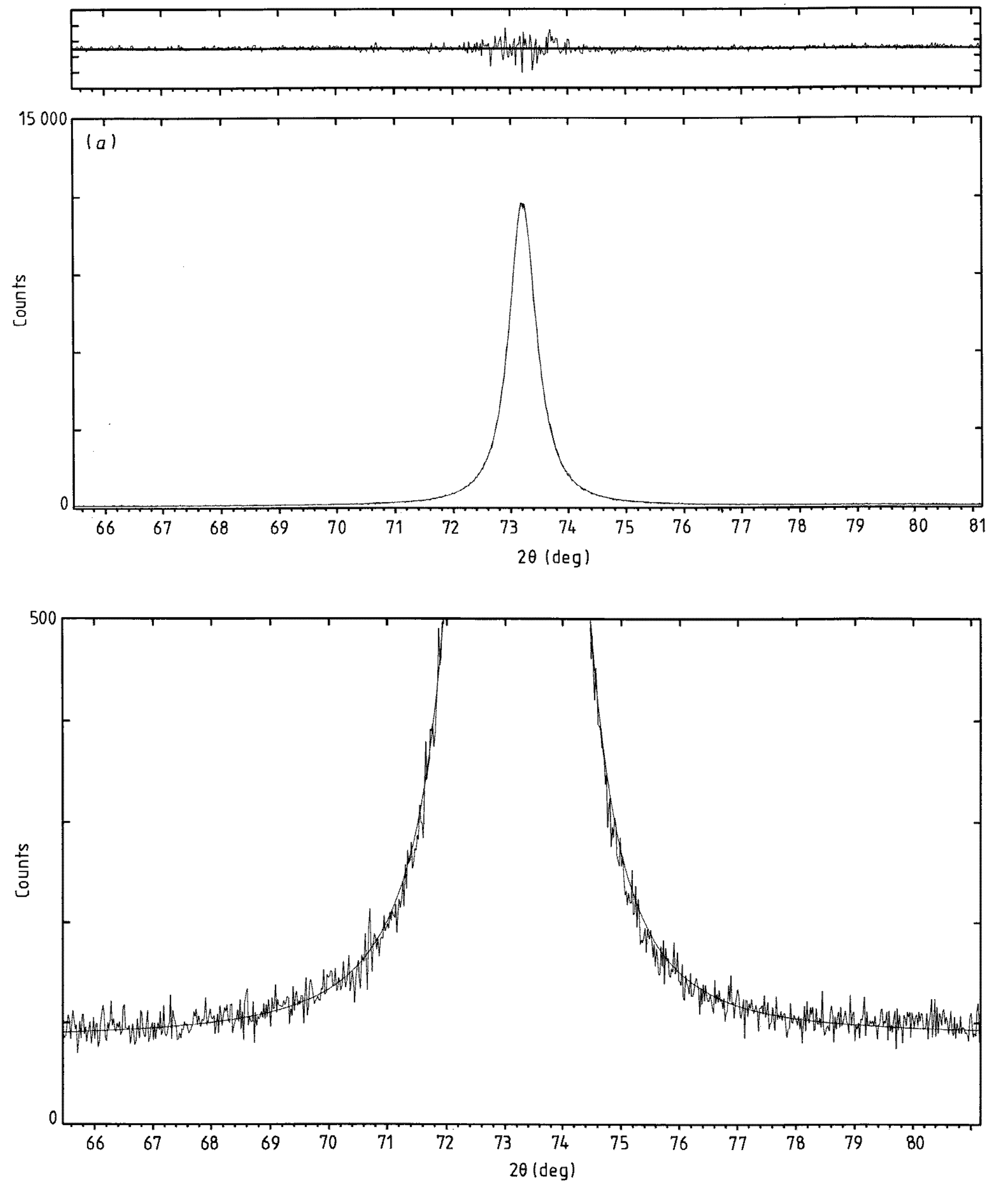

Figure 2. (*a*) Fitting of Pearson VII function to the 211 reflection for cold-worked tungsten powder, Cu $K\alpha_1$ radiation. The lower figure, with a $\times 30$ scale expansion, shows the quality of fit in the line-profile tails. Refined parameters are (see Appendix): $2\theta_0 = 73.206°$, $I_0 = 194.4$ c/s, Area=158.6 c/s.deg, $b = 1.4$ c/s, $FWHM = 0.577°$, $\beta = 0.816°$, $m = 1.21$, $\phi = 0.708$, $R_{wp} = 1.2\%$, $R_{\text{exp}} = 1.3\%$. The scale factor for the difference plot is 5. (*b*) Part of the diffraction pattern for a sample Y_2O_3, fitted with a Pearson VII function, Cu $K\alpha_1$ radiation. The line broadening is mainly due to crystallite-size effects. The $\times 20$ scale expansion again shows the 'fit' in the line-profile tails ($R_{wp} = 1.4\%$) (Louër 1994).

peaks, part of the diffraction pattern for yttria (Y_2O_3), is shown in figure 2(*b*), again with an expanded scale to show the degree of fit in the line-profile tails.

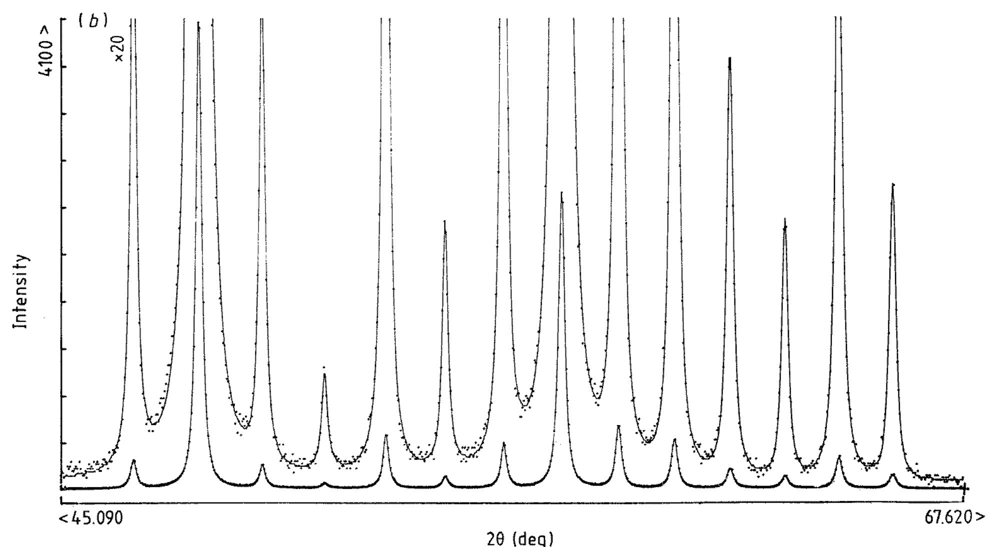

Figure 2. Continued.

A different strategy, in which $h(x_i)$ is replaced by $f(x_i)*g(x_i)$, was proposed by Taupin (1973a) and developed further by Huang and Parrish (1975). (See also Parrish, Huang and Ayers 1976.) This incorporates the deconvolution of $g(x)$, obtained in a separate experiment, from $h(x)$ to give $f(x)$, written as $A_j\Phi(x_i - x_j)$. Such a procedure, with a split Pearson VII function for $\Phi(x)$, was used by Toraya, Yoshimura and Sömiya (1983) and Howard and Snyder (1985). Enzo *et al* (1988) and Benedetti *et al* (1988) included a pseudo-Voigt function to model $f(x)$, with an exponential term to make allowance for any asymmetry of $g(x)$. The validity of the deconvolution operation then depends on how well $f(x)$ is represented by these functions.

3.3.2. Rietveld method. The method of total pattern fitting introduced by Rietveld (1967, 1969) requires two models at the start of the refinement, a structural model based on approximate atomic positions and a non-structural model which describes the Bragg reflections in terms of analytical or other differentiable functions. Both must be considered in order to obtain an optimum representation of the observed pattern. The main aim of the Rietveld method is to refine the positions of atoms by using powder diffraction data, but it also provides estimates of line-profile parameters. The total intensity of reflections and, to a first approximation, their positions, are determined by the structural model, but the form of the Bragg reflections depends on the instrumental function (g profiles) and on the effects of the microstructure of the sample (f profiles). These are included in the non-structural model. In this approach the calculated intensity at x_i is given by

$$y_{\mathrm{cal}}(x_i) = \sum_j \mathrm{I}_j G_j \Phi(x_i - x_j) + b(x_i) \tag{3.5}$$

the summation again being over all reflections which contribute to the intensity at x_i. In equation (3.5), G_j is a preferred-orientation function, I_j is the integrated intensity of the jth reflection, given by the well known relation (cf equation 2.1)

$$I_j = s m_j (LP)_j F_j^2 \tag{3.6}$$

where s is the scale factor, m_j is the multiplicity and $(LP)_j$ is the Lorentz-polarization factor. F_j is the structure factor given by

$$F_j = \sum_i N_i c_i \exp[2\pi i(hx_i + ky_i + lz_i)] \exp(-B_i) \tag{3.7}$$

where x_i, y_i, z_i are the coordinates of the ith atom in the unit cell, expressed as fractions of the cell edges, h, k, l are the Miller indices, N_i is the fractional occupancy for the ith atomic site, c_i is the X-ray scattering factor (f_i) or the nuclear scattering length (b_i) and B_i is the temperature factor. The non-structural model is represented by the reflection profile function Φ (see appendix), for which the various parameters are angle or energy dependent and which will, in general, also have a lattice-direction dependence. In the simplest case for angle-dispersive geometry, where the breadths of line profiles vary smoothly with d^*, the variation of $(FWHM)^2$ is usually expressed as a quadratic in $\tan\theta$, introduced by Caglioti, Paoletti and Ricci (1958) to describe the behaviour of the Gaussian instrumental broadening with neutron sources:

$$(FWHM)^2 = U \tan^2\theta + V \tan\theta + W \tag{3.8}$$

where U, V, W are refinable parameters.

3.3.3. Rietveld method programs. After the late 1960s the number of applications increased rapidly (see Hewat 1986), limited initially to neutron diffraction data and later extended to X-ray data obtained with a diffractometer (Cu$K\alpha$ doublet) (Young, Mackie and Von Dreele 1977) or a Guinier camera (Cu$K\alpha_1$) (Malmros and Thomas 1977). The popularity of the Rietveld method led to the development of more sophisticated programs, usually based on Rietveld's original work (1969). A list of the main programs is given in Table 15 of Gorter and Smith (1995). Among those most widely used are:

(i) the DBWS program (current version: DBWS-9411) written by Wiles, Sakthivel and Young for main frame computers and later adapted for PC use. The latest version (Young *et al* 1995) is an update of that described by Wiles and Young (1981). It operates with X-ray or neutron diffraction data collected in the angle dispersive mode. This program is the basis of other versions developed by different authors; e.g. LHPM (Hill and Howard 1986), ALFRIET1 (Howard and Snyder 1985) to refine only $f(x)$ by deconvoluting a split Pearson VII-modelled $g(x)$ from the observed data, ALFREIT2 (Matheis and Snyder 1994) to refine structures with incommensurate modulations and FULLPROF (Rodriguez-Carvajal 1990). The latter version has been written in to cover a variety of situations.

(ii) GSAS (Larson and Von Dreele 1987), which offers a high flexibility, runs on a VAX-VMS machine and was recently adapted for PC use. It works with angle dispersive and energy dispersive (time-of-flight) data. Single-crystal, X-ray and neutron diffraction data can be used simultaneously or independently in a structure refinement. The program includes provisions for applying constraints on bond lengths and angles.

(iii) XRS-82, *The X-ray Rietveld System* (Baerlocher 1982) is based on a collection of crystallographic programs for the refinement of structures from single-crystal data. Apart from extending the system to minimize S (equation 3.2), some additional features are

incorporated, such as the Learned Function, used to describe the actual peak shape, and geometric restraints based on stereochemical knowledge (soft constraints).

(iv) Others programs include RIETAN (Izumi 1995) and MPROF (Bendall, Fitch and Fender 1983). RIETAN was developed for angle-dispersive X-ray and neutron data and MPROF was the forerunner of a number of programs with provision for the refinement of two or more phases simultaneously.

An approximate size-strain analysis, on the basis of order dependence and modelling of anisotropy of microstructural effects, has been implemented in some programs. (See also section 6.1.5) Also, most programs incorporate an iterative procedure for pattern matching (Le Bail, Duroy and Fourquet 1988), by fitting a calculated pattern to the observed data without the use of a structure model, but using constraints on the positions of reflections allowed by the space group conditions. This facility is of importance in *ab initio* structure determination for extracting a set of integrated intensities rapidly, for subsequent use as input data for structure-solution programs (section 7.3).

3.3.4. Modelling of structural imperfections. Attempts to model patterns with various types of imperfection and for poorly crystalline materials have been reported. For instance, linear polymer structures are usually complex with many atoms per unit cell and their powder diffraction patterns generally show poor crystallinity. For modelling purposes it is appropriate to include in the model all structural and morphological parameters which are known. Constrained least-squares refinements from the complete powder diffraction pattern have been applied to isotactic polypropylene (Immirzi and Iannelli 1988). A program for refining the molecular structure of the crystalline phase of polymers based on an analysis of X-ray fibre diffraction patterns has been devised by Iannelli (1994). A non-linear least-squares procedure applied to the diffraction pattern of myelin membranes isolated from intact tissue was used for optimizing the structure factors and determining coherently diffracting domain sizes and lattice distortions (Inouye, Karthigasan and Kirschner 1989). A least-squares refinement procedure was used for comparing calculated and observed diffraction patterns for disordered lamellar solids (de Courville-Brenasin, Joyez and Tchoubar 1981). The $00l$ reflections are calculated by using parameters describing the mean number of layers and spacing fluctuations and the asymmetric hk bands are calculated by means of the theory of planar defects. The modelling of diffraction patterns for the $00l$ reflections from randomly stratified clay minerals was discussed by Wood and Brown (1988). The basis of this technique is similar to that of the Rietveld method and it includes the effects of disorder and crystallite size. A computer program dedicated to the simulation of wide-angle and low-angle scattering was introduced to provide a general description of complex patterns of poorly crystallized materials (Espinat *et al* 1993).

3.4. Reliability, precision and accuracy

3.4.1. Discrepancy factors. All the variable parameters used in the pattern fitting method are included in a refinement procedure that minimizes S (equation 3.2). An indication of the agreement between the observed [y_i(obs)] and the calculated [y_i(cal)] intensity distributions, and between the integrated intensities of the observed and calculated models for reflections j, is given by discrepancy factors listed in table 1 (Young and Wiles 1982; Hill and Fischer 1990). The weighted profile factor R_{wp} and the goodness of fit GoF, are the most meaningful for following the progress of the refinement, since their numerator contain the quantity S being minimized. On the basis of Gaussian statistics, the theoretical

minimum value for R_{wp} is given by the expected factor R_{exp} ($= R_{wp}/GoF$). In addition, graphical criteria of fit are also used, e.g. plots of the difference between observed and calculated patterns. In the Rietveld method, the validity of the crystal structure model is measured by the factors R_B and R_F, which are based on the integrated 'observed' I_j ('obs') and calculated I_j(cal) of the individual j Bragg intensities. (The use of '. . . ' is a reminder that the observed intensities are generally obtained by partitioning the raw data on the basis of the ratio of the contributing calculated intensities.) It should be noted that the R_p and R_{wp} factors incorporate the observed $y(x_j)$ discrete intensities, which include the background contribution, in their denominator. By adding artificially a constant intensity to a complete dataset, Eriksson, Louër and Werner (1989) showed that the profile indicators R_p and R_{wp} can provide misleading values if they are obtained from datasets with different background levels, the lower profile R values being obtained from the dataset having the higher level. It was concluded that, in order to follow the progress of a structure refinement with a particular dataset, the R_{wp} factor is appropriate, but for comparison of datasets only the structure model factors R_B and R_F should be used. Similar discussions on the R factors used in the analysis of powder diffraction data by the Rietveld method have been reported (Maichle, Ihringer and Prandl 1988; Hill and Fischer 1990; Jansen, Schäfer and Will 1994).

Table 1. Numerical criteria of fit used in the Rietveld method and other pattern-fitting precedures. w_i is the observation weight, usually assigned the value $y_i(\mathrm{obs})^{-1}$. N is the number of observations, P the number of adjusted parameters and C the number of constraints applied.

Criterion	Definition
R-pattern:	$R_p = \dfrac{\Sigma\lvert y_i(\mathrm{obs}) - y_i(\mathrm{cal})\rvert}{\Sigma y_i(\mathrm{obs})}$
R-weighted pattern:	$R_{wp} = \left[\dfrac{\Sigma w_i(y_i(\mathrm{obs}) - y_i(\mathrm{cal}))^2}{\Sigma w_i(y_i(\mathrm{obs}))^2}\right]^{1/2}$
R-Bragg factor:	$R_B = \dfrac{\Sigma\lvert I_j(\text{'obs'}) - I_j(\mathrm{cal})\rvert}{\Sigma I_j(\text{'obs'})}$
R-structure factor:	$R_F = \dfrac{\Sigma\lvert I_j(\text{'obs'})^{1/2} - I_j(\mathrm{cal})^{1/2}\rvert}{\Sigma I_j(\text{'obs'})^{1/2}}$
Goodness-of-fit indicator:	$GoF = \left[\dfrac{\Sigma w_i(y_i(\mathrm{obs}) - y_i(\mathrm{cal}))^2}{(N - P + C)}\right]^{1/2}$

3.4.2. Precision and accuracy in Rietveld analysis. When the minimum value of S (equation 3.2) is reached, the estimated standard deviations (e.s.d.s) σ_i associated with the ith parameter are normally used as indicators of precision; they are given by the simple relation:

$$\sigma_i = [M_{ii}^{-1} S/(N - P + C)]^{1/2} \tag{3.9}$$

where M is the matrix of the least-squares algorithm. The term $S/(N-P+C)$ is an indicator of the overall variance of the fit. The e.s.d. values are often used as indicators of precision in a Rietveld analysis (see, for example, Taylor 1985). They can be artificially low and should be interpreted with caution, as shown by extensive discussions on this topic (Sakata and Cooper 1979; Prince 1981; Scott 1983; Hill and Madsen 1987). As noted by Young (1995), a calculated e.s.d. is not the experimental probable error; it is the minimum possible

probable error arising from random errors alone. In fact, some discrepancies between the models used and the actual data, e.g. in the description of the line profiles, in the unit cell parameter model for the peak positions, in the modelling of preferred orientation effects, etc., can introduce a bias in the calculation of e.s.d.s and the precision and accuracy of the parameter estimates cannot be validly assessed by statistical methods (Prince 1981). If serial correlation is present, then none of the e.s.d. values is a valid measure of uncertainty. To test for serial correlation between adjacent steps in a powder diffraction pattern, Hill and Flack (1987) proposed the use of the Durbin–Watson d_{DW} statistic. They used it in a weighted form:

$$d_{DW} = \frac{\sum_{n=2}^{N}(w_i \Delta y_i - w_{i-1}\Delta y_{i-1})^2}{\sum_{n=2}^{N}(w_i \Delta y_i)^2} \tag{3.10}$$

where $\Delta y_i = y_{obs}(x_i) - y_{cal}(x_i)$ and w_i is the weight assigned to each intensity. The ideal value of d_{DW} is 2.0. A simple correction for serial correlation was derived by Bérar and Lelann (1991), which in practice increases the e.s.d. values by a factor of 2 to 3. Andreev (1994) suggested the use of a function which takes into account local correlation, and recommended its minimization in the final stage of the fitting procedure, after S (equation 3.2) has been reduced to a minimum. This two-step technique was tested with success on two widely-distributed datasets, for $PbSO_4$ (Hill 1992) and $Ca_5(PO_4)_3F$ (Wiles and Young 1981).

Some comparisons between single-crystal and Rietveld refinement results for the same materials have been reported. However, for a meaningful comparison the data should correspond to the same upper limit of $\sin\theta/\lambda$, which is rarely the case. Young, Mackie and Von Dreele (1977) obtained e.s.d.s (not corrected for serial correlation) which were 2 or 3 times as large as in single crystal studies and the co-ordinate parameters generally were in agreement within 2 or 3 combined e.s.d. values.

4. Instrumentation and experimental considerations

4.1. Sources of radiation

4.1.1. Sealed-tube X-ray sources. The most widely used source of radiation in powder diffraction continues to be the conventional sealed X-ray tube, though neutron sources, both continuous and pulsed, and synchrotron radiation are available world-wide at central research facilities. The disadvantages of a conventional source are its low brilliance, non-tunability and relatively high beam divergence, but these factors are more than offset by its accessibility, low cost and high reliability. Target materials for angle-dispersive experiments range from Cr ($Z = 24$) to Ag ($Z = 47$), corresponding to wavelengths in the range 2.9 Å to 0.56 Å for $K\alpha$ characteristic radiation. The choice of wavelength depends on the range in reciprocal space to be probed in a particular application and on the composition of the sample; it is clearly desirable to avoid the excitation of fluorescence from the specimen, if possible. However, by far the most commonly used target material is Cu($Z = 29$), for which the generally accepted wavelength is currently 1.5405981 (10) Å for Cu$K\alpha_1$ radiation (Deslattes and Henins 1973).

The brightness of a conventional X-ray source is limited by the rate at which heat can be dissipated from the target and a power rating of 3 kW (equivalent to about 600 W mm^{-2} for

a fine-focus tube) is the maximum currently available commercially. By rotating the anode, the rating can be increased to about 20 kW for a broad-focus tube. The corresponding increase in the brightness of the source reduces the time taken to acquire data with a given statistical quality by a factor of ~ 2.5, but at the expense of resolution. However, when operating in fine-focus mode, the powder density can be increased to ~ 4500 W mm^{-2}. Rotating-anode sources are used to advantage in dynamical experiments, for studying non-equilibrium phenomena on a time scale of seconds, or when only small samples are available, as in ultra-high-pressure studies (section 11.2).

In addition to the $K\alpha_1$–$K\alpha_2$ doublet, with intensities approximately in the ratio 2:1 and a relative separation of about 2.5×10^{-3}, there is a group of four or five satellite lines, depending on the target material, on the high-energy side of the $K\alpha_1$ line. The total intensity of these 'non-diagram' lines is about 1% of that for the $K\alpha_1$. For many years this structured wavelength distribution for $K\alpha$ radiation limited progress in a number of powder diffraction applications, particularly for materials having low and intermediate symmetry. Attempts were made at an early stage to remove the $K\alpha_2$ component analytically (e.g. Rachinger 1948). Improved procedures were introduced by Ladell, Zagofsky and Pearlman (1970), Delhez and Mittemeijer (1975) and Platbrood (1983) and nowadays the 'Rachinger correction' is usually included as standard in software packages for data reduction and analysis provided by diffractometer manufacturers. However, the parameters used to model the doublet are only approximate and normally do not take into account the differing widths and asymmetries of the two lines, nor is provision usually made for the satellite group. A more rigorous approach was introduced by Parrish, Huang and Ayers (1976) in their procedure for pattern decomposition (section 3.3.1). They modelled the wavelength distribution and other instrumental contributions to an observed line profile by means of five Lorentzian functions, two for each side of the $K\alpha_1$ and $K\alpha_2$ components and one for the $K\alpha$ satellite group. Parameters defining these functions are refined in the usual way

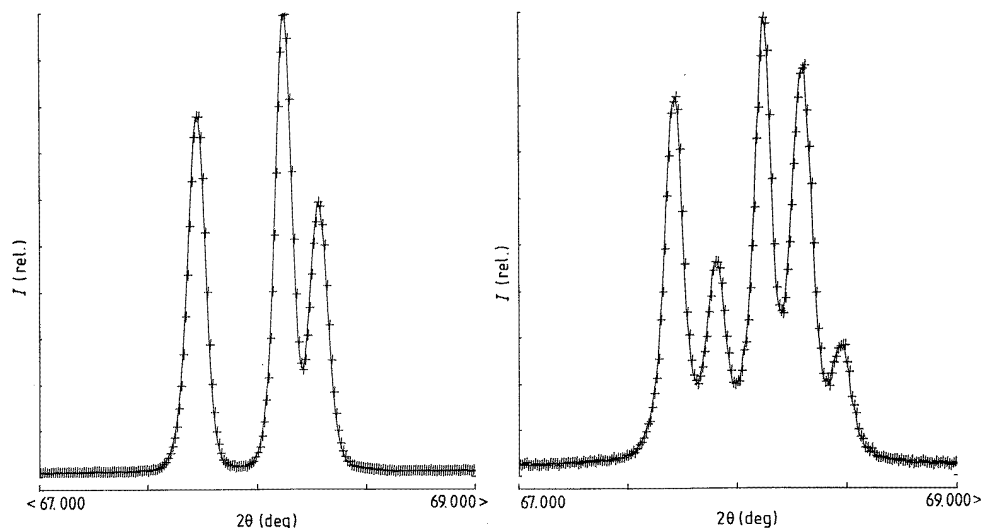

Figure 3. The quartz triplet 212, 203, 301, Cu$K\alpha$ radiation, showing the dramatic improvement in resolution and pattern quality achieved with an incident-beam monochromator and Cu$K\alpha_1$ radiation (left), compared with the Cu $K\alpha_{1,2}$ doublet (right).

until an optimum 'fit' is achieved.

The procedure devised by Parrish, Huang and Ayers is an improvement on '$K\alpha_2$-stripping' techniques and is an adequate approximation in some applications of powder diffraction. However, the introduction of systematic errors is inevitable with analytical techniques currently available and, for the more demanding requirements of advanced methods in modern powder diffraction, it is desirable to remove unwanted radiation at source by means of a focusing monochromator (e.g. Louër and Langford 1988). This is customarily placed in the incident beam, though a focusing monochromator in the diffracted beam has the additional advantage of removing sample-induced fluorescent radiation. Such monochromators can now be supplied as a standard item with commercial diffractometers. There is some reduction in the intensity of the $k\alpha_1$ line, though a β filter and incident-beam Soller slits (section 4.2.1) are no longer required. The resulting spectrum is essentially monochromatic ($\Delta\lambda/\lambda \sim 4\times 10^{-4}$) and the wavelength distribution can readily be modelled by one of the analytical functions listed in the appendix. Also, the number of peaks in a diffraction pattern is halved (figure 3), thereby significantly reducing peak overlap. Indeed, the use of a focusing monochromator to remove the $K\alpha_2$ component and $K\alpha$ satellite lines is an essential requirement for studying microstructural properties by means of pattern decomposition (section 10.3), if high precision is required, and is highly desirable in most other applications of powder diffraction, e.g. structure refinement by means of the Rietveld method (section 3.3.2), powder pattern indexing (section 7.2) and extraction of structure-factor amplitudes (section 7.3).

4.1.2. Synchrotron sources. The first synchrotron radiation facility was introduced in 1961, when a beamline was incorporated in the 184 MeV synchrotron at the National Bureau of Standards, Washington (Madden and Codling 1963), and there are currently about 60 such facilities world-wide, operational or under construction (Hasnain, Helliwell and Kamitsubo 1994). Radiation from a synchrotron source can extend from 'hard' X-rays to the infra-red region and beyond, with a high flux over a wide range of wavelengths. At the Daresbury Laboratory 2 GeV Synchrotron Radiation Source (SRS), for example, commissioned in 1981 and the first of many 'dedicated' sources, the exploitable wavelength range is $\sim$ 10 pm (100 keV) to $\sim$ 1 cm (10^{-4} eV). Some storage rings, such as the Daresbury SRS, are optimized for brightness, and others (e.g. the 6 GeV European Synchrotron Radiation Facility (ESRF) at Grenoble, France), are designed to achieve high brilliance. The maximum flux usually occurs at too low an energy for some diffraction experiments and magnetic devices, such as 'wigglers' or 'undulators' are inserted between the bending magnets of storage rings to shift the peak flux to higher energies. In addition to an increase in intensity of several orders of magnitude, compared with a conventional source, a major advantage of synchrotron radiation is the extreme parallelism of the beam; the divergence is $\sim$ 1 mrad or less in the vertical direction and is only slightly more in the plane of the storage ring. (The vertical divergence decreases, and the resolution thus improves, as the energy of the source increases.) This means that powder-diffraction experiments with exceptionally high resolution can be carried out. Among the many consequences of this feature is the recent development of micro-diffractometry. There are two types of microdiffraction: data can be collected from very small samples (e.g. section 11.2) and information can be obtained from individual crystallites or grains in a polycrystalline material. For example, structure solution has been carried out with data from $\sim$ 10–20μm crystallites (e.g. Harding and Kariuki 1994; Harding *et al* 1994) and the variation in microstructure within grains of plastically-deformed copper has been determined (e.g. Langford *et al* 1992). Another advantage of synchrotron

radiation is tunability of wavelength; any value in the X-ray régime can be selected simply by rotating an incident-beam monochromator, usually channel-cut Si or Ge, to the appropriate angle. By this means, the wavelength can be finely tuned to exploit resonant diffraction (anomalous dispersion: section 8), and it can be set to eliminate sample fluorescence, adjusted for maximum intensity from the source or optimized to probe the region of interest in reciprocal space. Another attribute of synchrotron sources is total linear polarization of the beam in the plane of the storage ring and it tends to be circularly polarized out of the plane, but these features are not yet widely exploited in powder diffraction.

In addition to high-resolution studies at fixed wavelength, synchrotron radiation is used to advantage in energy-dispersive experiments. The very intense 'white beam' is ideally suited to time-resolved diffraction, when a complete diffraction pattern can be obtained in a few seconds, and to non-ambient experiments generally. Since scattering is at a fixed angle, ancillary equipment, such as a cryostat, furnace or pressure cell, can readily be inserted in the beam path. Access to synchrotron facilities is necessarily limited and experiments usually have to be planned a year or so in advance, but the proliferation of dedicated sources throughout the world has greatly extended the range of science which can be studied by means of powder diffraction.

4.1.3. Neutron sources. Since neutrons behave as a gas with the usual Maxwell–Boltzmann distribution of velocity, it follows from the de Broglie equation that the maximum (λ) of the corresponding wavelength distribution depends on the inverse of the effective temperature T, or

$$\lambda^2 = h^2/3mkT = 632.9/T \tag{4.1}$$

where h, m and k have their usual meaning and λ is in Å. It is thus a fortunate coincidence that the wavelength distribution for neutrons in thermal equilibrium at 273 K has a maximum at 1.52 Å, remarkably close to that for Cu$K\alpha$ characteristic radiation. Neutrons are thus eminently suitable for carrying out diffraction experiments and for many years powder diffraction has been practised at a dozen or so conventional reactors, mainly in the U.S.A. and Europe. The range of wavelengths available at a beam port depends largely on the temperature of the moderator which it views. Short wavelengths predominate if a graphite moderator at temperatures up to almost 2000°C is used, whereas a 'cold' source, such as liquid hydrogen, gives long-wavelength neutrons. Such sources are mainly used for angle-dispersive experiments, a narrow range of wavelengths being selected by means of a monochromator. Somewhat more recently, the spallation source was introduced as a means of producing neutrons (Carpenter 1977). The interaction of a high energy pulsed proton beam with a heavy metal target produces bunches of neutrons by 'spallation' reactions and these are moderated to thermal energies for use in diffraction experiments. Such sources are used for powder diffraction at the Rutherford Appleton Laboratory (ISIS), the Los Alamos National Laboratory (LANSCE) and the Argonne National Laboratory (IPNS).

Neutrons are distributed spatially according to their velocity, and hence wavelength, so the time t taken to travel from the moderator to a detector is proportional to the wavelength and the total flight path L or, again from the de Broglie equation,

$$t = \lambda Lm/h = 2dLm\sin\theta/h \tag{4.2}$$

$$= 0.5055dL\sin\theta\text{ms} \tag{4.3}$$

if L is in metres and d in Å. Thus, if the distance from the moderator to the detector is 10 m, then $t \sim 5$ ms for $d = 1$ Å and a high scattering angle. This property led to the introduction of time-of-flight (TOF) powder diffractometers (Jorgensen and Rotella 1982). Such diffractometers are effectively energy-dispersive instruments and the scattering angle is usually high [$> 90°$ (2θ)]. Advantages of a TOF diffractometer are that, for a given scattering angle, the resolution ($\Delta d/d$) is essentially constant, whereas it tends to be inferior for larger values of d in the angle-dispersive case, and that a much greater region of reciprocal space can be probed. The resolution mainly depends on the path length, which is about 100 m for the ISIS high resolution powder diffractometer (HRPD).

The main advantages of the use of neutrons in diffraction experiments are that the scattering cross-section does not vary with $\sin\theta/\lambda$ and is thus constant for all scattering angles or energies and, with a few exceptions, its magnitude is similar for all elements, as noted in section 2.1. Accordingly, the main use of neutrons in powder diffraction has been the refinement of crystal structures by the Rietveld method (section 6), particularly for determining the positions of hydrogen atoms, which hitherto has rarely been accomplished with X-rays, and the distribution of cations among various atomic sites. The former is normally based on deuterated samples, since scattering from a hydrogen atom is dominated by a very large incoherent component, which is not the case for deuterium. With neutrons there is usually sufficient contrast between the scattering cross-sections for the site occupancy of cations with similar atomic number, or of different isotopes, to be determined. The diffracted intensity is considerably lower for neutrons than for X-rays and thus large samples (typically 10–20 gm) are required in order to achieve comparable data quality. However, an advantage of the low absorption of neutrons by most elements and isotopes means that

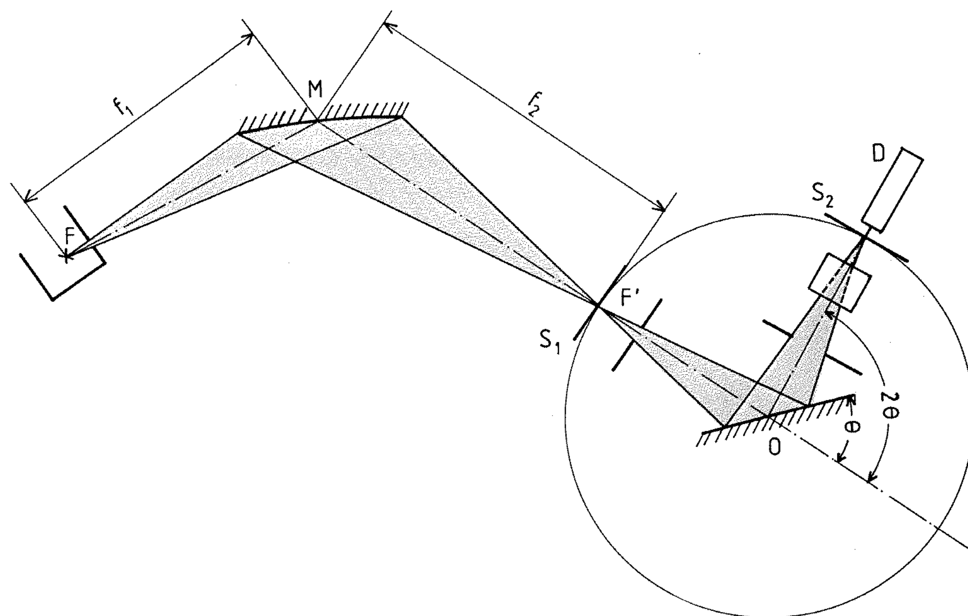

Figure 4. Geometry of the Bragg–Brentano (Parrish) powder diffractometer with a conventional X-ray source (F) and incident-beam monochromator (M), short focal distance f_1, long focal distance f_2 and focusing point F′. O is the diffractometer axis, D the detector and S_2 the receiving slit. S_1 is an optional slit at F′.

furnaces, cryostats and other ancillary equipment can be inserted in the beam path without significant loss of intensity. Neutron and X-ray experiments are thus complementary and it is sometimes advantageous to use both sources of radiation in structure solution or refinement (section 7.5; see also Von Dreele 1995). Von Dreele (1989) also gives further information on neutron sources in general and David and Jorgensen (1995) discuss TOF instruments and their use in structure refinement.

4.2. Diffractometers and cameras

4.2.1. Powder diffractometers. The modern high-resolution powder diffractometer is the result of continuous development, largely by the late William Parrish, since the late 1950s. (See Parrish 1992.) The instrument most commonly used with conventional divergent-beam X-ray sources is based on Bragg–Brentano parafocusing geometry (figure 4), whereby the source, sample and receiving slit lie on the 'focusing circle', which has a radius dependent on θ. Coherently scattered rays from a flat sample then converge (are 'focused') on the receiving slit, which is placed immediately in front of the detector. The detector normally rotates about the diffractometer axis through twice the angular rotation of the sample ($\theta/2\theta$ scans), though for some instruments the sample is stationary and the X-ray tube and detector rotate (θ/θ scans). This configuration is mainly used to study liquid samples. Instruments with horizontal or vertical axes are available. The former has some advantages, if automatic sample changing is required, and for the latter the torque imposed by the detector is constant at all angles. Samples are normally studied by reflection, but the transmission mode can also be used. Monochromatic radiation can be obtained by inserting a focusing monochromator in the incident or diffracted beams (figure 4 and section 4.1.1) and sample fluorescence can be eliminated by means of a monochromator, usually graphite, in the diffracted beam. The source size is typically about 0.05 mm in the plane of the instrument (the equatorial plane) and about 10 mm axially. If there is no incident-beam monochromator, beam dimensions are limited by a divergence slit, usually with an aperture of 1°–2°, in the equatorial plane and by Soller slits, parallel foils with an aperture in the region of 2°, in the axial plane. The receiving slit normally has an aperture in the range 0.01° to 0.10°, depending on the desired resolution. The receiving-slit aperture in fact dominates the instrumental line width at low and intermediate angles; typically this is about 0.06° for a 0.05° receiving slit, corresponding to a resolution $\Delta d/d$ of $\sim 2 \times 10^{-3}$. A feature of the Bragg–Brentano geometry is that the resolution improves dramatically at higher angles, by an order of magnitude.

A less common type of powder diffractometer is based on the Seemann–Bohlin geometry (Parrish and Mack 1967; Mack and Parrish 1967), in which the specimen is stationary and is mounted on a radial arm, instead of on the axis of rotation. The detector rotates around a fixed-radius focusing circle and is arranged to point towards the sample at all angles. Diffraction is from planes inclined to the sample surface by different amounts, whereas only planes which are nearly parallel to the surface contribute in the Bragg–Brentano case. A third form of diffractometer is based on the Guinier camera (section 4.2.2). This has an incident-beam monochromator and samples are viewed in transmission. Diffraction is then from planes which are nearly normal to the surface. The effects of instrument geometry on line position and breadth have been evaluated by Wilson (1963) for the Bragg–Brentano case and are listed by Parrish and Wilson (1992) for Seemann–Bohlin geometry. The relative merits of various diffractometer configurations, together with the associated experimental procedures, have been reviewed by Jenkins (1989b).

The parallel-beam optics used with synchrotron radiation means that a variety of diffractometer configurations is possible. The diffractometer axis is usually horizontal and

the most widely used method in powder diffraction is standard $\theta/2\theta$ scanning, with a rotating flat specimen or a spinning capillary sample. Since there is no restriction on the path lengths of the incident and diffracted beams, this is often termed Debye–Scherrer geometry, by analogy with the standard powder camera. The resolution is largely governed by the width of the incident beam, if this is greater than the sample size, and by the receiving-slit aperture. The resolution can be improved somewhat if the receiving slit is replaced by an analyser crystal which has a small mosaic spread (Cox *et al* 1983; Hastings, Thomlinson and Cox 1984). 2θ scans with a fixed sample position are used for analysing texture, preferred orientation and grazing-incidence diffraction. Energy-dispersive experiments are normally performed with a fixed $\theta - 2\theta$ setting and a solid-state detector coupled to a multichannel analyser, but higher resolution can be achieved by rotating a monochromator in the incident beam, to select the desired range of wavelengths.

A very recent development is the introduction of a parabolically-bent multilayer device with a laterally-graded period (Schuster and Göbel 1995), to condense divergent X-rays from a sealed-tube source to a parallel beam. This technique results in a gain by a factor of 100 in intensity and allows the use of parallel-beam geometry with conventional sources.

4.2.2. Powder cameras. Powder diffractometers have largely replaced film cameras in laboratories where powder diffraction is practised. This is particularly true of the cylindrical Debye–Scherrer camera, in which the sample is mounted in a thin glass capillary tube, normally manufactured from light elements or silica. The other type which is still favoured in some laboratories, is the Guinier focusing camera, with a flat transmission specimen and a cylindrical film (Guinier and Dexter 1963). An advantage of this camera is that, by suitable adjustment of the monochromator crystal, the $K\alpha_1$ line can be selected. Werner (1992) has discussed the relative merits of powder cameras and diffractometers.

4.3. Detectors

4.3.1. Photographic film. The use of photographic film for the detection of X-rays has largely been superseded by electronic devices in powder diffraction. Aside from the convenience factor, this is mainly due to the inherent low resolution of film and the difficulty of obtaining digital data of the quality required in modern diffraction methods. Nevertheless, a Guinier–Hägg camera, coupled with a densitometer to obtain a digital representation of intensity, has been used successfully for pattern indexing and structure analysis (Werner 1986) and is still used in some laboratories to obtain standard data for the Powder Diffraction File (section 5.1.1). It should, however, be remembered that photographic film is an inexpensive 2-dimensional detector which gives a visual indication of the presence of preferred orientation (section 6.1.3). Also, from the appearance of Debye–Scherrer rings which may occur for different phases, film can be used as an aid to identifying a mixture of unknown materials.

4.3.2. Counter detectors. The majority of detectors used with X-ray sources are of the proportional or scintillation type, the former having a greater energy resolution ($\sim$ 15%, compared with $\sim$ 50% for the latter), but lower quantum-counting efficiency. Both produce an output voltage proportional to the energy of the incident X-ray photon and, when used with a pulse-height analyser, a degree of energy discrimination can be achieved. Far greater energy resolution ($\sim$ 2–3%) can be obtained with a solid-state detector, usually a Li-drifted silicon crystal, though other materials are used. Such detectors have the added advantage

that the quantum counting efficiency is $\sim$ 100%, but earlier versions needed to be held at the temperature of liquid nitrogen at all times, to avoid loss of Li, which can be inconvenient for routine use. This disadvantage was overcome in the early 1980s by the introduction of a compact silicon detector with Peltier thermoelectric cooling. Solid-state detectors have been reviewed by Bish and Chipera (1989) and further details of the construction and performance of counter detectors have been given by Parrish (1992).

4.3.3. Position-sensitive detectors. If high-resolution data are required from an angle-dispersive experiment, then scanning the diffraction pattern in small angular increments with one of the above detectors is the best approach. However, the time taken to accumulate data can be prohibitively long, if routine measurements for a large number of samples are to be made or if the time-dependent behaviour of a sample is of interest. Such applications led to the development of position-sensitive detectors (PSDs) in powder diffraction. These are mostly based on the proportional counter and early versions were linear, with the subtended angle limited to about 10°. Thus, unless a narrow angular range is acceptable in a particular application, the detector needs to be re-positioned throughout the range of interest. Göbel (1981) introduced a method for repositioning a PSD which permits a very rapid automated data collection by using approximate Bragg–Brentano geometry. The aberration introduced by de-focusing of the diffracted beam was overcome by the introduction of curved detectors in X-ray diffractometry in the late 1970s (Ortendahl *et al* 1978), which effectively takes the place of a film in Debye–Scherrer geometry. A commercial version was developed for use with an incident-beam focusing monochromator, which employs a gold-plated tungsten anode confined magnetically to a radius of 130 mm and subtending an angle of 80° (Wölfel 1983). Included in the pressurized enclosure containing the anode wire and magnets is a delay line with spatial resolution of 105 μm, corresponding to an angular resolution of about 0.07° (2θ). At about the same time, a more robust version, employing a stainless-steel blade as the anode, was introduced (Ballon, Comparat and Pouxe 1983). This has a radius of 250 mm, corresponding to an angular aperture of 120°, and a resolution of 0.03° (2θ). A commercial version of this detector is also available.

The maximum counting rate for PSDs is less than for normal proportional or scintillation detectors by an order-of-magnitude or so, but in most applications this is not a serious limitation. Also, the instrument resolution is somewhat inferior, which may be a disadvantage in cases where line breadths are not dominated by sample broadening. A more serious problem is that the response, both spatially and in terms of intensity, is not necessarily linear throughout the length of the detector. Curved PSDs in particular require careful calibration and the data are subjected to somewhat elaborate correction procedures (e.g. Shishiguchi, Minato and Hashizume 1986). Nevertheless, the introduction of curved PSDs in angle-dispersive experiments, whereby a complete pattern can be obtained without moving the detector, has revolutionized time-dependent studies (section 11.1) and even routine work where high resolution is not the main consideration. Further information on the design and performance of various types of PSD has been provided by Arndt (1992).

4.3.4. Area detectors. In general there is no particular advantage in using a 2-dimensional detector in X-ray powder diffraction, if a sufficient quantity of an 'ideal' sample (section 4.5.1) is available. However, there are some applications where area detectors are proving to be indispensable, notably in studies of texture and in quantifying preferred orientation, or in ultra-high-pressure work, when the sample volume is small (section 11.2). The most widely used area detector in powder diffraction at present is the image plate, introduced

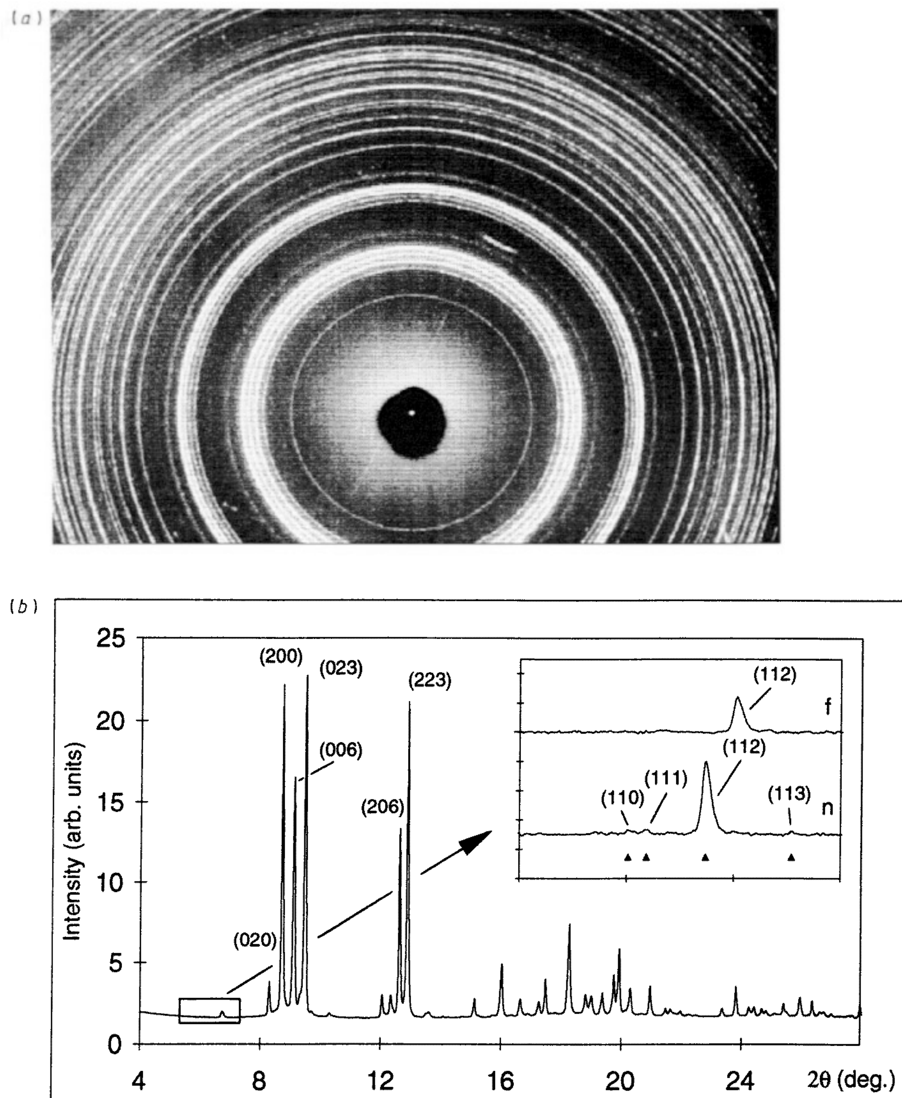

Figure 5. Powder diffraction pattern obtained with an image-plate detector and synchrotron radiation (Daresbury SRS). (*a*) 2-dimensional image from InSb-IV at 5.1 GPa, 0.4445 Å, 8 hr exposure time. (*b*) Integrated profile of the 2-dimensional image. The inset shows, on a common scale, an enlarged view of the low-angle region recorded at 0.4635 Å, far (f) from the In *K*-edge (0.4439 Å), and at 0.4445 Å, near (n) the *K*-edge (Nelmes and McMahon 1995).

by Fujii *et al* (1988) for energy-dispersive high-pressure experiments carried out with a diamond anvil cell. This uses a storage phosphor, such as a Eu-activated Ba halide, which is exposed in the same way as photographic film and then scanned with a laser beam. The intensity of the light emitted is proportional to the energy of the original X-ray photon and this is measured with a photomultiplier. The image plate is used repeatedly, since the image can be erased. It has a low background, a large ($\sim 10^5$) dynamic range and a reasonable spatial resolution.

The extension of the use of the image plate detector to angle-dispersive experiments transformed high pressure research, since the problem of small sample volume, inherent with diamond anvil cells, is then overcome by recording and integrating the intensity around a substantial part of each Debye–Scherrer ring. This technique was pioneered at the Photon Factory (Kikegawa 1992) and was further developed at the Daresbury Laboratory SRS (Piltz *et al* 1992; Nelmes and McMahon 1994) (figure 5). The combined advantages of the image plate and the high resolution attainable with angle-dispersive system means that data of sufficient quality for structure solution or refinement can now be obtained at pressures up to about 200 Gpa (2 Mbar). The use of the image-plate detector with synchrotron radiation has been reviewed by Amemiya (1995). Charge-coupled devices (CCDs) and fast-scanning television monitors (Arndt 1992) have not hitherto been widely used as 2-dimensional detectors in powder diffraction, but this is likely to change in future, particularly with high brightness synchrotron sources.

4.3.5. Neutron detectors. Neutrons can be detected in powder-diffraction experiments by inducing a nuclear reaction with a highly absorbing isotope, such as ^{3}He or in ^{10}BF gas, and then detecting the resulting γ ray or heavy-particle emission in a proportional counter in the usual way. Alternatively, detection can be achieved by interaction with a scintillator which is coupled by means of a light guide to a photomultiplier. This arrangement is more efficient than a proportional counter and an area detector can be formed by mounting scintillators in a 2-dimensional array. The HRPD at ISIS has a ring of such scintillators, each being connected to three out of a total of 64 photomultipliers. The detection of light in all three then identifies the location of the incident neutron unambiguously.

4.4. Non-ambient diffraction

4.4.1. High-temperature diffraction and reaction cells. Furnaces for carrying out *in situ* diffraction studies of phase changes and other phenomena at temperatures up to 2500°C have been available for many years and the different designs and desirable features have been reviewed by McKinstry (1970). A significant advance during the last decade or so has been the development of high-temperature cells for *in situ* characterization of samples in reactive gas environments or for following solid-state reactions. The impetus for this work has largely been catalyst development and, in addition to the reaction cell, the apparatus consists of a gas mixing rig and some means of analysing the product gases, usually a gas chromatograph and a mass spectrometer. Two main types of cell have emerged. In one the gases are passed over the surface of the sample (e.g. Mamott *et al* 1988; Terblanche 1989) and in the other they pass through the sample (e.g. Moggeridge, Rayment and Lambert 1992). An example of the latter type, which incorporates the best features of earlier equipment, is the cell devised by Puxley, Squire and Bates (1994) to study heterogeneous catalysts under simulated reaction conditions at temperatures up to 1000°C. A feature of the cell is optimization of the interaction between gas and sample, an essential requirement if a measurable degree of gas conversion is to be achieved. The cell was mainly intended for studying the catalytic oxidative coupling of methane, but it was also used to investigate solid-state reactions and phase transitions.

The increased use of *in situ* powder diffraction has in fact led to the development of a variety of cells for studying samples under special environmental conditions and also to the design of powder diffractometers to accommodate large attachments (e.g. Arnold *et al* 1989). An autoclave cell has been devised for time-resolved analysis, by means of

neutron diffraction, of dynamical processes occurring during hydrothermal syntheses under hostile conditions (Polak *et al* 1990). Electrochemical cells have been designed for use with neutrons and synchrotron sources and a cell for *in situ* energy dispersive X-ray powder diffraction of intercalation reactions has been described by Clark *et al* (1994).

4.4.2. Low-temperature diffraction. Experiments at low temperature have been carried out since the early days of powder diffraction and the considerable number of cryogenic devices which evolved have been described in detail by Rudman (1976). Any temperature down to ~ 1 K can be obtained by using different coolants and methods of cooling. The sample can be cooled by means of a stream of cold gas, conduction, Joule–Thomson expansion or immersion, or by enclosing the sample or entire apparatus in a cold environment. The choice of cooling mechanism depends to some extent on the radiation used and the nature of the experiment, but increasing use is being made of the 'cryostream' system for temperatures down to 77 K (Cosier and Glazer 1986). This embodies a continuous nitrogen-flow cooling device. The disadvantages of thermal instability and high coolant consumption which were inherent in earlier devices are overcome by a combination of precise control of gas flow and a large thermal capacity of the heat exchanger/evaporator. The temperature at the sample is stable to within ± 0.1 K and the 'cryostream' only consumes 0.5 lhr^{-1} of liquid nitrogen. The system can be used with any type of diffractometer or camera.

4.4.3. High-pressure cells. Experiments at non-ambient pressure, which are frequently carried out at non-ambient temperature, can be broadly classified as low, medium and high pressure, according to the type of cell used. Low-pressure studies, up to 0.7 GPa (7 kbar), can be carried out with gas- or oil-driven cells. These can accommodate a large volume of sample, the pressure throughout the cell is hydrostatic and temperatures as high as 1500°C can be produced. Such cells are particularly suited to the study of organic materials.

For the next régime, to about 20 GPa, a Bridgman anvil cell can be used. This consists of two opposed anvils made of a hard material, such as tungsten carbide, with flat parallel surfaces between which the sample is compressed as the anvils are driven together. The sample volume is limited to a few mm^3 and sample temperatures up to 2000°C have been reached with these cells. Other cells used in powder diffraction are the belt device, which employs a tapered piston, and the Drickamer cell (Häusermann, Daghooghi and Sherman 1990, 1992).

Multi-anvil cells, whereby a single ram induces a compression of the sample along the three axial directions, are used to pressures of about 30 GPa. The sample size can be $\sim 10\mathrm{mm}^3$ or more, with temperatures up to 2500°C. Multi-anvil cells have been used for energy-dispersive diffraction (EDD) since the early 1980s, but the advantages of large sample volumes and high temperatures are offset by their size and weight, the latter being in the region of 0.5 to 1 tonne. Their use has thus been restricted to central research facilities, for example, the MAX80 press at the Photon Factory, Japan, to which MAX90, operating at higher pressures, was added a decade later (Kikegawa 1992), and the SAM85 device at the National Synchrotron Light Source (NSLS), Brookhaven (Weidner *et al* 1992a). The latter has a 250 tonne hydraulic ram which simultaneously drives an assembly of six anvils into the sample. Although mainly intended for use in the energy-dispersive mode, fixed wavelength data can be obtained over a restricted range of scattering angle. A more compact (50 kg) cell of the Bridgman type, employing a torroidal anvil arrangement, has been developed by Besson *et al* (1992) for EDD experiments with synchrotron and neutron sources at pressures of 3 GPa or more. A problem inherent with multi-anvil cells is non-uniformity of stress

throughout the sample and also a temperature gradient, if the sample is heated. Although the stress exerted by a cubic-anvil arrangement is essentially hydrostatic, the sample geometry is normally cylindrical and the stress distribution within it is uniaxial. This departure from hydrostatic conditions, known as deviatoric stress, can be monitored by including a cubic material whose equation of state is known, such as NaCl or Au, with the sample. The effect is not large at lower pressures, since only a small region of the sample is available for diffraction, due to the parallel-beam optics of synchrotron radiation, but it is nevertheless measurable and it increases at higher pressures. Weidner *et al* (1992a, b) have thoroughly investigated the precision of pressure measurement, the deviatoric stress and temperature gradient for a cubic-anvil press.

Pressures in excess of 400 GPa (4 Mbar) have been obtained by means of the diamond anvil cell (DAC). The different types of DAC used in high pressure investigations of physical properties have been described by Jayaraman (1983) and the deviatoric stress for this type of cell has been considered by Meng, Weidner and Fei (1993). Temperatures of about 2000°C can be attained with resistive heating, or more if a laser is used, but only very small quantities of sample can be studied. Even higher pressures can be induced by shock waves, but this technique is not widely used in powder diffraction. Further information on pressures cells is given in Chapter 1 of Liu and Bassett (1986).

4.5. Sample preparation and experimental strategy

4.5.1. Sample preparation. A careful and systematic procedure for sample preparation is always desirable and is an essential requirement in many applications of powder diffraction. Failure to observe basic criteria for preparing powder samples can influence the position, intensity and shape of reflections, leading to frustration at the analytical stage and the likelihood of significant errors in the results. In order to achieve a uniform distribution of intensity around each Debye–Scherrer ring there needs to be $\sim 10^6$ crystallites/cm^2 and ideally the greater part of the crystallites should thus have sizes in the range 5–10 μm (Parrish and Huang 1983; see also Cline and Snyder 1983, Jenkins *et al* 1986). Smaller crystallites introduce measurable line broadening and larger sizes degrade crystal statistics and give rise to extinction effects (Sabine 1985, 1988; see also section 6.1.4). Also, large crystallites can introduce an unacceptable displacement of reflections; with focusing geometry the peak shift for 50 μm particles is $\sim 0.01^\circ$ (2θ). If a limiting size of about 10 μm cannot be achieved directly by sieving, sedimentation or some other means of fractionation, then grinding or milling can be used, if sample microstructure is not of interest. However, it should be borne in mind that some substances undergo a phase change when subjected to mechanical treatment (Smith, Snyder and Brownell 1979a). In structure solution or refinement, line-profile overlap can sometimes be reduced, and the quality of data improved, by annealing the sample.

In most cases it is important to avoid preferential orientation of crystallites when preparing specimens and there are various ways in which this can be achieved. If a flat sample is used, it is customary to load the sample holder from the side rather than the front, in order to reduce the effects of preferred orientation. A general method for the elimination of preferred orientation, spray drying, was introduced by Smith, Snyder and Brownell (1979b). Spray drying consists of atomizing a slurry of the powder containing a small amount of adhesive. The droplets ($\sim 50\mu$m) are dried in air and form spherical agglomerates. Details of this procedure are given by Cline and Snyder (1987). The sample surface must be coincident with the axis of rotation, perpendicular to the diffraction vector and smooth, since roughness also introduces peak displacement. Specimen-surface displacement is the

commonest and often the largest source of error in peak position with focusing geometry; typically, a surface displacement of 10 μm displaces peaks by $\sim 0.01^\circ$ (2θ) in a direction which depends on whether the sample is behind or in front of the diffractomerter axis. Further information on sample preparation is given in Methods & Practices (Jenkins 1989a).

4.5.2. Experimental strategy. Experimental conditions are optimized to obtain the best quality data in the time available for a particular task, but are invariably a compromise between resolution and intensity; for example, the use of wider slits increases the latter, but degrades the former. In the majority of angle-dispersive experiments, the step length should be between 1/5 and 1/10 of the *FWHM*, but a smaller step ($\sim FWHM/20$) is needed if a Fourier representation of line profiles is required. Unless software for subsequent analysis requires a constant step throughout a dataset, it is convenient to increase the step length for broader reflections at higher angles. For a single receiving slit the choise of aperture in principle depends on the breadth of line profiles and ideally should be approximately equal to the step length. However, in practice it is customary to use a fixed aperture, typically $\sim 0.05^\circ$, for most applications, since the zero error usually has to be redetermined each time the receiving slit is changed. An overview of experimental strategy has been discussed by Parrish and Huang (1980) and further information is again included in Methods & Practices (Jenkins 1989a).

The precision of line-profile parameters depends on counting statistics and this in turn is determined by the maximum intensity and the background level. Various authors have considered random errors in the measurement of line-profile position, intensity and breadth due to counting statistics (e.g. Wilson 1967; Langford 1980; van Berkum *et al* 1995). In practice it has been found that ideally, in applications based on pattern decomposition, a maximum count of at least 10 000 (a precision of 1%) should be accumulated for each reflection, but this may well be impracticable for weak lines. For phase identification, counting statistics are decided by the desired level of detection for minor phases, relative to the background level.

4.6. Instrument characterization and Standard Reference Materials

Well characterized standard materials play an important rôle in every aspect of powder diffraction, from determining the performance of instruments to improving the precision of experimental data. The most widely used standards are those produced and marketed by the US National Institute of Standards and Technology (NIST, formerly the National Bureau of Standards), based in Gaithersburg, Maryland. These are known as Standard Reference Materials (SRMs) and, depending on the application, they are used as an independent specimen (external standard) or are mixed with the sample of interest (internal standard). Various other standards are available commercially and they are also produced in individual laboratories to suit particular applications.

It is important that the crystallite sizes for standard materials should mostly lie within the range 5–10 μm, for the reasons stated in section 4.5. A high linear absorption coefficient μ is desirable, though not essential. (In the following, the values given for μ correspond to the wavelength of Cu$K\alpha$ radiation. μ^{-1} is also included, to give an indication of the penetration depth at this wavelength.) Also, materials with high crystal symmetry (cubic or hexagonal) are normally used, to avoid undue overlap of reflections when they are used as internal standards. In general, materials with a tendency to exhibit preferred orientation should be avoided, an esential requirement for intensity standards. Examples of the use of

standards are given by Wong-Ng and Hubbard (1987) and full specifications of SRMs and other information are included in *Methods & Practices* (Jenkins 1989a).

4.6.1. d-spacing standards. The main SRM marketed by NIST for the precise determination of the position of line profiles is Si 640*b* ($a_0 = 5.430940$ (11) Å at 25°C). In addition to acting as a d-spacing standard, this SRM is also widely used for determining the wavelength in angle-dispersive experiments with synchrotron radiation. NIST also provides fluorophlogopite (SRM 675, a synthetic mica with $d_{001} = 9.98104$ (7) Å at 25°C) for calibration at low angles or large d spacings. Unlike other SRMs, this standard has relatively large particles (up to 75 μm), to encourage total orientation of platelets, so that only $00l$ reflections are observed. Both these standards introduce measurable peak displacements due to sample transparency, unless thin ('smear') specimens are used. μ for Si is 133 cm^{-1} ($\mu^{-1} = 75\mu$m) and is considerably less for mica. For a 'thick' specimen of the former, the 422 reflection (Cu$K\alpha$ radiation) is displaced by $-0.01°$ (2θ). Ag ($a_0 = 4.08651$ (2) Å at 25°C; $\mu = 2500\,\text{cm}^{-1}$, $\mu^{-1} = 4\mu$m), for which the corresponding peak displacement is only about $-0.0005°$ for a 'thick' specimen, is also widely used as a d-spacing standard.

The first reflection with Cu$K\alpha_1$ radiation for SRM 675 occurs at 8.853° (2θ) and a material which extends the coverage of SRMs down to very low angles is silver behenate (Huang *et al* 1993). The long spacing for this material, obtained with synchrotron radiation and by using SRM 640*a* as an internal standard, is $d_{001} = 58.380$ (3) Å and, for Cu$K\alpha_1$ radiation, there are 13 well defined and evenly spaced $00l$ reflections in the range 1.5° to 20° (2θ). Additional information is given in the report of a 'round robin' organized by the ICDD on the measurement of this large d spacing (Blanton *et al* 1995). This material is suitable for use as an external or an internal low-angle calibration standard for the analysis of materials with large unit-cell dimensions and modulated multilayers with large layer periodicity.

4.6.2. Intensity standards. The primary intensity standard is α-Al_2O_3 (corundum) and its main use is in quantitative analysis. Data in the Powder Diffraction File often include the ratio of the intensity of the strongest peak to that of the corundum 113 reflection, the Reference Intensity Ratio (RIR), which is listed as I/I_c. (See section 9.) This greatly facilitates the quantitative analysis of phases for which I/I_c is known, since an internal standard in then not required. It should, however, be remembered that the RIR is based on maximum intensities, whereas weight fractions are proportional to line-profile areas (integrated intensities). Four secondary standards are also supplied by NIST, ZnO (wurtzite, $I/I_c = 5.17$ (13) for 101 line), TiO_2 (rutile, $I/I_c = 3.39$ (12) for 110 line), Cr_2O_3 (corundum structure, $I/I_c = 2.10$ (5) for 104 line) and CeO_2 (fluorite structure, $I/I_c = 7.5$ (2) for 111 line). These five standards are marketed as SRM 674.

4.6.3. Instrument line-profile shape standards. The need for standard reference materials to calibrate instrumental line profiles arose from the increased emphasis in recent years on the use of complete diffraction patterns in several applications of powder diffraction (section 6 *et seq.*). There are in fact two reasons for having instrumental standards. One is to characterize instrument resolution, as a check that alignment has been optimized or to compare the behaviour of different diffractometers, and the other is to obtain sample line profiles $f(x)$ from the observed data $h(x)$ (section 2.3). Different standards may therefore be required if samples of interest do not have a high absorption coefficient for the radiation used.

In addition to the usual requirements for standard reference materials, suitable substances for instrument characterization should clearly not exhibit any measurable sample broadening, even when used with high resolution diffractometers. Also, unless very thin samples are used, they should have a high linear absorption coefficient. With Bragg–Brentano geometry, for example, the contribution to line breadths due to transparency from a sample with $\mu = 1000\text{cm}^{-1}$ [$\mu^{-1} = 10\mu\text{m}$] typically has a maximum value of only $\sim 0.002^\circ$ (2θ). Various materials were considered by the Technical Committee of the ICDD, in association with NIST, and lanthanum hexaboride (LaB_6) ($\mu = 1138\text{cm}^{-1}$; $\mu^{-1} = 9\mu\text{m}$) was selected for use as an instrumental standard (Fawcett *et al* 1988). This was subsequently marketed by NIST as SRM 660 and it also serves as a line position standard ($a_0 = 4.15690$ (5) Å at 26°C). Other materials used as instrumental standards include BaF_2 ($\mu = 1394\text{cm}^{-1}$; $\mu^{-1} = 7\mu\text{m}$) (Louër and Langford 1988) and KCl ($\mu = 247\text{cm}^{-1}$; $\mu^{-1} = 41\mu\text{m}$) (Scardi, Lutterotti and Maistrelli 1994). Both are low cost materials, are available in large quantities and can readily be annealed to minimize sample broadening. Although KCl may introduce a measurable breadth contribution due to sample transparency, it can be used to advantage for correcting data from materials having a similar absorption coefficient, such as many ceramics.

A different approach was adopted by van Berkum *et al* (1995), who selected a 5–10 μm size fraction from the NIST Si SRM 640*a* and deposited about 1.5 mg cm^{-2} uniformly on a (510) oriented Si single-crystal wafer. The whole assembly was then annealed. At angles below about 100° (2θ) the resulting line-profile widths were found to be slightly less than for LaB_6 which had been prepared in the same way, but without heat treatment. However, the time taken to acquire data with sufficient precision for the Si sample, more than a week, would be prohibitively long for routine instrument characterization. van Berkum *et al* give a useful overview of the criteria for preparing an optimum instrumental standard and describe their optimization procedure in detail.

Line profiles arising from geometrical and physical aberrations were calculated in the early days of powder diffractometry (e.g. Klug and Alexander 1974), but recently there has been a revival of interest in convoluting these functions with a wavelength spectrum to obtain instrumental line profiles $g(x)$. This was carried out by Cheary and Coelho (1992) for Bragg–Brentano geometry and later (1994) extended to include a linear position-sensitive detector. In a similar approach, Kogan and Kupriyanov (1992) synthesized the overall instrumental line profiles by obtaining the Fourier coefficients of the profiles due to individual aberrations. However, not all the relevant aberration functions are known precisely, or can be described analytically, and at present $g(x)$ is normally obtained by means of a suitable SRM.

The characteristics of a diffractometer are normally represented by the Instrument Resolution Function (IRF), the variation of the $FWHM_g$ of the standard line profiles $g(x)$ with 2θ, in the angle-dispersive case. Typical IRFs for a conventional and synchrotron X-ray sources are given in figure 6. The nature of this curve depends on the geometry and dimensions of the instrument and slit system and on the radiation used. For a conventional diffractometer with an incident-beam focusing monochromator and a receiving-slit aperture of 0.05°, the IRF typically has a shallow minimum of $\sim 0.07^\circ$ (2θ) at intermediate angles, this being largely due to the width of the receiving slit, increasing to twice this value at $\sim 120^\circ$–125° (2θ), as the contribution from the wavelength spectral distribution increases. At low angles the instrumental line broadening increases rapidly, due to the effects of axial divergence. The influence of the apertures of the divergence, receiving and Soller slits on the form of the IRF and on the symmetry of $g(x)$ has been considered by Cheary and Cline (1994). This work clearly demonstrates the importance of selecting an optimum slit

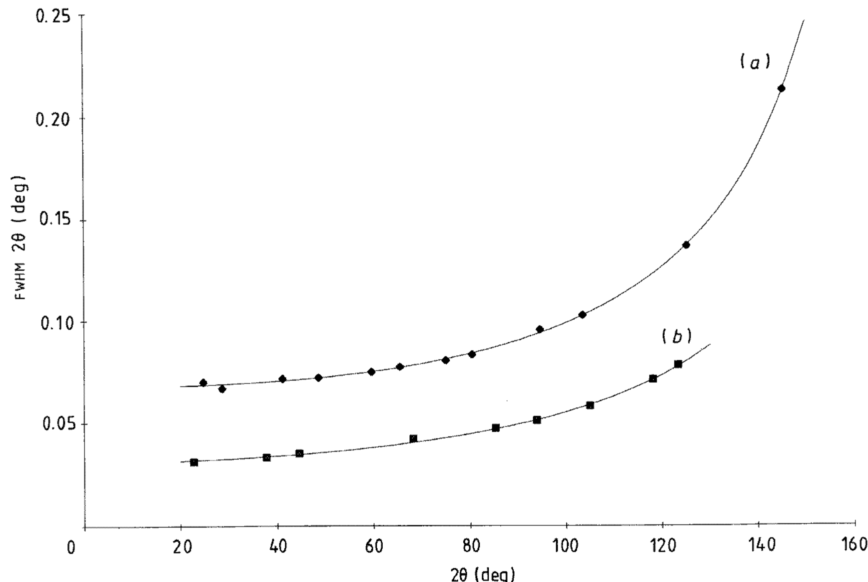

Figure 6. Typical Instrument Resolution Functions (IRFs) (a) for a conventional Cu $K\alpha_1$ X-ray source, incident-beam monochromator and Bragg–Brentano diffractometer, 0.05° receiving slit, and (b), the high resolution station 9.1 powder diffractometer at the Daresbury Laboratory SRS, 0.026° receiving slit.

configuration if reasonably symmetrical instrumental line profiles are required. In order to obtain interpolated values of width in a particular application, a quadratic in $\tan\theta$ is normally fitted to $(FWHM_g)^2$ (equation 3.8), but a function which models the form of the IRF more closely at lower angles and makes allowance for sample transparency ('thick' specimen) is (Langford 1987)

$$(FWHM_g)^2 = A\tan^2\theta + B + C\cot^2\theta + D\sin^2 2\theta. \tag{4.4}$$

Equation (4.3), which is based on the variances (mean square breadths) of the individual contributions to instrumental line profiles (Wilson 1963), can also be used to model the variation of the integral breadth β_g with angle. The fourth term can be omitted for highly absorbing samples.

5. Databases and phase identification

5.1. Databases

Ordered collections of crystallographic data have been available since the early days of powder diffraction, but their use increased steadily after the introduction of magnetic storage media and dramatically since the mid 1980s, with the advent of the CD-ROM and PC systems, together with general access to world-wide communication networks. A list of currently available crystallographic databases, with the type of storage medium used,

38-1433

Ba2Cu3YO7

Barium Copper Yttrium Oxide

Rad.: CuKa1 λ: 1.5405 Filter: Graph d-sp: Diffractometer

Cut off: 17.7 Int.: Diffract. I/Icor.:

Ref: Wong-Ng, W., McMurdie, H., Paretzkin, B.,Hubbard, C., Dragoo, A., NBS (USA), ICDD Grant-in-Aid, (1987)

Sys.: Orthorhombic S.G.: Pmmm (47)

a: 3.8856(3) b: 11.6804(7) c: 3.8185(4) A: 0.3327 C: 0.3269

α: β: γ: Z: 1 mp:

Ref: Wong-Ng, W et al., Powder Diffraction, 2, 192 (1987)

Dx: 6.383 Dm: SS/FOM: F_{30}=66(.0091, 50)

Color: Black
Peak height intensity. The temperature of data collection was 25.5 C. The sample was obtained from F. Beech of the Reactor Radiation Division, NBS. A stoichiometric mixture of CuO, Y2 O3 and Ba C O3 were intimately mixed and fired at 500 C overnight. Reaction with container was avoided by placing the pellet on a support of the same material. The resulting powder was ground and pressed into pellets and refired at 900 C overnight. The pellets were reground, pressed and fired at 950 C overnight. Final annealing took place at 750 C for 27 hours under oxygen. The oxygen content was analyzed by differential thermal gravimetric analysis. Superconductor with Tc of 92 K. The structure was determined by Siearist, T. and Sunshine, S. et al. (1). The sample was characterized by neutron Reitveld refinement technique by A. Santoro, at NBS. The compound was first reported by Cava and Batlogy. Silicon, fluorophlogopite used as an internal stands. PSC: oP13. Mwt: 666.20. Volume[CD]: 173.30.

Wavelength= 1.5405981

d Å	Int	h	k	l	d Å	Int	h	k	l
11.689	<1	0	1	0	1.3619	12	2	0	2
5.8361	4	0	2	0	1.2977	1	0	9	0
3.8912	10	0	3	0	1.2950	<1	3	0	0
3.8188	4	0	0	1	1.2865	2	1	6	2
3.2346	3	1	2	0	1.2656	<1	2	7	0
3.1960	5	0	2	1	1.2565	1	0	7	2
2.9175	<1	0	4	0	1.2340	<1	2	4	2
2.7496	55	1	3	0	1.2309	4	1	9	0
2.7248	100	0	3	1	1.2286	6	0	9	1
2.6530	2	1	1	1	1.2263	5	3	0	1
2.4682	3	1	2	1	1.2098	5	0	3	3
2.3357	13	0	5	0	1.2015	3	2	7	1
2.3191	5	0	4	1	1.1843	1	1	2	3
2.2316	14	1	3	1	1.1763	2	2	5	2
1.9909	2	1	4	1	1.1702	<1	3	3	1
1.9461	22	0	6	0	1.1683	1	0	10	0
1.9425	21	2	0	0	1.1551	1	1	3	3
1.9095	12	0	0	2	1.1187	3	1	10	0
1.7732	4	1	5	1	1.1161	6	2	8	1
1.7408	3	1	6	0	1.1114	4	1	8	2
1.7344	4	0	6	1	1.0860	1	3	5	1
1.7143	2	0	3	2	1.0791	1	2	9	0
1.6683	2	0	7	0	1.0733	1	0	9	2
1.6595	1	2	2	1	1.0617	1	0	11	0
1.5837	26	1	6	1	1.0550	1	2	7	2
1.5685	13	1	3	2	1.0377	4	3	6	1
1.5334	<1	1	7	0	1.0333	4	3	3	2
1.5291	1	0	7	1	1.0273	4	1	6	3
1.4938	2	2	5	0					
1.4899	2	2	4	1					
1.4782	3	0	5	2					
1.4225	2	1	7	1					
1.3751	5	2	6	0					
1.3666	5	1	8	0					
1.3634	13	0	8	1					

©1994 JCPDS–International Centre for Diffraction Data. All rights reserved.

Figure 7. Data for fully oxygenated 'YBCO', $YBa_2Cu_3O_7$, No. 38-1433 in the Powder Diffraction File (PDF-2). ©1994 JCPDS-ICDD. All rights reserved.

source and other details, is given in Table 1 of Gorter and Smith (1995). The more important datasets, in so far as powder diffraction is concerned, are considered below.

5.1.1. The Powder Diffraction File. The principal method for the identification of unknown materials is based on a comparison of experimental data with standard d spacings and peak intensities ('ds and Is') contained in a database known as the Powder Diffraction File (PDF). This database was introduced in the late 1930s by Hanawalt, Rinn and Frevel (1938) and has been issued annually since 1950. It is currently maintained, updated and marketed by the International Centre for Diffraction Data (ICDD). Two versions of the file are available and a third is under development. In addition to 'ds and Is', a typical entry in the main database, known as PDF-2, contains hkl values for each reflection if the pattern has been indexed, the chemical name and, if appropriate, the mineral name, the chemical formula, cell dimensions and the space group, selected physical properties, a chemical analysis and other details of the sample, references and an indication of the quality of the data. Originally supplied on 3″ × 5″ cards, the database is currently provided in book form, as microfiche, on 9-track magnetic tape or on a CD-ROM. The last was introduced in 1987 (Jenkins and Holomany 1987) and it is by far the most convenient storage medium. A new set with about 2000 entries is added each year and in 1995 the PDF contained data for over 70,000 substances, occupying about 200 MByte of storage. A typical entry in the database, PDF No. 38-1433 for fully ogygenated 'YBCO' ($YBa_2Cu_3O_7$), is shown in figure 7, which was obtained as a 'card image' from the CD-ROM. For convenience, the database has organic

and inorganic materials as main categories, but it is also divided into other subsets; cements, corrosion products, explosives, forensic materials, high T_c ceramics, minerals, metals and alloys, pharmaceuticals, pigments, polymers and zeolites are available and other subsets can be obtained by the user to suit a particular application. Although PDF-2 is invaluable as a database, it can be unwieldy for on-line identification, even if a search is restricted to one or other of the above subsets, and a version containing only d spacings, intensities, name and chemical formula, known as PDF-1, is available and this only requires about 10 MByte of storage. Another database, PDF-3, containing full digitized patterns in addition to the information in PDF-2, is under development by the ICDD. (See section 5.2.2.)

5.1.2. Other databases. There are several other crystallographic databases of interest in powder diffraction. Of these, the most widely used is the Crystal Data File (CDF) (Stalick and Mighell 1986; see also Allen, Bergerhoff and Sievers 1987, pp 133–43), a compilation of unit cell data which have been reported in the literature. Each entry includes unit-cell parameters, crystal system, space group, chemical name and formula and literature references and there are currently (1995) data for about 200 000 unit cells. The CDF can be used as a means of identifying an unknown substance if the crystal system and cell dimensions are known. The Inorganic Crystal Structure Database (ICSD), developed by Bergerhoff and Brown (1987) and based at the Fachsinformationzentrum-4 in Karlsruhe, contains structural information for inorganic compounds other than metals. The Metals Structures Database (MSD) (Rodgers and Wood 1987) contains similar data, but for metals and alloys and their corrosion products. The MSD is based at the National Research Council of Canada in Ottawa. The Cambridge Structural Database (CSD) (Allen, Bergerhoff and Sievers 1987, pp 31–132) has data for organic and organo-metallic materials. The ICSD, MSD and CSD are primarily of interest in single-crystal work, but they can be used to calculate powder diffraction patterns or to generate a starting model, based on an isostructural compound, for structure refinement by means of the Rietveld method. Also, if a structure is unknown, but the unit cell has been found from powder diffraction data (section 7.2), these databases can be consulted to ascertain if an isostructural material exists. All these databases except the last are, or will be, available in CD-ROM form. The CSD can be accessed through Internet.

5.1.3. Crystallographic Information File Format. In order to meet the need for a universal mechanism for the archiving and electronic transmission of data, text and other material, the IUCr developed the Crystallographic Information File (CIF) format (Hall, Allen and Brown 1991). A CIF file is completely self-descriptive, in that data items are identified by unique names which are listed in a dictionary of core definitions. It is composed of ASCII characters and can thus be edited in the usual way by using any computer operating system. Various programs are available free of charge from the IUCr for producing and handling CIF files. Although CIF format is already used widely by the single-crystal community, its application to powder diffraction is a relatively recent development. A supplement to the core dictionary, which contains definitions pertaining to data obtained from all types of powder diffractometer and any of the sources of radiation used in diffraction experiments, has been compiled (Toby, Langford and Hall 1993). CIF format has been adopted by the ICDD for the PDF-3, which is in fact its first major application in powder diffraction. The use of CIFs by crystallographers is increasing steadily and, in order to facilitate the archiving, transmittal and publication of information, all who generate and analyse powder data are encouraged to use this format.

5.2. Phase identification (Search/Match)

The set of d spacings and intensities obtained from an X-ray diffraction pattern for a random powder sample of a given material is unique and it was appreciated early in the history of powder diffraction that this provided a means of identifying unknown substances or of confirming materials present. Compounds with the same chemical formula, but different structures, such as polymorphs of SiO_2, TiO_2 or ZnS, can readily be distinguished. Data for compounds having the same structural arrangement, but containing different elements, are similar and the differences are sometimes small (e.g. lanthanide compounds). Nevertheless, such materials can again be distinguished by means of diffraction data. Indeed, powder diffraction is frequently the only means available for the identification of unknown materials, particularly if only small quantities (e.g. a few mg) of sample are available, and X-ray data are extensively used world-wide for this purpose.

5.2.1. Manual Search/Match. In order to identify an unknown phase, the PDF is searched until an entry is found which matches the experimental ds and Is, a procedure thus known as Search/Match. If this is carried out manually, it is clearly impracticable to search the entire database and an index is used. Various indexes have been devised over the years, but the one most widely used is that introduced by Hanawalt, Rinn and Frevel (1938). The Hanawalt Index (or the Hanawalt Search Manual) is based on the d spacings of the strongest lines in the diffraction pattern. The database is divided into groups containing the strongest line, regarded as having a maximum intensity of 100%, and within each group the spacing of the second strongest line is listed in descending order of d. The eight most intense lines are included for each entry and, to minimize the effects of preferred orientation, each pattern can occur up to four times, according to certain permutation rules. The section of the Hanawalt Search Manual which contains the data for fully oxygenated 'YBCO' is shown in table 2(a). This is taken from the Hanawalt group for d_{100} in the range 2.74 to 2.70 Å. The Hanawalt Index is updated and issued annually by the ICDD. Again, indexes to various subsets of the PDF are published from time to time. An alphabetical listing of all entries in the PDF is also published and this sometimes provides the quickest means of identifying phases. The section of the Alphabetical Index which includes 'YBCO' is shown in table 2(b). A comprehensive account of the strategy employed in manual search/match is included in *Methods & Practices* (Jenkins 1989a). It is usually evident from prior knowledge (sample origin and history, chemistry, etc.), experience or simply intuition, whether or not a match is the correct solution, but various Figures of Merit (FoMs) have been devised to quantify the result. (See, for example, Smith, Hoyle and Johnson 1993, 1994.) The quality of data contained in the PDF also needs to be considered when assessing the validity of a match. Modern diffractometers are capable of producing high quality data routinely, whereas many of the earlier datasets, particularly those obtained with a Debye–Scherrer camera, are less accurate. So that allowance can be made for this, an indication of the quality of data is given for each entry in the PDF. One such indicator is the figure of merit F_N, given by equation 7.3 (Smith and Snyder 1979). Additionally, during the 1980s all earlier datasets were assessed by the ICDD for accuracy and precision and, if necessary, upgraded or replaced. The observed ds and Is can be influenced by instrumental aberrations, preferred orientation and sample imperfections, so there is unlikely to be an exact match with standard data, even if these do not contain significant errors. Minerals belonging to isomorphous series and alloys require special treatment, since d spacings will depend on composition, over a limited range, and the PDF only contains data for 'end members' and selected intermediate cases. However, such errors and differences in ds and Is are taken into account by the

experienced user when comparing the experimental pattern with standard data. In order to characterize further such materials, PDF data are used to index the reflections and a least-squares lattice-parameter program (tables 8 and 9 in Gorter and Smith 1995) is used to obtain precise cell dimensions. The position of the sample within a series, and hence its composition, can then often be deduced.

In addition to being an invaluable and readily accessible source of powder data, the CD-ROM version of PDF-2 provides a powerful means of carrying out a computer-aided manual search (Jenkins 1994). In addition to ds and Is, most of the information stored for each entry in the database can be included in the search, up to 19 items in total (table 3). With each CD-ROM PDF-2, the ICDD supplies a program for this purpose and, since the attributes can be linked by the operators 'AND', 'OR' or 'NOT', the procedure is known as a Boolean search (Jenkins and Holomany 1987). An equivalent procedure is available for searching the CDF and again the ICDD supplies the necessary software. Additionally, an experimental program PC-QUEST to greatly extend the scope of computer-aided search/match is under development by the ICDD (Jenkins 1994).

5.2.2. Computer Search/Match. Manual search/match can be laborious and time-consuming, if the sample contains a mixture of several phases, though the effort involved is greatly reduced if carried out in conjunction with the CD-ROM version of PDF-2. However, search/match is largely a matter of pattern recognition, a procedure which can be carried out rapidly and exhaustively by means of a computer, and some 20 programs for this purpose are currently available (table 6 in Gorter and Smith 1995). About two thirds of these are suitable for use with PCs or equivalent computers and a third are commercial products, mainly supplied with Automatic Powder Diffractometers (APDs). The first search/match program was that developed by Frevel (1965), which used a database containing about 300 commonly occurring phases. This was followed by the programs of Nichols (1966) and Johnson and Vand (1967). Both carry out a 'reverse search' of the entire database, whereby each standard value is compared with the experimental data, rather than vice versa. The Johnson–Vand program uses a sequential file structure and produces an ordered list of best matches, together with figures of merit, from which the user decides which is the correct solution. The strategy adopted by Nichols, on the other hand, employs an inverted file, in which the d spacings for the reference data are ordered by decreasing relative intensity. Nichols only included d values for the strongest lines, but otherwise the procedure is analogous to the Hanawalt method. When a component has been identified, the corresponding standard pattern can be subtracted and the procedure repeated until all lines in the measured pattern have been identified.

Many subsequent search/match programs are based on one or other of the above strategies. An improved program, SEARCH, based on inverted files and the Hanawalt search strategy, was developed by Snyder (1981) for use with laboratory-based minicomputers, which were widely used in the 1970s and 1980s. In order to overcome the problem of poor quality reference patterns which existed at that time, he adopted a hierarchical approach, as had been used earlier by Frevel. A MICRO file containing the 300 most common phases was searched first. If this did not provide a solution, then a MINI file containing 2500 entries designated as frequently encountered phases was searched. Finally, if necessary a search was made of a MAXI file containing the full PDF, then up to set 28. A match criterion based on a figure of merit was adopted, the acceptance level depending on whether or not elemental information was included in the search. Cherukuri and Snyder (1983) compared the performance of the program with one based on the Johnson–Vand approach. It was found

Table 2. (*a*) Entry for fully oxygenated 'YBCO', No. 38-1433, in the Alphabetical Indexes to the Powder Diffraction File, Sets 1-44. ©1994 JCPDS-ICDD. All rights reserved.

(*a*)

o Barium Copper Yttrium Oxide: $YBa_3Cu_4O_z$	3.11_x	2.97_x	1.87_x	41–455
o Barium Copper Yttrium Oxide: $Ba_3Cu_7Y_2O_x$	3.08_x	3.03_x	2.66_3	41–454
* Barium Copper Yttrium Oxide: $BaCuY_2O_5$	2.99_x	2.93_7	2.83_5	38–1434
o Barium Copper Yttrium Oxide: $Ba_3Cu_2YO_x$	2.88_x	2.91_5	1.67_3	41–456
* Barium Copper Yttrium Oxide: $Ba_6YCu_3O_{11}$	2.87_g	2.94_g	2.98_g	41–62
o Barium Copper Yttrium Oxide: $YBa_2Cu_3O_{9-z}$	2.87_x	2.47_8	3.12_5	41–453
Barium Copper Yttrium Oxide: $YBa_3Cu_2O_x$	2.85_x	2.87_7	2.03_3	41–16
i Barium Copper Yttrium Oxide: $Ba_4YCu_3O_9$	2.85_g	1.65_g	2.02_g	41–61
o Barium Copper Yttrium Oxide: $Ba_3Cu_2YO_z$	2.83_x	1.66_8	1.65_6	42–443
* Barium Copper Yttrium Oxide: $Ba_2Cu_3YO_6$	2.76_x	2.73_5	1.93_3	39–1496
* Barium Copper Yttrium Oxide: $Y_2Ba_4Cu_7O_{15}$	2.75_x	2.72_x	2.63_5	43–410
o Barium Copper Yttrium Oxide: $Ba_2Cu_3YO_{6.5}$	2.74_x	2.71_7	1.58_4	42–11
i Barium Copper Yttrium Oxide: $YBa_2Cu_3O_{9-x}$	2.74_x	2.34_2	1.58_2	40-411
i Barium Copper Yttrium Oxide: $Ba_{0.4}Y_{0.1}Cu_{0.5}O_x$	2.74_x	1.94_7	2.33_6	40–1058
Barium Copper Yttrium Oxide: $Ba_{0.3}Y_{0.3}Cu_{0.4}O_x$	2.73_x	2.75_6	1.59_4	40–1059
* Barium Copper Yttrium Oxide: $Ba_2Cu_3YO_{6.8}$	2.73_x	2.75_6	1.58_3	39–486
i Barium Copper Yttrium Oxide: $Ba_4Cu_7Y_2O_{14}$	2.73_x	2.75_6	1.58_2	40–199
i Barium Copper Yttrium Oxide: $YBa_2Cu_3O_{6.1}$	2.73_x	2.75_6	1.58_3	43–545
* Barium Copper Yttrium Oxide: $Ba_2Cu_3YO_{6.56}$	2.73_x	2.74_9	2.75_8	39–1434
i Barium Copper Yttrium Oxide: $BaYCuO_3$	2.73_x	1.58_6	1.94_5	41–1081
* Barium Copper Yttrium Oxide: $Ba_2Cu_3YO_7$	2.72_x	2.75_6	1.58_3	38–1433
* Barium Copper Yttrium Oxide: $YBa_2Cu_4O_8$	2.71_x	2.74_7	1.93_3	43–402

(*b*) Part of Hanawalt Group 2.74–2.70 (±0.01) Å, which includes fully oxygenated 'YBCO', from Hanawalt Search Manual (Inorganic Phases), Sets 1-44. ©1944 JCPDS-ICDD. All rights reserved.

(*b*)

2.73_x	2.75_6	1.59_4	2.34_3	1.57_2	1.95_2	1.91_2	1.37_2	$Ba_{0.3}Y_{0.3}Cu_{0.4}O_x$	40–1059
* 2.73_x	2.75_x	1.59_6	1.95_5	3.90_3	2.23_3	1.58_3	1.57_3	$DyBa_2Cu_3O_7$	40–211
* 2.73_x	2.75_8	1.58_2	2.24_2	1.59_2	1.57_2	1.94_2	2.33_1	$Ba_2Cu_3YO_{6.56}$	39–1434
i 2.73_x	2.75_6	1.58_3	2.24_2	1.94_2	2.34_1	1.57_1	1.95_1	$YBa_2Cu_3O_{6.1}$	43–545
i 2.73_x	2.75_6	1.58_2	2.23_2	1.94_2	3.89_1	2.33_1	1.57_1	$Ba_4Cu_7Y_2O_{14}$	40–199
c 2.73_g	2.75_g	1.58_g	2.23_g	1.57_g	1.94_g	1.91_g	11.7_g	$Ba_2YCu_3O_7$	40–159
* 2.73_x	2.75_6	1.58_3	1.94_2	2.23_2	1.95_1	1.91_1	1.57_1	$Ba_2Cu_3YO_{6.8}$	39–486
* 2.73_x	2.75_5	1.58_3	1.94_2	1.57_2	1.37_2	1.92_1	2.24_1	$YBa_2Cu_{3-x}Pd_xO_z$	43–269
2.72_8	2.75_x	2.79_8	1.94_8	1.57_8	1.58_7	3.47_6	1.59_6	Na_3AlH_6	20–1072
* 2.72_x	2.75_x	2.63_5	1.94_4	1.95_3	2.84_3	2.23_2	1.92_2	$Y_2Ba_4Cu_7O_{15}$	43–410
* 2.72_x	2.75_7	1.58_3	1.95_3	1.94_3	2.23_2	3.89_2	2.34_2	$Ba_2Cu_3HoO_7$	39–1400
* 2.72_x	2.75_6	1.58_3	1.95_2	1.94_2	2.23_1	2.34_1	1.57_1	$Ba_2Cu_3YO_7$	38–1433
* 2.72_x	2.75_6	1.58_3	1.94_2	3.88_2	1.95_2	1.57_2	1.91_1	$Ba_2Cu_3ErO_7$	39–1404
i 2.71_x	2.75_8	3.86_5	1.93_5	1.57_3	2.52_3	2.26_3	2.22_3	$BaCa_2Mg(SiO_4)_2$	31–129
* 2.71_x	2.75_x	2.74_x	2.73_x	3.51_8	3.49_8	4.90_7	2.60_6	$LiCu(PO_3)_3$	23–358
2.71_x	2.75_6	2.68_6	1.56_x	1.36_x	1.21_x	1.92_6	1.91_6	$SmGaO_3$	21–1060
c 2.70_9	2.75_x	2.59_6	3.13_5	2.81_4	2.91_2	1.57_2	1.51_2	$GaPr_2$	33–566
2.70_9	2.75_x	2.23_8	1.60_8	5.51_6	3.98_6	1.99_6	1.90_6	$(NH_4)_2NiCl_4 \cdot 2H_2O$	21–32
i 2.70_8	2.75_x	2.04_7	1.82_7	2.08_6	5.43_5	2.01_4	1.83_4	$NiRh_2Se_4$	22–742
2.70_x	2.75_5	1.96_5	3.85_4	3.03_4	1.91_4	1.66_4	2.99_3	Cd_2GeO_4	34–585

that the inclusion of chemical information in the Hanawalt approach made little difference to performance, except for a significant reduction in the search time, whereas elemental data resulted in a dramatic improvement to the behaviour of the Johnson–Vand method. It was

Table 3. Data which can be included in a Boolean search of PDF-2.

No.	PDF data included in search	No.	PDF data included in search
1	PDF number	11	Mineral Group Code
2	Subfile	12	Reduced unit-cell parameters
3	Inorganic chemical name	13	Principal author
4	Mineral name	14	Year of journal
5	Organic chemical element	15	Journal CODEN
6	Chemical element	16	Colour
7	Three strongest lines	17	Density
8	Chemical Abstracts Service number	18	Volume of reduced unit cell
9	Organic chemical name	19	'Long' Lines (largest d values)
10	Inorganic chemical name fragments		

found that solutions from the Hanawalt approach were seldom wrong, but the list produced by the Johnson–Vand program required user evaluation to select correct solutions.

A significant advance in computer search/match was the introduction of the series of interactive programs PDIDENT by Goehner and Garbauskas (1983, 1984). For the first time the user could control the search/match strategy interactively, in a manner similar to that carried out manually by an experienced analyst. As in earlier programs, optional chemical constraints were incorporated, there was provision for varying the 2θ error window and the number of strongest lines required for a match could be set. Another important feature was a facility for displaying ds and Is from the database, along with the experimental pattern, for visual verification of a match. Toby, Harlow and Holomany (1990) later produced a suite of programs based on that of Goehner and Garbauskas. The main improvement was in accessing and searching the database and entries can be selected by means of chemical information, peak positions and name. Two modes of operation are available, 'novice friendly' with simple menus and a more advanced, and versatile, mode for the experienced user. Also, The Powder Suite was designed to be expandable by adding additional programs or subroutines to suit particular applications.

All the programs considered so far were developed for mainframe machines or mini-computers, mostly VAX/VMS, though a PC version of SEARCH is now available, and are public-domain software. Version 20 of the Johnson–Vand program (PDIDENT) and The Powder Suite are supplied by the ICDD free of charge to purchasers of the VAX/VMS version of PDF-2.

Perhaps the most important innovation in search/match procedures in recent years is the use of complete digitized diffraction patterns, after removal of the background, rather than simply a list of ds and Is (Caussin, Nusinovici and Beard 1988, 1989). This procedure is less dependent on the quality of data than is the use of peak location programs and it is particularly effective for patterns containing a large number of unresolved lines, as frequently occurs with complex multiphase samples. The program which incorporates these features, developed by Socabim as part of the Siemens DIFFRAC-AT package, was also the first to incorporate a search of a PC version of the complete PDF, which is currently achieved in less than 8 s with an Intel 486/66-based PC (Nusinovici and Winter 1994). The most reliable method for deciding whether or not the sample contains a particular PDF entry is to compare data for the latter with regions of zero intensity in the pattern for the unknown. Subtraction of the background, including any amorphous contribution, is thus an essential step and this is achieved interactively, by fitting a parabolic function tangentially to appropriate points in the pattern. No other treatment of the raw data is carried out; smoothing

of the data to reduce 'noise' is neither necessary nor desirable. The program employs the Johnson–Vand strategy and lists possible matches in order of increasing FoM, a low value being indicative of a likely solution. (This is in contrast to some other figures of merit, where a high value is used, but unambiguous interpretation is then less straightforward.) The FoM in the Socabim program is in fact based on that used in standard pattern-recognition methods. The criteria for ascribing 'bonus' or 'penalty' factors can be controlled by the user, depending on whether the pattern for the unknown is regarded as simple, average or complex. As with earlier programs, possible matches are displayed as 'stick diagrams' (ds and Is) superimposed on the experimental pattern, for visual selection of the correct solution. These can be derived from the PDF, or can be generated by the user, a valuable facility when dealing with solid solutions. As each phase is identified, its diffraction lines can be removed and the procedure repeated by using the remaining lines until all have been identified.

The error window associated with search/match based only on ds and Is is normally $\sim \pm 0.02^\circ$ (2θ) (Jenkins and Schreiner 1986), but Nusinovici and Bertelmann (1993) demonstrated that, by using the full-pattern approach of DIFFRAC-AT search/match, unambiguous identification of pure phases is still possible if the window width is increased by an order of magnitude. In fact, the width of a diffraction line profile provides a convenient and logical error window in this approach. Another feature of using the complete pattern is the ability to detect impurities at a much lower level than previously an intensity as low as 0.1% of that of the strongest line can be detected if the data are of sufficiently high quality (Nusinovici and Winter 1994). To date, no search/match program has proved to be completely satisfactory in all cases, but the interactive and versatile Socabim program appears to emulate the technique of a skilled analyst undertaking manual search/match, but in a fraction of the time.

Before powder-diffraction laboratories were equipped with APDs, a common form of search/match, in cases where a limited range of materials was of interest, was based on a visual comparison of the unknown data with chart recordings for selected standard patterns. These were obtained by the analyst, by using identical experimental conditions throughout, and they provided a convenient and rapid means of identifying certain classes of material, such as clay minerals, cements, catalysts, etc. This approach has been revived recently by applying it to complete experimental patterns in conjunction with the digitized-pattern database PDF-3 (Smith, Johnson and Hoyle 1991; Smith, Hoyle and Johnson 1993). The program MATCHDB is used for this purpose and, although PDF-3 so far only contains about 500 phases, initial results are promising. A limitation is that the instrumental contributions to the unknown pattern and the standard data will usually differ. Ideally, instrumental effects should be eliminated from both datasets by the deconvolution of data obtained from an instrument standard, such as LaB_6 (section 4.6.3), but this is not practicable at the present time. Additionally, there may well be differences due to sample imperfections or to a variation in chemical composition, such as occurs with solid solutions. These limitations are considered further by Smith, Hoyle and Johnson (1994). Nevertheless, the use of PDF-3 for the identification of unknown samples may well become a standard technique at some time in the future.

6. Crystal structure refinement from powder data

6.1. Factors affecting precision and accuracy

6.1.1. Experimental considerations. Factors governing the choice of experimental conditions for structure refinement have been considered in detail by Hill and Madsen (1987), as part of a general discussion of accuracy and precision in the Rietveld method. A basic requirement in angle-dispersive experiments is the choice of a suitable wavelength. Complex structures with a large number of structural parameters require a considerable number of resolvable peaks, but the use of a short wavelength to achieve this impairs the peak separation. The optimum wavelength will thus be a compromise between resolution, which may be dominated by sample-induced broadening, and maintaining a reasonable observations-to-parameters ratio. The latter will depend on various factors, but a value in the region of 10 is probably adequate for most purposes. (See section 2.1 for the approximate number of reflections in a powder pattern up to a given value of d.)

Hill and Madsen noted that, for published Rietveld analyses at fixed wavelengths, step lengths ranged over two orders of magnitude and maximum intensities over almost three and there is clearly a need to optimize these parameters. Although it is desirable to have a small step and good counting statistics for the successful application of pattern decomposition (section 3.3.1), this is not necessarily the case for the Rietveld method. Hill and Madsen (1987) determined the optimum values of step length and counting time per step beyond which no additional structural information is obtained by further increasing the number of observed discrete intensities $y_{\mathrm{obs}}(x_i)$ or by improved counting statistics. Their systematic study of diffraction data from materials with orthorhombic or higher symmetry indicated that the optimum value of the maximum intensity at each step is only a few thousand counts and that the optimum step length is between one-fifth and one-half the minimum *FWHM* of well resolved diffraction lines. Poor counting statistics is usually observed at high angles for X-ray powder diffraction data, as a consequence of the combined effects of the fall-off in scattering factor with increasing $\sin\theta/\lambda$, the Lorentz-polarization factor and thermal vibrations. These contribute to a ‘scrambling’ of the pattern and are a significant source of imprecision in Rietveld refinement. The quality of the data is improved by using a longer counting time per step for the high angle region. A procedure has been described which uses a systematic variable-counting-time strategy (Madsen and Hill 1992, 1994); the counting time at each step is increased in a manner that is inversely proportional to the decrease in line profile intensity.

6.1.2. Background and truncation. During the decade or so following its introduction, the Rietveld method was mainly applied to relatively low-resolution neutron data, obtained at a fixed wavelength. In these experiments the line profiles were usually dominated by instrumental effects and were closely Gaussian in form. As instrument resolution improved, the reporting of erroneous thermal parameters became common place and even negative values were given in some cases. Also, when X-ray data came to be used, it was soon evident that instrumental line profiles are not even approximately Gaussian. Ahtee *et al* (1984) compared structure refinements from observed and simulated data for $NaTaO_3$ and Ni. They used Gaussian and Voigtian profile functions truncated at different ranges, in order to ascertain the influence of the function used, and its range, on the estimated thermal parameters and background. They found that the intensity ‘lost’ to the background in the Gaussian case, truncated at the customary range of $\pm 3FWHM$, had the effect of increasing the values of the thermal parameter substantially. For simulated data, modelled with a Voigt

function, the correct thermal parameter for Ni was obtained for a range of $\pm 40 FWHM$, though the structural parameters were barely affected by this increase in truncation range. Also, by modelling the profile tails correctly, the background was constrained to a level which was close to the true value. Thus, if meaningful thermal parameters are required in a particular application, an accurate representation of the diffraction line profiles is essential and the function must be fitted over an adequate range. Smrcok (1989) used the theory of error propagation to compare structure refinements of Y_2O_3, by using the rigid modified Lorentzian and the more flexible Pearson VII functions (see appendix).

6.1.3. Preferred orientation. The grains or crystallites in many powder samples tend to have a shape which does not approximate to a sphere, due to cleavage or growth mechanisms. When compacted into a sample holder or deposited on a flat surface, such crystallites tend to orient preferentially in a particular crystallographic direction. The same can be true of capillary samples, though the effect is usually less severe. In general two habits can occur; crystallites can approximate to platelets, having one shorter dimension, or they can have an acicular habit, with one longer dimension. Ideally, the Rietveld method, and indeed most other applications of powder diffraction, require data from a random sample, since preferred orientation clearly has a marked influence on the relative intensities of Bragg reflections. An extreme case is the mica group of minerals, where all reflections other than $00l$ have zero intensity unless steps are taken to randomize the sample. Simple sample preparation techniques can be used for reducing preferred orientation (section 4.5.1).

The present treatment of preferred orientation in the Rietveld method is less rigorous than other corrections for extraneous factors and it is highly desirable to minimize its effect by careful sample preparation. However, it should be noted that the problem is usually less severe in the neutron case than with X-rays; larger sample volumes are used and the tendency for crystallites to align preferentially is less. The effect can be reduced in the X-ray case if a capillary sample is used and is rotated about its axis. At the outset, Rietveld (1969) introduced a 'preferred orientation function', G_j in equation 3.5, of the form

$$G_j = D_2 + (1 - D_2)\exp(-D_1\alpha_j^2) \tag{6.1}$$

where D_1 and D_2 are refinable parameters and α_j is the angle between $\boldsymbol{d}_j^*$ and the preferred-orientation direction. This approach has since been implemented in most Rietveld programs. For asymmetric diffraction, as in the Seeman–Bohlin geometry, for example, and cases of inclined texture, additional empirical corrections have been proposed (Cerny, Valvoda and Chladek 1995). Dollase (1986) introduced an improved treatment based on the March function (March 1932):

$$G_j = (D_1^2\cos^2\alpha_j + D_1^{-1}\sin^2\alpha_j)^{-3/2}. \tag{6.2}$$

This correction, known as the March–Dollase function, is now incorporated in several Rietveld programs.

Another approach to correcting for preferred orientation, based on a harmonic expansion, is that of Ahtee *et al* (1989), for which an improved model has been described by Järvinen (1993). These authors modelled the effects of an orientation distribution by means of spherical harmonics. It was found that quite large corrections could be applied successfully, but this potentially important approach is less straightforward and so far has not been widely

implemented. Another approach for obtaining information about the presence of preferred orientation effects, based on a statistical analysis of normalized structure-factor moduli, has been described by Altomare *et al* (1994). The method was found to be useful and efficient when applying direct methods to determining the structural model (section 7.4). The influence of preferred orientation on the statistical precision of normalized structure factors, for the case of disc-shaped crystallites and a spinning sample, has been considered by Peschard, Schenk and Capkova (1995). A technique based on an exponential preferred-orientation model $\exp(-D_1 \sin^2 \alpha_j)$ was derived to correct integrated intensities before structure determination.

6.1.4. Extinction. An important component of the model used in the Rietveld method is provision for extinction. In the context of a polycrystalline material, this is a reduction in the intensity of a Bragg-reflected beam by re-scattering in the direction of the incident beam as it passes through successive planes in a crystallite. Extinction is thus dependent on the size of coherently-diffracting domains. Sabine (1985) made a systematic study of extinction effects in structure refinement. By using fixed wavelength neutrons, he obtained data for samples of MgO with mean grain sizes in the range 0.7 μm to 20 μm and found that the reduction in intensity due to extinction was about 40% for the 20 μm grains, but was negligible for sizes of 1–2 μm. Over this range the estimated thermal parameters increased by a factor of two. Sabine also devised a correction for extinction based on spherical grains of diameter D, whereby each ordinate of a Bragg peak is multiplied by a factor $(1+x)^{-1/2}$, where

$$x = (3/4)^2 (NF\lambda D)^2 \tag{6.3}$$

N being the number of unit cells in the crystal and F the structure factor per unit cell. He obtained good agreement between theory and experiment to a level at which extinction reduces the intensity by a factor of two. However, it is better to minimize the effect whenever practicable by using a sample containing small grains (section 4.5.1); clearly the optimum size depends on the nature of the material, but a diameter of about 5–10 μm is probably suitable in most cases. Although each grain is likely to be a single crystal for brittle materials, it should be noted that in many instances the domain size may well be less than that of the grains. However, Cline and Snyder (1987) showed that, in the X-ray case, the effects of extinction are detectable for crystallites as small as 1 μm.

6.1.5. Line breadth and shape. Both the shape and breadth of line profiles vary with d^* and for most materials there is likely to be an additional lattice-direction dependence due to sample imperfections (section 2.4.2). In some cases it may be possible to minimize the latter by annealing the sample, but otherwise both effects should be modelled in the Rietveld method. An essential preliminary stage is to examine the variation of the *FWHM* (or integral breadth) with 2θ or d^* and to compare this with the resolution curve for the instrument used. If the two curves are identical, indicating that sample effects are negligible, then some polynomial describing the instrumental resolution function (IRF) can be used to model the breadth variation. The nature of this is unimportant and the function normally used in Rietveld programs is a quadratic in $\tan\theta$ (equation 3.8; see also equation 4.3). If the curves differ, but the scatter for the sample curve is no greater than would be expected from counting statistics or there is no marked 'anisotropy', on average, then (3.8) can again be used, but with U, V and W as refinable parameters. However, the sample curve

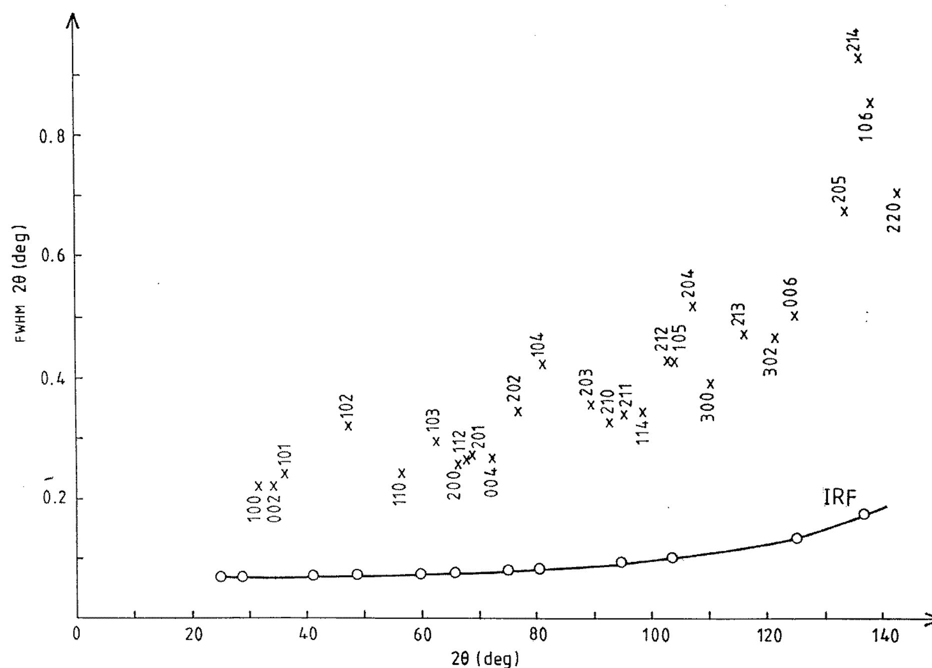

Figure 8. Variation of *FWHM* with scattering angle 2θ for ex-oxalate ZnO, Cu $K\alpha_1$ radiation, showing marked 'anisotropy' of breadth due to the presence of stacking faults. Also included is the IRF, obtained with a BaF_2 standard (Langford *et al* 1993).

frequently exhibits a scatter which is d^*-dependent and may be large (e.g. figure 8). The nature of this 'anisotropic' breadth variation must then be ascertained and the dependence of breadth on *hkl* modelled (see below). A similar approach is adopted for the variaion of line-profile shape. In many cases the shape factor appropriate to the fitted profile function varies smoothly, and sometimes linearly, with 2θ or d^* and a suitable polynomial is then used to model the variation. Otherwise, the *hkl* dependence should be ascertained and modelled.

As noted in section 2.4, a variety of microstructural phenomena can exist in a powder or polycrystalline sample, giving rise to complex diffraction effects, and these are considered further in section 10. In general, sample-induced line broadening includes contributions which are independent of d^*, known as 'size effects', and which depend on d^* ('strain effects'). There have been various attempts to make allowance for smoothly varying ('isotropic') microstructural effects in Rietveld programs. David and Matthewman (1985) modelled experimental line profiles by means of a Voigt function and assigned the Lorentzian and Gaussian components to 'size' effects and the instrumental broadening respectively. A different approach was introduced by Howard and Snyder (1989) in the program SHADOW, who convoluted Lorentzian sample line profiles, assumed to be due to crystallite size and/or microstrains, with experimentally-determined instrumental profiles, to match the observed data. The simultaneous presence of isotropic 'size' and 'strain' effects has also been considered by Thompson, Cox and Hastings (1987). These authors used a pseudo-Voigt function to model the overall line broadening and assigned the Lorentzian component of the equivalent Voigt function to 'size' effects and the Gaussian component to the combined

'strain' and instrumental contributions. Such procedures are unlikely to yield accurate estimates of microstructural parameters, but are probably adequate for the purpose of structure refinement, provided that there is a reasonably smooth variation of the breadth and shape of line profiles with d^*.

An early attempt to model anisotropic line broadening in the Rietveld method was made by Greaves (1985), who assumed that crystallites had the form of platelets with thickness H and infinitely large lateral dimensions. In this case the contribution to the integral breadth of reflections from planes parallel to the surface, in reciprocal units, is simply $1/H$. In order to allow for the direction dependence of microstrain, some assumption must be made regarding the stress distribution. If this is assumed to be statistically isotropic, then the anisotropy of elastic constants leads to an *hkl* dependence of strain. Thompson, Reilly and Hastings (1987) expressed microstrain as a function of *hkl* and refined appropriate strain parameters based on elastic compliances. Simultaneous anisotropic 'size' and 'strain' broadening was incorporated in the Rietveld method by Le Bail (1985) and Lartigue, Le Bail and Percheron-Guégan (1987). The *hkl*-dependent nature of these quantities was modelled by means of ellipsoids and Fourier series were employed to represent line profiles. The number of microstructural parameters to be refined was restricted by adopting a Lorentzian function for 'size' contributions and an intermediate Lorentz–Gauss function for 'strain' broadening. In a similar approach, Lutterotti and Scardi (1990) included crystallite size and microstrain as refinable parameters, in the place of the usual angular variation of line-profile width (equation 3.8). Microstructural analysis was then based on the approximate single-line Fourier method introduced by Nandi *et al* (1984). (See section 10.2.2.) The program LS1 based on this approach (Lutterotti, Scardi and Maistrelli 1992) was applied to data from $Ni(OH)_2$ and CeO_2-stabilized zirconia, which both exhibited anisotropic line broadening. In addition to obtaining microstructural data for these samples, modelling of direction-dependent broadening improved the agreement between the observed and calculated patterns and yielded positive temperature factors for light atoms, which would otherwise have had spurious negative values.

At present no Rietveld program makes allowance for all possible cases of sample-induced modifications to the g profiles and it would be difficult to make such a provision. If plots of breadth and shape parameters versus 2θ or d^* exhibit significant 'anisotropy', then it is better to adopt a two-stage approach (Delhez *et al* 1995). In the first stage the position, intensity, breadth and some shape parameter (e.g. Lorentzian/Gaussian fraction, Pearson VII index or Voigt parameter; see appendix) of individual lines are obtained by pattern decomposition (section 3.3.1), for which no structural information is required. From these parameters the dependence of breadth and shape on radial distance and direction in reciprocal space (i.e. d^* and *hkl* dependence) can be determined for all peaks. The corresponding quantities can then be predicted for reflections not found during pattern decomposition, owing to extreme overlap or too low intensity. If desired, the results of pattern decomposition can be interpreted in terms of microstructural properties. Also, the pattern can be indexed, if the unit cell is not already known, and precise cell dimensions can be obtained from selected reflections, after line positions have been corrected for systematic errors. These are likely to be more accurate than are obtained from Rietveld programs, since refinement of cell dimensions along with other parameters merely absorbs peak displacements due to any instrumental aberrations for which no allowance has been made and also to shifts due to lattice imperfections. If the cell parameters are known, a constrained pattern-decomposition method can be applied. Another advantage of using pattern decomposition is that intensities of indexed Bragg reflections can be used in *ab initio* structure determination (section 7.3) or for structure refinement by the conventional least-

squares approach based on separate Bragg intensities (section 6.4). In the second stage, (semi-) empirical relationships describing the behaviour of breadths, shapes and perhaps position of lines as functions of d^* and hkl, obtained from stage 1, are used in the Rietveld refinement.

6.2. Current practices with the Rietveld method

In order to evaluate errors related to the practical application of the Rietveld method, the Commission on Powder Diffraction of the IUCr undertook a comparison of the use of the method in various laboratories by means of a round robin. The aims of the project were: (i) to evaluate a cross section of currently used Rietveld refinement software; (ii) to examine the range and effect of various refinement strategies; (iii) to assess the precision and accuracy (spread) of the parameters derived by a Rietveld analysis; (iv) to compare and contrast various instruments and methods of data collection. Results concerning the refinements from two constant-wavelength X-ray and neutron powder diffraction patterns for $PbSO_4$, which had been distributed to participants, were reported by Hill (1992). In a second report (Hill and Cranswick 1994), results from data collected by the participants on a sample of monoclinic ZrO_2, using their in-house instruments, were reported. The major factors limiting the accuracy of the derived $PbSO_4$ crystal structure were carefully analysed. Rietveld analysis of the $PbSO_4$ X-ray powder diffraction data provided atomic coordinates and isotropic thermal parameters for the Pb and S atoms which were in reasonable agreement with the values derived from a single-crystal study, but the 'light' O atomic parameters had a wide spread of coordinates about the weighted mean. For the neutron diffraction data, crystallographic parameters for Pb and O atoms were precise, with a narrow distribution relative to the single-crystal results. This is in agreement with a previous comparison between powder neutron diffraction and single-crystal investigations of fosterite Mg_2SiO_4, in which comparable uncertainties in positional parameters were found (Lager *et al* 1981). In the second part of the round robin, in which participants collected their own data for a sample of monoclinic zirconia, the results revealed worker-to-worker disparities which were greater than anticipated. In addition to the difference in refinement strategies, the discrepancies were largely related to the quality of data collected by the participants. This is illustrated in figure 9, where a complex section of the diffraction patterns provided by the participants is shown. Figures 9(a), 9(b) and 9(c) are data collected with conventional sources (Cu$K\alpha$ radiation), with markedly different counting statistics, corresponding to a maximum count of 29, 420 and 4000 respectively. The poor quality of the data in figure 9(a) means that it is difficult to distinguish between the individual reflections and to determine the background level. A comparison between figures 9(b) and 9(c) indicates the substantial improvement in resolution for the former, for which the data were obtained by using an incident-beam focusing monochromator to remove the $K\alpha_2$ component (section 4.1.1). An immediate consequence is a better stabilization of the refinement procedure and an improvement in background determination. Figures 9(d), 9(e) and 9(f) show analogous angular ranges for neutron data. The intensities and angular resolution again differ significantly.

6.3. Some applications of the Rietveld method

The Rietveld method has been used for structural investigations of polycrystalline materials having a variety of properties, e.g. solid electrolytes, intercalates, zeolites, superconductors, hydrides, non-stoichiometric phases etc. (For a review of early applications, see Hewat

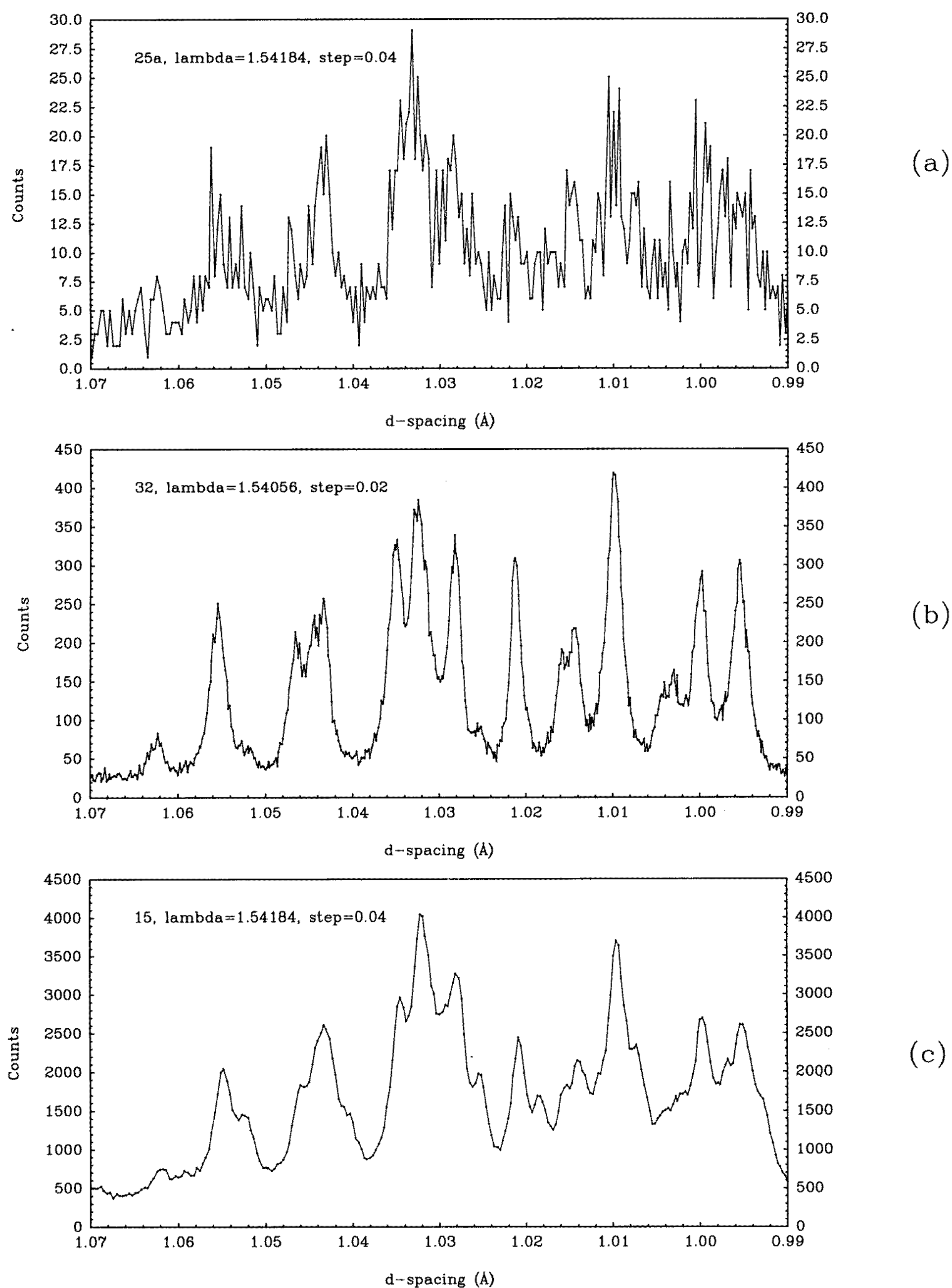

Figure 9. Parts of powder diffraction patterns for ZrO_2 provided by six participants in the Rietveld method 'round robin'. (*a*) and (*c*) Cu$K\alpha_{1,2}$ radiation; (*b*) monochromatic Cu$K\alpha_1$ radiation; (*d*), (*e*) and (*f*) neutron data with wavelengths of 1.0505 Å, 1.1126 Å and 1.0907 Å respectively. (Hill and Cranswick 1994).

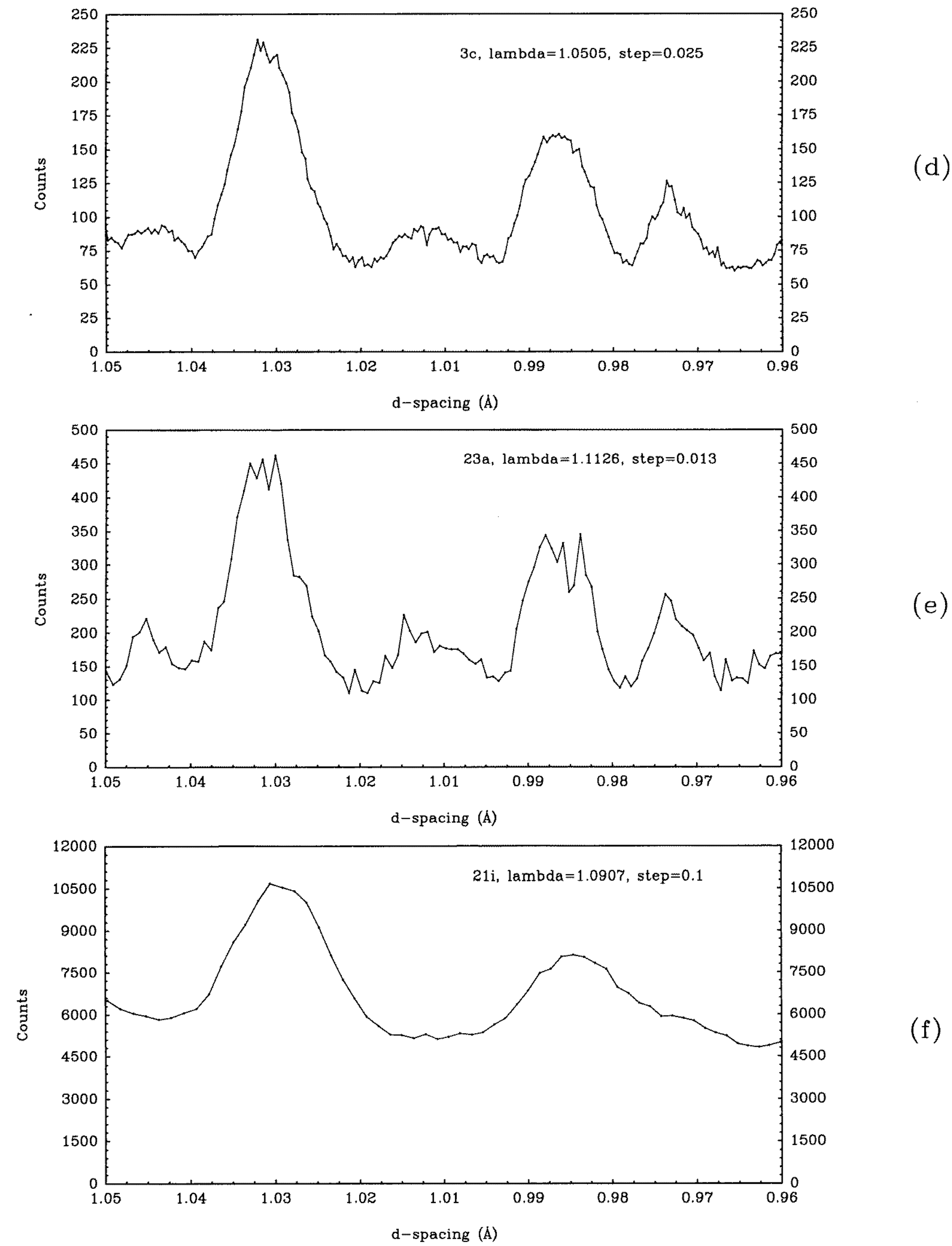

Figure 9. Continued.

1986.) Among the more complex structures reported is the simultaneous refinement of 161 parameters for the triclinic structure of $UO_2DAsO_4.4D_2O$ at 4 K from powder diffraction data (Fitch, Wright and Fender 1982). In this study, the sample investigated was contaminated by ice and its structure was refined simultaneously. An important application of the Rietveld method is the study of materials which undergo phase transitions and which often disintegrate when subjected to thermal treatment or produce multi-domain crystals not suitable for single-crystal studies. The method is also a powerful tool for investigating phase transformations in solids as a function of temperature. The detailed structure of deuterated Cu(II) Tutton's salt has been determined at low temperatures, from 5 to 295 K, by neutron powder diffraction (Hathaway and Hewat 1984) and it was possible to determine the structure and bond lengths at many more temperature values than is customary with single-crystal methods. From an accurate study of the bond lengths in CuO_6 polyhedra, the results were interpreted as order-disorder transitions of Jahn–Teller type, with an elongated Cu–O axis. Additionally, the strong libration of the $(ND_4)^+$ ion was observed from neutron diffraction data. X-ray powder diffraction has also been used for studying the structures of fast ionic conductors as a function of temperature. At elevated temperatures, Bragg reflections are superimposed on a background arising from ion disorder. The study of the three polymorphs of Ag_2Te between ambient temperature and its melting point at 1233 K has recently been reported (Schneider and Schulz 1993). β-Ag_2Te crystallizes with the space group $P2_1/c$, whereas the α modification has the space group $Fm\bar{3}m$ with a statistical distribution of Ag ions. The structure of γ-Ag_2Te was also refined with space group $Im\bar{3}m$ and it is isostructural with α-AgI.

Perhaps the most noteworthy recent success of the Rietveld method has been its contribution to an understanding of the structures of the high-temperature oxide superconductors, due to the lack of suitable single crystals and the need to locate oxygen atoms, and their occupancy, in the presence of heavy metal atoms such as Ba, Tl and Bi. In the case of $YBa_2Cu_3O_{7-x}$, X-ray single-crystal diffraction had already located the heavy atoms, but the work was inconclusive concerning oxygen, because crystals were microscopically twinned. Neutron powder diffraction experiments were carried out in atmospheres with controlled oxygen partial pressures (Jorgensen *et al* 1987). From the data, the occupancies of particular oxygen sites were obtained by Rietveld method and it was shown that there is a structural transition at high temperature to a tetragonal non-superconducting phase as oxygen is removed from the CuO-chains. A number of studies of metal ordering and oxygen non-stoichiometry has been reported for this class of materials, e.g. in $(Nd, Sr, Ce)_2CuO_{4-y}$ (Izumi *et al* 1989). One of the first uses of combined X-ray and neutron diffraction data in Rietveld refinement was the study of cation disorder in this high T_c superconductor (Williams *et al* 1988). The crystal structure of a number of copper oxide superconducting phases has been investigated from powder neutron diffraction data and the earlier applications have again been reviewed by Hewat (1990). Also, considerable effort has been devoted to solving the crystal structure of $BaBiO_3$, since superconducting phases occur in the $BaPb_{1-x}Bi_xO_3$ system. High-temperature crystal structures of $BaBiO_{3-x}$ were studied *in situ* by neutron and X-ray powder diffraction by using controlled oxygen pressures (Kusuhara *et al* 1989). Rietveld refinement of the neutron data for $BaBiO_3$ at 900K revealed that the structure is cubic, with large anisotropic thermal vibration amplitudes of the O atoms in the direction perpendicular to the Bi–O bonds. For oxygen-deficient $BaBiO_{3-x}$, it was shown that the system is not a single phase. The Rietveld method has also been used for the refinement of incommensurate structures (Elsenhans 1990; Matheis and Snyder 1994). The calculation of peak positions and structure factors for 1-dimensional incommensurate structures is based on four integers, *hklm*. The incommensurate structure

of the superconductor $Bi_2(Sr_{1-x}Ca_x)_3Cu_2O_{8+z}$ was refined by combining X-ray and TOF neutron powder diffraction data (Yamamoto *et al* 1990).

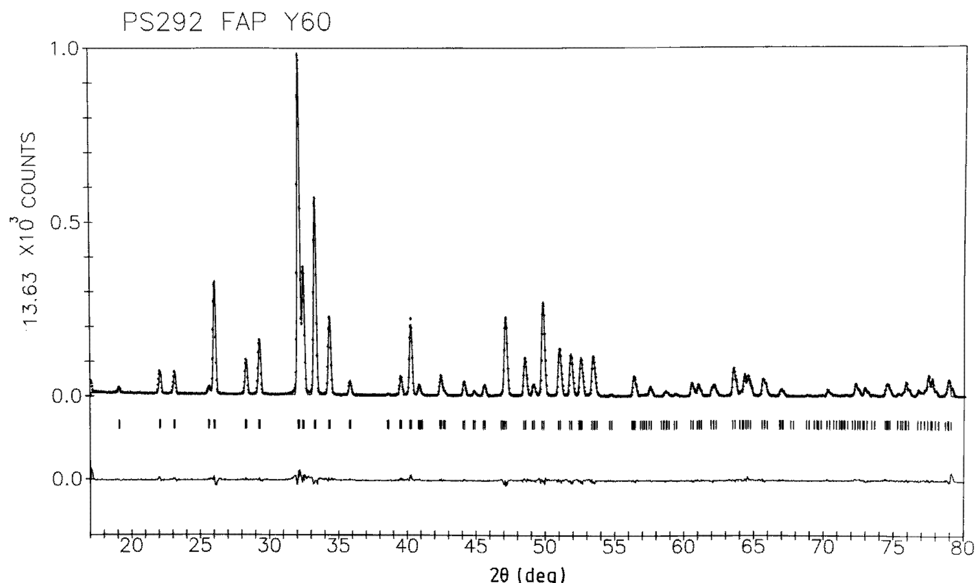

Figure 10. Example of a typical Rietveld plot. The observed intensity data for fluorapatite are plotted as points and the calculated pattern is shown as a continuous line. The short vertical bars indicate the positions of possible Bragg reflections and below these is the difference plot, observed minus calculated data (Young 1995; by permission of Oxford University Press).

The Rietveld method has been applied, by using neutron diffraction data, to structural studies of the recently discovered class of carbon-cage molecular compounds known as fullerenes. At room temperature the C_{60} molecules are orientationally disordered and their centres are located on a face-centred cubic lattice. Below 249 K, powder diffraction has revealed that the molecules become orientationally ordered (David *et al* 1991). Recent results for the structure and dynamics of 'buckyball' C_{60} molecules have been reviewed by Copley, David and Neuman (1993). The structures of RbC_{60} and KC_{60} have also been analysed through Rietveld refinement from X-ray synchrotron powder diffraction data. A covalent bonding between neighbouring C_{60} molecules has been confirmed, demonstrating the existence of polymeric chains in these compounds (Stephens *et al* 1994). New phases of C_{60} have also been synthesized at high pressure (Iwasa *et al* 1994). However, experimental diffraction patterns exhibited significant line broadening and only patterns calculated from structural models by using the computer program LAZY-PULVERIX (Yvon, Jeitschko and Parthe 1977) were reported.

The studies of magnetic structures is a typical application of neutron diffraction, since, unlike X-rays, neutrons interact with the magnetic moments of atoms. The powder method is a primary and simple tool for obtaining information on the arrangement of magnetic moments in crystals. Advances in magnetic structure determination by means of neutron powder diffraction were reviewed recently by Rodriguez-Carvajal (1993).

The determination of site occupancy in minerals, and in inorganic materials generally, has been carried out by the Rietveld method for compounds with simple structures, such as that of farringtonite and graphtonite, in which cations are found in five- and six-

coordinated sites (Nord 1986). Compared with spectroscopic methods, the diffraction technique gives information on inter-atomic distances and angles. Also, the site-occupancy factors can be refined, if the cations scatter with sufficient contrast. Cation distributions in $(Fe_{1-x}Mn_x)_3(PO_4)_2$ solid solutions were determined by combining neutron diffraction and Mössbauer spectroscopy (Nord and Ericsson 1982). The study of four $(Zn, Mg)_3(PO_4)_2$ solid solutions from X-ray powder diffractometer data demonstrated that the Zn/Mg cation distribution is ordered, with zinc preferring the five-coordinated sites and magnesium the six-coordinated metal sites (Bénard *et al* 1992). Similar results of almost constant cation distribution factors, irrespective of composition, were found in isostructural series of Fe-containing materials from Mössbauer spectroscopy.

The sensitivity of the Rietveld method to structural detail has been revealed in a number of studies, but attention must be paid to the possibility of false minima during the refinement. For example, the orientation of the two inner hydroxyl ions in kaolinite was uncertain from X-ray data (Suitch and Young 1983) and neutron data suggested that the H atoms of these ions were positioned differently. Consequently, the space group $P1$ was proposed (Young and Hewat 1988). However, a Rietveld refinement of non-hydrogen atomic positions in kaolinite by Bish and Von Dreele (1989) favoured of the presence of C-centring and previous results were explained by false minima due to a poor modelling of preferred orientation and to the presence of dickite as a second phase. The sensitivity of the Rietveld method was also demonstrated by a comparison of X-ray powder diffraction data from a 2.2 wt% antimony-substituted calcium fluorapatite (0.185 Sb atoms per unit cell) with those from an undoped sample. This indicated a substitution of one of the Ca atoms by Sb (Deboer *et al* 1991).

Structure refinement from powder diffraction data is widely used in the study of zeolites. Once a reasonable model has been generated (see section 7.4.3.2), a comparison between the calculated and observed patterns will indicate whether or not the model is likely to be correct. Rietveld refinement of the zeolite ZSM-12 structure from synchrotron data revealed the true symmetry ($C2/c$) although the topological symmetry was $C2/m$ (Fyfe *et al* 1990). The structure of VPI-5, an aluminophosphate, was found to have a low symmetry; in a structure refinement from synchrotron data the correct space group $P6_3$ was proved, the suggested framework was confirmed and interesting structural features were revealed (McCusker *et al* 1991). In order to stabilize the early stages of refinement and to facilitate refinement of complex zeolite structures, geometric constraints can be included as additional information. McCusker, Baerlocher and Nawaz (1985) determined the structure of the zeolite mineral gobbinsite from X-ray data, refining 64 structural parameters and using 50 soft constraints on bond distances and angles. For further information the reader is referred to a review by McCusker (1991). In the complex structure of ZSM-5, details of the arrangement of the organic cation tetrapropyl-ammonium were revealed by including restraints (distances and angles) in the refinement data from a conventional Cu$K\alpha_1$ source (Baerlocher 1984). Neutron diffraction is also used for locating light atoms in zeolites, e.g. Li^+ cations in Li–X and Li–Y zeolites (Forano *et al* 1989).

Least-squares Rietveld refinement has been used for the study of intercalation or insertion phenomena in layered materials. Neutron diffraction with samples of FeOCl and $FeOCl(TTF)_{1/8.5}$ established that tetrathiofulvalene (TTF) molecules intercalated between FeOCl layers contribute to the diffraction pattern and exhibit a long-range order (Kauzlarich *et al* 1986). The electrochemical insertion of lithium in potassium tungsten bronze was also investigated from neutron diffraction data, to localize Li in the structure of $Li_xK_yWO_3$ (Slade *et al* 1989).

6.4. Pattern decomposition and structure refinement

An alternative approach to the Rietveld method, based on a two-stage procedure, has also been used for structure refinement. In the first step, estimates of the Bragg intensities are extracted from the diffraction pattern by means of a pattern-decomposition method in which the peak positions of individual reflections are constrained by the unit-cell parameters. Programs have been adapted for producing integrated intensities and their standard deviations, as for a single crystal data set (Pawley 1981; Jansen, Schäfer and Will 1988). In the second step, the indexed Bragg intensities thus derived are used as input data for a subsequent structure refinement. W. Hamilton wrote the first least-squares program for two-stage structure refinement from powder diffraction data in the early 1960s. This program, known as POWLS, was not published (see Will 1989), but it was subsequently updated by Will (1979). The procedure has been used for the refinement of simple structures, such as silicon, quartz and corundum, after correcting for preferred orientation and collecting data from suitably prepared specimens (Will, Parrish and Huang 1983). A direct comparison of the atomic parameters of monoclinic $Na_2Al_2Ti_6O_{16}$ refined under the same conditions with both a two-stage analysis and the Rietveld technique has shown that the results agree within the estimated standard deviations (Toraya 1995). Additional comments on integrated-intensity methods and the Rietveld method, and estimates of parameters and their standard deviations, have been reported by Cooper, Rouse and Sakata (1981), Prince (1981), Taylor, Miller and Bibby (1986) and Will *et al* (1990). The pattern-decomposition method was also used to calculate electron-density maps directly from the observed diffraction data for orthorhombic Mg_2GeO_4 (Will *et al* 1988) and CeO_2 (Sakata *et al* 1990; see section 7.4.3.1).

7. *Ab initio* structure determination

7.1. Historical overview

Single-crystal X-ray diffraction is the technique most frequently used for solving and refining crystal structures. A basic requirement of the technique is that data for individual reflections are uniquely indexed and intensities measured accurately. In experiments with a powder material, the 3-dimensional location of each reciprocal lattice point is lost by projection on to a single dimension, which results in a considerable loss of information. Consequently, observed diffraction lines are partially or totally superimposed. The situation is further aggravated by the number of lines, which increases as d^{*3} (see equation 2.2) and by the intrinsic line broadening arising from structural imperfections (section 2.4). The geometric reconstruction of the reciprocal lattice and the treatment of the overlap of diffraction lines are the central problem for structure determination from powder data. In the last two decades, the advent of powerful indexing methods and the Rietveld structure-refinement approach to overcome the line overlap problem, combined with the new generation of high-resolution powder diffractometers, have contributed to significant advances in *ab initio* structure determination from powder data. The pioneering efforts of Swedish workers (see Werner 1986), combining *ab initio* indexing, structure determination and Rietveld refinement for data collected by means of Guinier–Hägg cameras, were the basis for subsequent intense activity in this field. In 1977, Berg and Werner (1977) solved *ab initio* the crystal structure of monoclinic $(NH_4)_4[(MoO_2)_4O_3](C_4H_2O_5)_2 . H_2O$ from powder diffraction data. A 3-dimensional Patterson function was calculated from 120 integrated intensities, from which

were derived the Mo atomic positions, and the localization of light non-hydrogen atoms was revealed by a series of Fourier calculations. In 1980, the crystal structure of a new tricline modification of MnP_4 was solved by means of direct methods (Noläng and Tergenius 1980). After these early results, solutions of a variety of new structures have been reported for data collected with different instrumental configurations and sources of radiation, e.g. $ZrNaH(PO_4)$ with a conventional diffractometer and $CuK\alpha_{1,2}$ radiation (Rudolf and Clearfield 1985), $Nd(OH)_2NO_3.H_2O$ with a diffractometer using monochromatic $CuK\alpha_1$ radiation (Louër and Louër 1987), α-$CrPO_4$ with synchrotron X-rays (Attfield, Sleight and Cheetham 1986), $FeAsO_4$ from TOF neutron data (Cheetham *et al* 1986), $Al_2Y_4O_9$ and I_2O_4 from combined synchrotron X-ray and neutron diffraction data (Lehman *et al* 1987), $LiB_2O_3(OH).H_2O$ from data collected by means of a curved position sensitive detector, Debye–Scherrer geometry and $CuK\alpha_1$ radiation (Louër, Louër and Touboul 1992). A partial compilation of the earlier structures to be solved from first principles from powder data has been made by Cheetham (1995). Many examples have been reported for various classes of material, mainly inorganic, but also for a few organic structures (e.g. Cernik *et al* 1991) and molecular inorganic compounds (e.g. Lightfoot, Glidewell and Bruce 1992; Petit *et al* 1993).

Ab initio structure determination from powder diffraction data involves a series of discrete steps from the collection of raw data to the refinement stage: (i) a careful sample preparation is required to reduce preferred orientation of crystallites and data are collected by means of a high resolution instrument; (ii) the powder pattern is indexed, including the derivation of the space group from systematic absences; (iii) the integrated intensities, and hence structure factor amplitudes $|F_{hkl}|$, are extracted from indexed reflections; (iv) the structure solution is determined using direct, Patterson, Fourier or other methods; (v) the atomic coordinates of the crystal structure are refined by means of the Rietveld method.

Compared to single-crystal data, the phase problem poses further difficulties in the case of powder data, owing the the limited number of measured unambiguous Bragg intensities available. This is currently the subject of intensive study. Indeed, although a number of structure solutions of powder materials with low symmetry have been solved successfully by means of standard direct or Patterson methods, the problem of exact overlap (e.g. the 550, 710 and 543 reflections for cubic material) encountered in cases of high symmetry poses additional problems for which new algorithms have been developed. These are based on the maximum entropy technique and the Sayre squaring method, to evaluate the intensity of overlapping reflections (David 1987). There is currently considerable interest in the application of these principles to the phase problem (see sections 7.4.2 and 7.4.3.1).

7.2. Powder pattern indexing

The indexing of powder diffraction patterns, i.e. the determination of crystal symmetry, unit cell dimensions and hkl indices of each reflection, is an essential step in *ab initio* structure determination. Compared to single crystal data, where the problem can easily be solved from the 3-dimensional location of the nodes of the reciprocal lattice, the solution from powder data can only be found from the lengths of the diffraction vectors, since the angles between the vectors have been lost in the rotational projection of the reciprocal lattices. Efficient methods are now available for indexing a powder pattern, regardless of crystal symmetry; these are computer-based and their use requires that errors are minimized (see Shirley 1980 and Louër 1992). The rôle of data quality was clearly shown by de Wolff (1957), who noted that indexing should be quite an easy puzzle if errors of measurement did not exist. He also proposed a figure of merit for selecting the correct result from false

solutions (de Wolff 1968); this important contribution can be considered a milestone in the field of powder pattern indexing.

7.2.1. Basic principles and solution reliability. The underlying physical principle of indexing is the reconstruction of the 3-dimensional reciprocal lattice from the radial distribution of the lengths d^* of reciprocal-lattice vectors. The basic relation used for indexing a powder diffraction pattern is obtained by squaring the $\boldsymbol{d}^*$ vector (equation 1.2):

$$Q(hkl) = \boldsymbol{d}^{*2} = h^2A + k^2B + l^2C + 2klD + 2hlE + 2hkF \tag{7.1}$$

where $A = \boldsymbol{a}^* \cdot \boldsymbol{a}^*$, $B = \boldsymbol{b}^* \cdot \boldsymbol{b}^*$, $C = \boldsymbol{c}^* \cdot \boldsymbol{c}^*$, $D = \boldsymbol{b}^* \cdot \boldsymbol{c}^*$, $E = \boldsymbol{c}^* \cdot \boldsymbol{a}^*$ and $F = \boldsymbol{a}^* \cdot \boldsymbol{b}^*$. The solution to this equation is not unique and it was recognized that the indexing problem cannot be solved by ordinary algebra because, however many equations are taken, the number of unknown variables is always greater than those known (see Vand and Johnson 1968). Moreover, the solution strongly depends on the precision and completeness of data. It has been shown that the interdependence of these features and the reliability of a solution can be evaluated by a figure of merit which takes into account the average discrepancies between $Q_{\rm obs}$ and $Q_{\rm cal}$, $\langle \Delta Q \rangle$, or the average angular discrepancy, $\langle \Delta(2\theta) \rangle$, and the size of the unit cell, through the number of calculated lines $N_{\rm cal}$ up to the Nth observed line. This should not include lines disallowed by the space group, if the latter is known. Although the most widely used criterion for indexing is the de Wolff (1968) figure of merit:

$$M_N = Q_N / 2\langle \Delta Q \rangle \, N_{\rm cal} \tag{7.2}$$

another factor, the F_N index (Smith and Snyder 1979), is also used:

$$F_N = N / \langle \Delta(2\theta) \rangle \, N_{\rm cal}. \tag{7.3}$$

In addition to these figures of merit, a criterion based on the principles of information theory has been proposed by Taupin (1988). From a consideration of the respective merits of M_N and F_N (Shirley 1980; Werner 1980), it was considered that the index F_N is more appropriate for evaluating the quality of a powder diffraction dataset whereas M_N is preferable for indexing purposes. In general, both are reported with the indexing results. The figure of merit M_{20}, should not be lower than about 10 (de Wolff 1968) in order to accept a solution with confidence. Nevertheless, values greater than 20 give a higher probability of correctness of the solution. An interesting point concerning the F_N figure of merit is the form used for reporting results: $F_N = \text{value}(\langle \Delta(2\theta) \rangle, N_{\rm cal})$. Indeed, the average angular discrepancy, $\langle \Delta(2\theta) \rangle$, is another evaluation of the quality of the fit between observed and calculated 2θ values. Examples of the magnitude of figures of merit have been reported and discussed by Louër (1992) for various situations. For instance, the presence of a dominant zone, due to one cell edge being significantly shorter than other two, introduces a complementary degree of freedom. The pattern is then characterized by the presence of a common zero Miller index for all the first lines of the pattern and pseudo solutions with high figures of merit can be produced by a search strategy based on the first lines in the pattern. Geometrical ambiguities have been discussed by Mighell and Santoro (1975). These can occur if the lattice has high symmetry, e.g. the pattern of a solid with hexagonal

symmetry can be indexed by an orthorhombic unit cell with half the volume of the hexagonal cell. Additional information contained in a powder diffraction pattern, based on equation 2.2, is concerned with an estimate of the volume of a triclinic unit cell. Smith (1977) derived an empirical relation for the cell volume based on the d value of the 20th observed line ($V = 13.39\ d_{20}^3$). Attempts to generalize the estimated cell volume to higher crystal symmetries have been reported (Paszkowicz 1987).

7.2.2. Indexing methods and computer programs. Various computer programs have been introduced for indexing the powder diffraction patterns for materials with unknown crystal structures (table 7 in Smith and Gorter 1995). The main programs, and an evaluation of their success rates, were reviewed by Shirley (1978, 1980). Three principal procedures, regardless of the crystal symmetry, are used in these programs:

(i) The Runge–Ito–de Wolff method is based on specific relations in reciprocal space. For example from two $Q(0kl)$ and $Q(0\bar{k}l)$ values the inter-axial angle α^* is calculated and similar relations exist for other pairs. A program using these principles was written by Visser (1969) and it is particularly efficient for low symmetry cases.

(ii) The method based on a permutation of Miller indices for base lines, proposed by Werner (1964). This is a semi-exhaustive trial-and-error method, for which several computer programs have been written (Werner, Eriksson and Westdahl 1985; Taupin 1973b; Kohlbeck and Hörl 1976; Wu 1989).

(iii) The dichotomy method based on the variation, in direct space (except for triclinic symmetry, for which Q-space was found to be preferable), of the lengths of cell edges and inter-axial angles over finite ranges, followed by a progressive reduction of these intervals by means of a dichotomy procedure. This method was introduced by Louër and Louër (1972). The strategy is exhaustive, within input parameter limits. A recent optimized program, DICVOL91, is available (Boultif and Louër 1991). The strategy for indexing starts from the cubic end of the symmetry sequence and finishes with the triclinic case. This method is not strongly sensitive to the presence of a dominant zone (Louër 1992).

Precise and accurate data are required for all programs. The absolute error on the peak positions has to be lower, on average, than 0.03° (2θ). Such precision can be obtained by a good adjustment and calibration of the instrument (section 4.6; see also Louër 1992). A comparison between powder pattern indexing from data collected by means of a conventional powder diffractometer and a synchrotron source has recently been reported, demonstrating the high precision of data collected in the latter case (Cernik and Louër 1992).

For indexing purposes, only the first (generally 20) diffraction lines of the pattern are used. In order to derive possible space groups, all reliable lines available in the pattern must be used. Programs for reviewing complete powder diffraction datasets are useful for this analysis, e.g. NBS $*$ AIDS83 (Mighell, Hubbard and Stalick 1980). Some additional techniques which are sensitive to symmetry can also be used for space group determination, e.g. electron diffraction, NMR (see, for example, Bell *et al* 1994; Fyfe *et al* 1991). From an interpretation of intensities corresponding to superimposed reciprocal-lattice points, Ohmasa and Ohsumi (1995) have shown that Laue classes of polycrystalline materials with high symmetry can be identified from concentrations of vectors in vector space, i.e. from distributions of Patterson peaks. As a final resort, intuition taking into account the symmetry of Wyckoff sites according to the chemical formula of the compound can help space group determination.

7.3. Extraction of integrated intensities

The number of available unbiased integrated intensities is the major factor in circumventing the phase problem. This number can be increased experimentally by collecting data with the highest possible resolution. Pattern decomposition methods, based on fitting procedures (see section 3.3.1), are used for extracting the intensity of Bragg components. In reported *ab initio* structure determinations two strategies have been employed.

In the first results reported, Bragg intensities with unambiguously indexed reflections, including low intensity and non-observed lines, but allowed by space group, were used. The number of available data is limited and depends on the instrument used, the symmetry of the material and its microstructure. For instance, 120 integrated intensities (Guinier camera data, Cu$K\alpha_1$) were used for the calculation of a Patterson function in a study of $(NH_4)_4[(MoO_2)_4O_3](C_4H_3O_5)_2.H_2O$, from which the heavy-atom positions were obtained (Berg and Werner 1977); 40–50 data were used in the case of $Zr(HPO_4)_2.H_2O$ (diffractometer data, Cu$K\alpha_{1,2}$) (Rudolf and Clearfield 1985); 68 well-resolved peaks were used to generate a Patterson map which yielded two heavy-atom positions in the structure of α-$CrPO_4$ (synchrotron X-ray data) (Attfield, Sleight and Cheetham 1986); 92 intensities were employed in the case of $KCaPO_4.H_2O$ (Louër, Plévert and Louër 1988) and, from 136 integrated intensities, Zr atom positions were found in the structure of triclinic $Zr(OH)_2(NO_3)_2.4.7H_2O$ (Bénard, Louër and Louër 1991a). Cu$K\alpha_1$ diffractometer data were used for the last two examples.

A second approach for extracting Bragg intensities is the use of symmetry information and unit-cell dimensions to generate intensities for all possible reflections in the pattern (Pawley 1981). The problems of least-squares ill-conditioning due to substantial correlated overlapping reflections are overcome by additional slack constraints. The whole-pattern decomposition of symmetry-allowed reflections yields a list of reflections with their intensity and estimated standard deviations. Rather than using an empirical restraint algorithm, a Bayesian approach including the requirement of positive intensities has been proposed (Sivia and David 1994). The least-squares procedure with slack restraints has been used for extracting the structure-factor amplitudes in a number of ab initio structure determinations, e.g. Sigma-2 zeolite from synchrotron powder diffraction data (McCusker 1988) and cimetidine (Cernik *et al* 1991). A convenient improvement of this basic principle is the incorporation in Rietveld programs of an iterative fitting procedure without knowledge of a structure model (Le Bail, Duroy and Fourquet 1988; Le Bail 1992). This is a rapid and efficient approach to total pattern decomposition, by using space-group constraints on Bragg reflection positions. It is based on a simple modification to the approximate procedure used by Rietveld (1969) for the extraction of integrated intensities at the end of the structure refinement. An arbitrary set of structure factors is used as input and only the parameters of the non-structural model are refined. These values are then inserted as calculated values and the refinement is repeated until the best fit between observed and calculated patterns is achieved. The procedure generates a list of 'observed' intensities by using an equipartition of the overall intensity of overlapping reflections, easily used as input data with programs for direct and Patterson methods; see also Altomare *et al* 1995. The equipartition principle is acceptable if there are not too many overlapping reflections in the pattern. Otherwise, a more realistic partitioning of intensities is required and more recent alternative approaches are discussed in the following sections.

7.4. *Structure solution*

7.4.1. Traditional methods. Most of the *ab initio* structure determinations from powder data reported in recent years have been based on methods traditionally used for structural investigations from single-crystal data. Once integrated intensities have been extracted, the phase problem is analysed by Patterson and direct methods, combined with a Fourier analysis. Nevertheless, the overlapping of reflections, arising accidentally from the diffraction geometry or as a consequence of point-group symmetry, is a major obstacle in the determination of unknown crystal structures. With both 'noisy' and incomplete data, structure solution can be an ill-posed problem. The success of structure determination from conventional crystallographic techniques depends on the degree to which reflections overlap and the complexity of the structure. The integrated intensity datasets used for obtaining the phase can be divided into three categories: (i) the limited number of strictly unambiguous reflections, used in the earlier studies (ii) the 'complete' dataset of extracted intensities after equipartitioning the overall intensity for overlapping reflections and (iii) the complete dataset after evaluating the intensity of overlapping reflections through approaches based on probability.

The relative strength and robustness of the Patterson method in the case of small datasets has been demonstrated in a number of structure determinations. This has also been verified in a more systematic manner through selected dataset types, including single-crystal data in which the experimental structure factors have been altered in some random fashion, very small datasets with as few as ten reflections and small datasets comprising a subset with $|F_{hkl}|$ values estimated to be equal (Wilson 1989; Wilson and Wadsworth 1990). A comparison between Patterson-map calculations from a single-crystal dataset and a small number of unambiguous $|F_{\text{obs}}|$ values has also revealed the relative insensitivity of the Patterson function to large errors (Bénard, Louër and Louër 1991b). Rius and Miratvilles (1988) have proposed a strategy to assist in the determination of structures with large known molecular fragments. This is based on an automated Patterson search method developed to orient and position molecular fragments with rigid geometry in the unit cell. It allows one to use available 'molecular-skeleton' geometries, e.g. from crystal structure databases, to solve undetermined structures containing similar fragments. The method is suitable for solving crystal structures of organic molecular solids, for which the number of measurable intensities at high angles is considerably reduced and the absence of strong scatterers prevents a direct interpretation of the Patterson function from being carried out. The method, combined with rigid-body Rietveld refinement, has been applied to the determination of molecular packing in a 'hydrogen-bonded' molecular solid formed from a dihydroxyphenyl-nitronyl nitroxide radical (Cirujeda *et al* 1995) and to obtaining the structure of the zeolite RUB-10 from low-resolution data (Gies and Rius 1995). Determination of the structures of zeolites and layered materials by using multi-solution direct methods has been considered by Rius *et al* (1995). A new phase-refinement function derived by Rius (1993) was applied successfully to the tetragonal zeolite ZSM-11 and to the silicate RUB-15.

7.4.2. Improvement of existing methods. A promising development in structure solution from powder data based on the heavy-atom method is certainly the use of the maximum entropy technique to evaluate, from first principles, the intensities of overlapping reflections. This method has been used successfully in image reconstruction in a wide variety of fields. The maximum entropy solution is described as the 'most honest choice' because it is the one that is 'maximally non-committal' about the unknown information. David (1990) has applied this algorithm to the Patterson function obtained from powder diffraction data. The

Patterson function must faithfully represent the observed intensities of clusters of Bragg reflections. This is expressed through the χ^2 constraint. If the Patterson function P_k is divided into N 'pixels', the functional description of the observation may be expressed as a linear form of the 'Patterson entropy'

$$S = -\sum_{k=1}^{N} P_k \ln(P_k/Q_k) \tag{7.4}$$

where Q_k is a normalization factor. This relationship is then maximized in an iterative manner consistent with χ^2 criteria. An application to diffraction data for rutile (TiO_2) has been described by David (1990).

A fast iterative Patterson squaring method (FIPS) (Estermann and Gramlich 1993) has been developed for improving the Patterson function. Each point of a Patterson map calculated from the equipartitioned observed data is squared. The resulting map is back-transformed, leading to new Fourier coefficients which are extrapolated to give a new distribution of fractional intensity for overlapping reflections. This iterative technique enhances the peak and eliminates negative values. The structure of the aluminophosphate-based molecular sieve (SAPO-40) has been solved *ab initio* after a redistribution of the intensities by the FIPS method, for a pattern in which 65% of the reflections overlap severely (Estermann, McCusker and Baerlocher 1992).

Approaches based on probability theory have been devised for the evaluation of the fractional intensity contribution of exactly overlapping reflections (Jansen, Peschar and Schenk 1992; Cascarano, Favia and Giacovazzo 1992; David 1987). These are based on the derivation of intensity statistics and of probability relations between structure factors.

7.4.3. New methods

7.4.3.1. Entropy maximization and likelihood estimation. In contrast to the previous techniques, the maximum entropy (ME) method attempts to solve the overlap and phase problems simultaneously. The theoretical basis of the maximum entropy method has been presented by Bricogne (1984), who later described the adaptation of this approach to solving crystal structures from powder diffraction data (Bricogne 1991). The multi-solution method of phase determination, combining entropy maximization and likelihood evaluation, was extended to structure determination by Gilmore, Henderson and Bricogne (1991). In this method, overlapping data are treated in a rational manner. The method consists of considering an unknown structure as being composed of chemically identified atoms with unknown positions. The latter are initially considered as random with a uniform distribution in the asymmetric unit cell and the technique consists of a gradual removal of this randomness. The method has been applied successfully to the determination of the structure of $LiCF_3SO_3$ (Tremayne *et al* 1992). Detailed procedures for solving small crystal structures *ab initio* by means of ME and powder-diffraction data were reviewed recently by Sudo, Hashizume and Carvalho (1995). As a test of the technique, the multi-solution method was applied to the determination of the structure of a low pressure phase of magnesium boron nitride Mg_3BN_3.

It is worth noting the ME analysis is also widely applied to drawing the electron or nucleus density distribution map for known structures from X-ray or neutron powder diffraction data (Sakata *et al* 1990; Sakata *et al* 1993). For example, it has been used to recover the precise electron density distribution from accurate structure factors (Sakata *et*

al 1990) and applied to obtain a high-quality electron-density distribution for CeO_2 from X-ray diffraction data, the structure factor being represented as the Fourier transform of the electron density in the unit cell. The differences of the electron density distribution and the chemical bonding between d-electron type Y_2O_3 and f-electron type Tm_2O_3 and Yb_2O_3 have been examined by a combination of pattern decomposition and MEM from X-ray powder diffraction (Ishibashi, Shimomoto and Nakahigashi 1994). It was found that the valence electron distribution for the three compounds is nearly the same though neutral Tm and Yb have 30 and 31 electrons more than Y ($Z = 39$).

7.4.3.2. Direct space methods. For facilitating the solution of crystal structures, model-building methods which combine chemical, geometric, MAS NMR and electron microscopy, the unit cell size, symmetry and diffracted intensity information can be used. Once a model has been created, it can be optimized for the observed symmetry and unit-cell dimensions by means of commonly used distance and angle least-squares (DALS) methods, where atomic coordinates are adjusted to give ideal bond lengths and angles. This method is useful for studies of complex structures for which the ratio between the number of observations and variables is considerably less than ten. The use of restraints (also known as soft or slack constraints) increases the number of observations. Although the nature of the two sets of observations (diffraction intensities and geometric restraints) is quite different, they share the same variables and can be included in a common least-squares matrix. In a restrained Rietveld refinement, two minimization functions are combined, S (equation 3.2) and S_R (Baerlocher 1995):

$$S_R = \sum \omega[R_0 - R_{\text{cal}}(x)]^2 \tag{7.5}$$

where R_0 can be an expected bond length or angle, $R_{\text{cal}}(x)$ is the value calculated from atomic positions and ω is a weighting factor. A number of methods used for the study of zeolite materials have been reviewed by McCusker (1991) and similar principles were reviewed by Bish (1992). In an example of the use of high-resolution TEM images to elucidate the structure of an unknown material, Post and Bish (1988) recognized similarities between the chain structure of hollandite, $BaMn_8O_{16}$, and romanechite, $BaMn_5O_{10}.H_2O$, and TEM images of todorokite. They derived a starting model for the last compound by using a DALS refinement. The model building method is not strictly structure determination, but is the creation of a plausible structure. Another representative example is the structure of zeolite-23 (Marler *et al* 1993), for which the use of complementary methods, such as ^{29}Si magic-angle-spinning, nuclear-magnetic-resonance spectroscopy, electron diffraction and DALS refinement were necessary to determine the symmetry. An initial set of atomic coordinates of the framework atoms used for the refinement was then optimized by the DALS procedure.

Another method for generating realistic framework models is that of simulated annealing. This has been applied to zeolites (Deem and Newsam 1989) and also to predict simple inorganic crystal structures (Pannetier *et al* 1990). A model is automatically generated when the plausibility of a given atomic arrangement is quantified by cost functions or in energy terms. These may include constraints on ideal interatomic distances, bond angles, coordination features and Pauling's principles for ionic compounds. Models are created from an initially random distribution of the atoms within the determined unit cell and their optimization is accomplished by Monte Carlo techniques by using simulated annealing methods (Newsam, Deem and Freeman 1992). Structural models generated by the random

movement of a collection of atoms within the unit cell, and the acceptance or rejection of trial configurations based on comparison between experimental and calculated patterns, have also been considered by Harris *et al* (1994) and applied to known structures.

The atom–atom potential method (Kitaigorodskii 1973; Pertsin and Kitaigorodskii 1987) has also been employed to obtain crystal structure models for organic solids. A computational study was used for the structure solution of a metastable phase of piracetam (Louër *et al* 1995). This was carried out by minimization of the crystal-lattice potential energy, calculated with semi-empirical atom–atom potentials. In this study, the geometric parameters (bond distances, valence and torsional angles) of the piracetam molecule in known structures of polymorphs were used and the packing calculations were made using the PMC (Packing of Molecules in Crystals) program (Dzyabchenko, Belsky and Zorkii 1979).

Once a model has been created by these direct space procedures a comparison of the powder diffraction pattern generated from the optimized atomic coordinates with the observed pattern will indicate whether or not a model is likely to be correct and a successful Rietveld refinement may confirm the correctness of the solution.

7.5. Combined X-ray and neutron diffraction

The complementary nature of X-ray and neutron diffraction has been used in a number of applications for improving accuracy and providing additional information. The respective advantages of X-ray and neutron sources for structural investigation have been considered in section 2.1. Even if X-ray diffraction is the most convenient means of crystal structure determination, due to higher contrast between atoms, the accuracy of the atomic coordinates of light atoms may be considerably improved by Rietveld refinement from neutron diffraction data. Combined neutron and synchrotron X-ray experiments were used for a structural study of $Ga_2(HPO_3)_3.4H_2O$ containing 29 atoms in the asymmetric unit (Morris *et al* 1992). The benefit of using neutron diffraction can be appreciated from materials containing contrasted atoms and anionic groups with well known geometry. For $U(UO_2)(PO_4)_2$ (Bénard *et al* 1994), the X-ray diffraction pattern is strongly dominated by the scattering contribution from the metal atoms, since the ratio of atomic factors of U and O atoms is greater than 11.5, the ratio of atomic numbers, while the appropriate neutron scattering lengths for U and O atoms are in the ratio 1.45. The imprecision in O atomic positions in the X-ray case can be seen from the distortion of the PO_4 tetrahedra with P–O distances ranging from 1.46 to 1.62 Å. After refinement from the neutron diffraction data, the P–O distance is in the range 1.510–1.565 Å. X-rays and neutrons were also used in the structure determination of similar materials containing contrasting atoms, e.g. PbC_2O_4 (Christensen, Cox and Lehmann 1989) and $PbSO_3$ (Christensen and Hewat 1990). The complementary nature of X-ray and neutron diffraction has given rise to the use of both neutron and X-ray powder diffraction data in a simultaneous structure refinement (Maichle, Ihringer and Prandl 1988; Larson and Von Dreele 1987). Moreover, neutron diffraction data can in some cases be used as an aid to determining the correct space group. For instance, the space group obtained from synchrotron data for potassium uranyl phosphate trihydrate, $KUO_2PO_4 \cdot 3H_2O$, was $Pccn$, but the intense 011 reflection observed in the neutron powder pattern violated the extinction conditions for this space group. The reflections observed in the neutron data were in fact found to be compatible with the $P2_1cn$ space group (Cole, Fitch and Prince 1993).

7.6. Noteworthy examples of ab initio structure determination

In recent years many crystal structures have been solved *ab initio* from powder diffraction data. In the majority of cases, powder diffraction data collected with conventional X-ray sources were used, but a few were based on synchrotron X-ray data or monochromatic X-rays. The three following examples demonstrate the power of modern powder diffraction methods for solving crystal structures.

Sigma-2 zeolite (McCusker 1988): synchrotron X-ray powder diffraction data of Sigma-2 $[(Si_{64}O_{128}).4C_{10}H_{17}N]$, a clathrasil phase, were collected by using the Debye-Scherrer geometry. The pattern was indexed by means of a tetragonal cell with $a = 10.2387$ (1) Å and $c = 34.3829$ (1) Å ($V = 3604\,\text{Å}^3$), space group $I4_1/amd$, and the asymmetric unit cell contains 17 atoms. The extraction of integrated intensities was carried out by the Pawley method with an equipartition of intensity for overlapping reflections. A sum of 258 integrated intensities were entered in a direct-methods program. The best solution gave the position of all four Si atoms and four of the seven O atoms in the asymmetric unit. The first difference Fourier map showed the remaining three O-atom positions. Subsequent refinement coupled with Fourier syntheses revealed the location of the partially disordered 1-aminiadamantane in the large cage. The final Rietveld refinement was based on 451 contributing reflections and 47 structural parameters, leading to a structure-model indicator R_F of 0.10.

Gallium phosphite (Morris *et al* 1992): the structure of $Ga_2(HPO_3)_3.4H_2O$, with 29 atoms in the asymmetric unit cell, was solved *ab initio* from X-ray synchrotron powder diffraction data (Debye–Scherrer geometry). The unit cell is monoclinic with $a = 8.0947$ (2) Å, $b = 10.0336$ (2) Å, $c = 7.6711$ (2) Å and $\beta = 111.392$ (2)° ($V = 580$ Å^3) and space group $P2_1$. $551|F_{\text{obs}}|$ values were extracted by the iterative method (Le Bail, Duroy and Fourquet 1988) and entered in the direct-methods program (SHELX-86). From the normalized structure factors f_{hkl}, the best solution produced an E-map with two large peaks which were assigned to Ga atoms. Subsequent Fourier syntheses revealed four more atoms identified as two P and two O atoms. The model was refined by the Rietveld method with further Fourier synthesis, which revealed the positions of one further P and ten O atoms. The H-atom positions were obtained from neutron diffraction data and the final stage of the Rietveld refinement converged to $R_F = 0.03$.

$((CH_3)_4N)_4Ge_4S_{10}$ (Pivan *et al* 1994): the structure of this thiogermanate has been solved from conventional high resolution Cu$K\alpha_1$ powder diffraction data. From pattern indexing the symmetry was found to be cubic with a cell dimension $a = 19.5490$ (4) Å and only two space groups, $P\bar{4}3n$ and P$m3n$ were possible. In this example, the complexity of the pattern arises from the large unit cell volume (7471Å^3) and the exact overlap of a large number of independent reflections. From pattern decomposition combined with the principle of equipartition of overlapping reflections, the structure was solved by direct methods and one difference Fourier map. The application of direct methods was found to be very sensitive to limitations in $\sin\theta/\lambda$ of the datasets used. The refinement by the Rietveld method converged to $R_F = 0.06$.

7.7. Integrated software

With the growing development of this important application of the powder method, integrated software for solving crystal structures is now of interest (McCusker 1992) and some of the programs available to carry out the various steps in *ab initio* structure

determination are listed in section 7.1. (See also Smith and Gorter 1995.) The software combines programs for the treatment of powder diffraction data with those used in conventional structure determination by single-crystal methods. An important development is that solving and refining crystal structures from powder data can now be performed with a personal computer (Louër and Louër 1994). It is intended to provide an integrated suite of programs for structural investigations as part of the Collaborative Computational Project in Powder Diffraction (CCP14) (see section 1).

8. Resonant diffraction (anomalous dispersion)

An important aid to structure determination is the use of resonant X-ray diffraction, which is also known as anomalous dispersion or anomalous scattering. The atomic scattering factor for X-rays, f, has a 'normal' (Thomson) component, f_0, and a complex energy-dependent 'anomalous' contribution $f' + \mathrm{i}f'$, or

$$f = f_0 + f' + \mathrm{i}f''. \tag{8.1}$$

f_0 depends on the electron distribution and varies only with $\sin\theta/\lambda$, whereas the anomalous contribution is strongly dependent on energy. This is normally very much less than f_0, but in the vicinity of an absorption edge, when the energy of an incident photon is sufficient to excite a core electron, it is greatly enhanced. For example, f' for Fe is about 7 eV at the K edge, compared with 17 eV for f_0 at $\sin\theta/\lambda = 0.3\text{Å}^{-1}$, and considerably greater values of f ' have been reported for L edges (Phillips and Hodgson 1980). Resonant diffraction is thus a sensitive probe of atomic sites and it has been used for many years in single-crystal determination of macromolecular and protein structures. However, it is a relative newcomer in powder diffraction, a result of the increased availability of dedicated synchrotron sources with high intensity over a wide range of wavelengths in the X-ray region. By fine tuning a suitable monochromator, the appropriate wavelength for enhancing f' or f'' for an atom of interest can be selected. Resonant scattering is mainly used to obtain the distribution of the resonant element within a crystal structure, in the presence of elements with similar atomic numbers, or to obtain contrast between atoms of the same element, but with different valence states, for which the values of f' normally differ by a few eV. Attfield (1992) has discussed these uses of resonant diffraction in detail, together with the relevant experimental procedures. (See also Wilkinson and Cheetham 1992.)

The reliability of the results of a resonant-diffraction experiment depends on the accuracy with which f' and f'' have been determined, particularly in the vicinity of their resonant values (Hoyt, de Fontaine and Warburton 1984). These parameters can be calculated, but values determined experimentally are generally considered to be more reliable. Considerable effort was expended in the 1980s to determine f' and f''. These were mainly obtained from the measurement of X-ray absorption spectra (e.g. Bonse and Hartmann-Lotsch 1984), by means of X-ray interferometry (e.g. Begum *et al* 1986) and from powder diffraction data (e.g. Suortti, Hastings and Cox 1985; Will *et al* 1987).

An example of a straightforward application of resonant diffraction to achieve elemental contrast is the determination of Fe/Ni occupancies of the four distinct octahedral sites in the structure of $FeNi_2(BO_3)O_2$ by Perkins and Attfield (1991). A single resonant pattern was collected at 16 eV below the FeK edge and, in addition to the usual parameters refined, Fe/Ni occupancies were obtained with a precision of 0.6%. A somewhat different use of elemental

contrast was the study by Moroney, Thompson and Cox (1988) of isotropic temperature factors in yttrium-stabilized cubic zirconia $Y_{0.19}Zr_{0.81}O_{1.90}$. The Y/Zr occupancy of the cation site was fixed and resonant data were used to ascertain how each species is disordered around the ideal position, by determining its temperature factor independently. Resonant diffraction has proved to be invaluable in elucidating structural detail in 'YBCO' and other high T_c ceramics. For example, Howland *et al* (1989) partially replaced Cu in $YBa_2Cu_3O_{7-\delta}$ by Fe, Co, Ni or Zn and determined the dopant site occupancies. This was achieved by collecting data at energies near the absorption edges for the dopants. Cu in orthorhombic YBCO occupies Cu(1) ('chain') sites and Cu(2) ('plane') sites. Ni and Zn were found to behave similarly, in terms of site occupancy, and differently from Fe and Cu. The two sites play distinctly different rôles in determining the physical properties of this material, which can be modified significantly by the introduction of dopants. An example of the use of resonant scattering, coupled with an image-plate detector, to detect very weak superlattice reflections at high pressure is given in section 11.2.

Warner, Cheetham and Cox (1990) used resonant diffraction to study the important case of Fe^{2+} and Fe^{3+} in the mixed-valence compound α-Fe_2PO_5. There is a difference of about 3 eV between the absorption edges of Fe^{2+} and Fe^{3+} (Sarode *et al* 1979) and in this instance the ions were found to be located at two different crystallographic sites. A significant result of this work was that the two sites could clearly be distinguished as having different scattering powers close to an absorption edge, despite there being a comparable energy spread in the incident beam. Wilkinson, Cheetham and Cox (1991) carried out a similar investigation of oxide-state contrast in $Ga^+Ga^{3+}Cl_4$, by using the differences in f' between Ga^+ and Ga^{3+}, and Kwei *et al* (1990) studied the Cu^+, Cu^{2+} and Cu^{3+} sites in orthorhombic YBCO. K edges were used in this work and, as an example of resonant scattering in the vicinity of an L edge, Attfield (1990) used Eu L_{III} to contrast ordered valence states in Eu_3O_4. In this instance, Eu^{3+} was found to occupy one of three distinct Eu sites and Eu^{3+} fills the other two. Until recently, resonant diffraction was limited to elements with Z greater than about 20, but Mårdalen, Riekel and Müller (1994) successfully used soft X-rays near the K edge for sulphur ($Z = 16$) to obtain information on the behaviour of the main chain in the partially conducting polymer poly(3-octylthiophene) (P3OT). Only the 100 reflection could be recorded, but in this instance the unit cell and the basic structure had been determined previously by using harder X-rays and neutrons. Nevertheless, the experiment demonstrated the possibilities of resonant diffraction with low-Z elements, particularly in providing additional structural information on systems with few diffraction peaks.

Resonant diffraction experiments carried out with synchrotron X-ray sources have contributed significantly to our understanding of complex inorganic structures and have increased our knowledge of the behaviour of f' and f'' in the vicinity of absorption edges. Although the technique is somewhat limited in its application and is experimentally demanding, resonant diffraction is now firmly established as a valuable technique in powder diffraction, one which is likely to become more important with the increased availability of high brightness sources.

9. Quantitative phase analysis

9.1. Introduction

The integrated intensity of reflections for a compound in a multiphase powder diffraction pattern is related to the phase abundance in the mixture. This property has been used

for many years in quantitative phase analysis (Klug and Alexander 1974) and significant advances have occurred in the last two decades (see, for instance, Snyder and Bish 1989; Hill 1991; Davis 1992; Snyder 1992a). The method can be applied to a wide range of materials, but instrumental and sample-related effects can influence the accuracy of the results profoundly, e.g. preferred-orientation, extinction, micro-absorption and the detection of trace and amorphous components. Diffraction measurements of phase abundance can be performed in many ways, but traditional methods require the acquisition of standard reference data for each phase present in the mixture to be analysed. The introduction of the concept of a reference intensity ratio (RIR; section 4.6.2) contributed to the simple and powerful procedure described by Chung (1974a, b). With the advent of the Rietveld method (section 3.3.2) a new approach to quantitative phase analysis has been devised (Werner *et al* 1979; Hill and Howard 1987).

9.2. The internal-standard and the reference-intensity-ratio methods

The internal-standard method is based on elimination of the matrix absorption factors by computing the ratio I_i/I_s of the diffraction line intensity of phase i and the intensity of a line for an internal standard s. This ratio is then related to the weight fraction (W_i) of phase i through the equation:

$$I_i/I_s = kW_i/W_s. \tag{9.1}$$

This equation is the basis of the internal-standard method. To be applied, it is necessary to add a known amount of a standard material to the mixture and the k values must be known, or must be obtained, for each phase. The procedure is sensitive to systematic errors, e.g. the effects of micro-absorption in a heterogeneous material and preferred orientation have been discussed by Cline and Snyder (1985, 1987) and Herman and Ermrich (1989); Bish and Chipera (1988) have considered the separation of overlapping and broad diffraction lines and the detection of amorphous and trace phases. The procedure for using a calibration curve in quantitative analysis was improved for the case of analysing monoclinic-tetragonal ZrO_2 by using pattern decomposition techniques (Toraya, Yoshimura and Sömiya 1984). The problem of multiple calibration constants can be overcome by using the RIR. This has been given the notation I/I_c, the ratio of the maximum intensity I of the strongest line of the analyte to that of the corundum 113 reflection, I_c (Visser and de Wolff 1964; Hubbard, Evans and Smith 1976; de Wolff and Visser 1988). The concept of the intensity ratio as a materials constant has been extended to other reference phases (Hubbard and Snyder 1988). Selected RIR values and other parameters have been reported by Davis and Smith (1988) and Davis, Smith and Holomany (1989). However, it should be noted that the weight fraction of a component in a mixture of phases is proportional to line-profile area and the use of maximum intensities is an approximation. Nevertheless, a direct application of the RIR concept was introduced by Chung (1974a, b) who derived a simple relationship in RIR analysis. In the fundamental equation 9.1, relating phase concentration (W) and diffraction line intensity (I), W_s ($= W_c$) is the weight proportion of the standard (e.g. corundum) added to the sample and k is the RIR_{ic} for component i. Also, an 'adiabatic' method for analysing a mixture of identified phases without the addition of a standard, provided that all RIR ratios are known, has been described. This imposes the constraint that the sum of the percentage weight fractions of all crystalline phases in the mixture, including trace components, is 100%. Thus, the presence of any unanalysed amorphous phase, including the commonly

occurring amorphous surface layers on crystallites, invalidates this procedure. In these approaches the RIR, by nature of the basic standard used for all materials, 'flushes out' absorption effects. Chung (1974a) illustrated the 'matrix flushing' technique with various tests using synthesized corundum as the flushing agent. An interesting example of this technique is a study of the performance of lead-acid batteries, to determine the correlation between deep-discharge service with the composition of the positive plate material (Harris, Hill and Rand 1984). The measurement and use of RIRs is straightforward for random samples and materials for which the intensity does no vary with composition. The problems arising from a variable chemistry and/or strong preferred-orientation effects (e.g. feldspars and zeolites) have been considered by Chipera and Bish (1995). By using reflections from non-parallel planes (e.g. 001 and 110), or small regions which include multiple reflections, the measured RIR values can be averaged to compensate for these effects. Chipera and Bish showed that the precision and accuracy of quantitative analysis in such cases are then considerably improved.

Additional standardless methods have also been described by Fiala (1980) and by Zevin and Zevin (1989). The former is essentially an iterative procedure in which the concentrations of individual phases and the intensities of standards are compared and the differences minimized. The related technique of Zevin and Zevin involves preparing at least as many mixtures of known concentration as there are phases in the sample to be analysed. If sufficient 'control' samples are prepared, then a least-squares comparison of intensities can be carried out. This standardless technique is unsuitable for sporadic analyses of a few samples, but it is a powerful and potentially accurate method for large-scale analysis of many samples with similar composition. Zevin and Zevin applied the method to various mixtures of minerals and most of the observed weight fractions were within 10% (relative) or the actual values.

9.3. Quantitative phase analysis by the Rietveld method

It has been demonstrated (Hill and Howard 1987) that there is a simple relationship between the individual scale factors (equation 3.6) determined in a Rietveld structure refinement of a multicomponent sample and the phase concentration in the mixture. Information on the weight fractions (W_i) of the phases present in a mixture is thus obtained directly from the scale factors for each phase obtained from the refinement:

$$W_i = \mathrm{s}_i(ZMV)_i \Big/ \sum_j \mathrm{s}_j(ZMV)_j. \qquad (9.2)$$

where s_i, Z_i, M_i and V_i are the scale factor, the number of molecules per unit cell, the molecular weight and unit-cell volume of phase i, and the summation is over all phases present. A similar relationship, expressed as a function of the calculated density ρ_i ($= Z_i M_i / N_A V_i$, where N_A is Avogadro's constant), was also derived (Bish and Howard 1988). The quantity ZMV (which is proportional to ρV^2) for a particular phase is the Rietveld equivalent of the conventional RIR (Hill 1991) and has been derived in RIR notation by Snyder (1992b). A requirement of the method is that the crystal structure is known for each phase in the sample. This analysis has advantages over conventional quantitative analysis methods, since no experimental precalibration is required and the use of all reflections in a pattern reduces the uncertainty in the derived weight fractions by minimizing the effects of preferred orientation and extinction. The problem of contrast

effects due to micro-absorption in quantitative analysis by means of the Rietveld method has been discussed by Taylor and Matulis (1991). Provision for the determination of phase abundance by using the Rietveld method is now available in a number of a computer programs, e.g. QPDA (Madsen and Hill 1990) and SIROQUANT (Taylor 1991). Bish and Post (1993) describe a modified version of the Rietveld program DBW3.2 (Wiles and Young 1981), adapted for use with internal external standards. These two modifications are then analogous to the matrix-flushing and adiabatic methods, respectively, described by Chung (1974a, b). Programs for quantitative analysis are listed in table 16 of Gorter and Smith (1995).

Many applications of this important development in quantitative analysis have been reported. Partially stabilized zirconia containing various amounts of the cubic, tetragonal and monoclinic phases of ZrO_2 have been analysed by X-ray (Hill and Reichert 1990) and neutron (Howard *et al* 1990) diffraction. In these materials, transitions between the polymorphs occur during the preparation of samples for X-ray diffraction and the composition at or near the surface is then not representative of the bulk. X-ray diffraction was used to study near-surface regions and neutrons were used to determine the composition of the bulk. Other applications of quantitative phase analysis to complex mixtures, by using the Rietveld method, include a mixture of Fe_3O_4–$Li_xFe_3O_4$, of interest in solid-state battery electrodes (Rodriguez-Carvajal and Fontcuberta 1987), and a study of Portland cement (Taylor and Aldridge 1993). The use of quantitative analysis in mineralogy by using the Rietveld full-pattern fitting method has been discussed by Snyder and Bish (1989) and Bish and Post (1993).

10. Line-profile analysis and microstructural properties

10.1. Microstructure of materials

Polycrystalline materials invariably contain imperfections which modify the intensity distribution of a Bragg reflection (section 2.4). This departure from an ideal structure, generally known as microstructure, can profoundly influence the physical, mechanical and chemical properties of materials and the characterization of structural imperfections (line-profile analysis) is thus an important application of powder diffraction. With the exception of structure refinement by means of the Rietveld method (section 6.1.5), the techniques considered so far have been concerned with ‘ideal’ crystal structures, in that the effects of microstructure have largely been ignored, and have mostly been based on determining the position and intensity of reflections. However, the full distribution of intensity needs to be taken into account in studies of microstructure and line-profile analysis is thus one of the more demanding uses of powder data. There are two main approaches to obtaining microstructural parameters from diffraction. One is based on the representation of line profiles by Fourier series and the other employs line-profile parameters obtained from pattern decomposition (section 3.3.1).

10.2. Analysis of microstructure based on Fourier series

The diffraction line profile $f(s)$ due to sample microstructure for the reflection hkl can be expressed as the Fourier series given by equation 3.3, with $x = s/2\hat{s}$, where s is the radial distance from the corresponding reciprocal-lattice point and $\pm\hat{s}$ is the range over

which data are recorded for this reflection. There are two ways in which equation 3.3 is applied in line-profile analysis. One may be regarded as an analytical approach, since formulae based on diffraction theory (section 2.4.1) are applied directly to the experimental data, to estimate parameters which characterize the microstructural properties of interest (sections 10.2.1 and 10.2.2). In the alternative approach, a model, based on the expected microstructural properties (e.g. section 2.4.2), is used to calculate the sample line profiles $f(x)$ or to obtain parameters which characterize $f(x)$. These are then compared with the experimental data, ideally by a least-squares-refinement procedure. Model-based procedures are considered in section 10.2.3.

10.2.1. Crystallite (domain) size. Bertaut (1949) demonstrated that, if $f(s)$ is due solely to the size of coherently diffracting domains, then the inverse of the initial slope of normalized values of a plot of A_n versus n is the average number of unit cells in a direction perpendicular to the diffracting planes and that the second derivative of this curve is proportional to the distribution of column lengths. For convenience, n is usually replaced by $L(= n/2\hat{s})$ and $|\mathrm{d}A_n/\mathrm{d}L|_{L=0}^{-1}$ then gives ε_F, the area-weighted apparent size (section 2.4.1) directly. (It should be noted that the Fourier coefficients A_n correspond to the transform $V(t)$ in equation 2.12, normalized to unit volume and with $Y(t)$ constant, and n corresponds to discrete values of $2\hat{s}t$.) These important results are the basis for determining the size and shape of crystallites (section 10.2.3) and the distribution of apparent size (section 2.4.1) from the Fourier-series representation of $f(s)$. For the particular case of reflections from crystallites with parallel surfaces which are perpendicular to the direction [hkl], the line profile due to size effects is, from Bertaut (1950) equation (10),

$$f(s) \propto \int_0^\infty \frac{\mathrm{P}(L)\sin^2 \pi L s\, \mathrm{d}L}{(\pi s)^2} \tag{10.1}$$

where $\mathrm{P}(L)$ is the volume-weighted fraction of the sample for which the crystallite thickness lies between L and $L + \mathrm{d}L$ and is proportional to $[V''(t)]_{t=L}$ (Guinier 1963, equation 5.21 and section 2.4.1). The term $\sin^2\pi Ls/(\pi s)^2$ in equation (10.1) will be different for other forms of crystallite. A consequence of the low precision which normally occurs when obtaining the second derivatives of A_n versus L is the presence of spurious oscillations in the size-distribution curves. Also, an incorrect determination of the background leads to an initial 'hook' of the A_n versus L curve, which results in a physically impossible negative value of $\mathrm{P}(L)$ as $L \to 0$ (Young, Gerdes and Wilson 1967). Various approaches have been devised to overcome the problem of spurious oscillations, applicable only to data from well resolved reflections and cases where broadening due to lattice distortion is negligible. Pausescu *et al* (1974) eliminated negative minima by means of an iterative procedure, based on an extrapolated exponential function. Bley, Calvayrac and Fayard (1974) obtained smooth size distributions by fitting a Lorentzian function to the tails of observed line profiles. This method is related to the correction introduced by de Bergevin and Germi (1972), which is based on the linear variation of the variance (second central moment) of a line profile with range of truncation (Wilson 1962b). The representation of the distribution curve by a polynomial series modulated by a generalized Lorentzian function was proposed by Moraweck, de Montgolfier and Renouprez (1977), who used the simplex method to solve the resulting set of simulataneous equations. A procedure based on smoothing the A_n versus L curve before obtaining the second derivatives was applied by Petrov (1976) and by Pielaszek *et al* (1983). The over-determined set of equations

derived from (10.1) can also be solved by a least-squares procedure (Hossfeld and Oel 1966; Le Bail and Louër 1978); however, the spurious oscillations superimposed on the size distribution function, a consequence of the instability of the system, usually remain. Le Bail and Louër (1978) applied an algorithm which minimizes an approximate function, based on Tikhonov's regularization procedure (see section 2.3), to obtain smooth distribution functions. The validity of this technique was confirmed by applying it to data from samples containing two known, but different size distributions. Similar regularization schemes were applied by Ozerin *et al* (1986) and Kojdecki (1991).

10.2.2. The Warren–Averbach method. Subsequent to the pioneering work of Bertaut in extracting the mean domain size and distribution of size from diffraction data, Warren and Averbach (1950, 1952) introduced an analytical technique for dealing with combined order-independent and order-dependent line broadening (section 2.4.1). Full details of the method are given by Warren (1969) and a useful overview has been provided by Delhez, de Keijser and Mittemeijer (1982). The basis of the method is the multiplicative property of the Fourier transforms of convoluted functions, as is used to remove instrumental contributions from experimental line profiles by means of the Stokes method for deconvolution (section 2.3). An analysis of microstructure is normally based on the cosine (real) coefficients A_n in equation 3.3. This makes the assumption that the sine coefficients B_n are negligible and, although B_n are zero for size effects, for which the line profiles are symmetrical, this is not necessarily the case for lattice distortion. Accordingly, Wagner (1966) suggested using $F_n = (A_n^2 + B_n^2)^{1/2}$, rather than A_n. The coefficients A_n are considered to have an order- (and hence d^*_{hkl}) independent component A_n^S and an order-dependent part $A_n^D(l)$, where S denotes 'size' and D 'strain' (distortion), and l is the order of the reflection, or

$$A_n = A_n^S A_n^D(l). \tag{10.2}$$

(A_n in equation 10.2 corresponds to the product $V(t)Y(t)$ in equation 2.12, normalized to unit volume.) The order-dependent coefficients are

$$A_n^D(l) = \langle \cos[2\pi \ln e(n)] \rangle \tag{10.3}$$

where $e(n)$, the fractional displacement of a pair of unit cells a distance n cells apart, is a measure of strain in the direction perpendicular to the reflecting planes. Thus

$$A_n = A_n^S - A_n^S 2\pi^2 l^2 n^2 \langle e(n)^2 \rangle + \ldots \tag{10.4}$$

Most Fourier methods for separating 'size' and 'strain' effects are then based on equation 10.2 or 10.4.

The Fourier harmonic number n is again often replaced by a distance L. By considering only the first two terms of this equation (n small), the inverse of the initial slope of a plot of normalized values of A_n versus L is again the area-weighted apparent size ε_F, as in section 10.2.1. In the method devised by Warren and Averbach, order-independent ('size') and order-dependent ('strain') contributions are separated by plotting $\ln(A_n)$ versus l^2. This procedure is exact if the variation of $e(n)$ is Gaussian, though there is no particular reason a priori that the strain distribution should be of this form, and is a good approximation

if the lattice distortion is small. In order to avoid this restriction, Delhez, de Keijser and Mittemeijer (1980) used only the cosine expansion to separate size and strain contributions. This entailed plotting A_n versus l^2 (i.e. neglecting the third and higher terms in equation 10.4). These and related procedures clearly require data for at least two orders of a reflection. However, this is not always possible or practicable to achieve, e.g. for heterogeneous catalysts with very small crystallites, some polymers or studies of surface layers. Another instance is the technique of monitoring a single peak rapidly by using a position-sensitive detector, in a dynamical study of a sample which is not in a state of equilibrium. Various authors have discussed the application of the Warren-Averbach method to data from a single peak. For example, Mignot and Rondot (1975, 1977) fitted a quadratic to the A_n versus n curve for small n to obtain A_n^S and A_n^D. Single-line methods have been listed and reviewed by Delhez, de Keijser and Mittemeijer (1982). An approach which is rapid and less model-dependent, based on the assumption that $e(n)$ is small or zero as $n \to 0$, was introduced by Nandi *et al* (1984). A_n^S is again obtained from the initial slope of the A_n versus n curve, the mean-square strain $\langle e^2(n) \rangle$ being given by equation 10.4. This approach lends itself to on-line monitoring of diffraction effects and, although the method is only approximate, Nandi *et al* obtained good agreement with the results of other single-line methods and multiple-order analyses when applying it to a variety of materials. Schlosberg and Cohen (1983) also developed an on-line procedure for the collection and subsequent Fourier analysis of diffraction data, taking into account errors due to truncation and from other sources. Another modification of the Warren–Averbach procedure uses the first derivatives of the A_n versus n curve, rather than the complete curves (Delhez, de Keijser and Mittemeijer 1982). By assuming that $g(x)$ and $h(x)$, and hence $f(x)$, can be approximated by some analytical function, this approach can be applied to calculate initial derivatives, from which estimates of ‘size’ and ‘strain’ can be extracted (de Keijser, Mittemeijer and Rozendaal 1983).

A different approach to characterizing lattice distortion was proposed by Vogel, Haase and Hosemann (1974). By using the logarithm of the ratio of A_n for two orders of a reflection, the size term vanishes and a hypothesis regarding the nature of the disorder present can then be based on the behaviour of $\ln A_n(l)/A_n(l+1)$ as a function of n. A parabolic trend, equivalent to a constant mean-square strain $\langle e^2 \rangle$, is interpreted as a fluctuation in lattice parameter in different crystallites, whereas a linear trend ($\langle e^2 \rangle \propto 1/n$, approximately) is attributed to the presence of dislocations or to paracrystallinity (Crist and Cohen 1979).

Owing to the difficulty in obtaining reliable Fourier coefficients for even moderate overlap of reflections, the basic method is largely restricted to materials with high symmetry and even then serious errors due to the unavoidable truncation of line-profile tails can occur, as was noted in section 2.3. An early attempt to deal with the case of partially overlapping line-profile tails, based on the linear variation of $\ln\langle e^2 \rangle^{1/2}$ versus $\ln(\langle d \rangle n)$, was made by Adler and Houska (1979). An interesting alternative approach to the use of Fourier series, which to some extent overcomes the problem of line-profile overlap and thereby is applicable to materials having lower symmetry, was introduced by Enzo *et al* (1988). This uses pseudo-Voigt functions to model $f(x)$ and $g(x)$, the latter having been determined experimentally. The convolution of these functions, carried out by numerical integration, is then compared with $h(x)$ by refining the parameters which define $f(x)$. A_n can then be determined for subsequent use in the Warren–Averbach or Vogel–Haase–Hosemann methods. García-Martínez *et al* (1993) used this technique to characterize ‘nanocrystals’ of ZnO and CuO, for which the crystallite size was found to be $\sim$ 10 nm or less. Niepce and Benabad-Sidky (1986) treated line-profile overlap by carrying out pattern decomposition before obtaining the Fourier coefficients. Among the examples cited is the important case

of the change in separation and broadening of the 002/200 doublet which occurs as the tetragonal-cubic phase transition in $BaTiO_3$ is approached. Balzar (1992) avoided the use of numerical convolution by making the assumption that the line profile due to instrumental effects and sample imperfections can be modelled by Voigt functions, for which the Fourier transform is known (Langford 1978). Balzar and Ledbetter (1992, 1993) compared this approach with the normal Fourier/Warren–Averbach procedure and found that, subject to certain limitations, the same results were obtained. They used the Voigt approach to estimate domain sizes in Bi-Cu-O superconductors, to ascertain the relationship between the critical temperature T_c and microstructure in doped superconductors with nominal composition La_2CuO_4 (Balzar, Ledbetter and Roshko 1993).

The Warren–Averbach method has been widely used since its inception, notably in metallurgical applications. Several programs exist for carrying out deconvolution by the Stokes method and for applying the Warren–Averbach technique (see table 13 in Gorter and Smith (1995)) and the procedure is usually included in commercial software for automatic powder diffractometers. In cases where broadening from lattice distortion is negligible, reliable information can usually be obtained about the mean size of crystallites or domains and the distribution of size (section 10.2.3). However, when size effects are accompanied by strain broadening, the latter is simply interpreted in terms of diffraction effects and in general its physical interpretation is unclear. Furthermore, the approximation used to describe strain broadening, namely the truncation of equation 10.4 at the second term, is incompatible with the nature of the microstrain in a plastically deformed material (Wilkens 1979, 1984). If parameters which relate to specimen microstructure in a way which is physically meaningful are required, then a model-based approach must be used. Nevertheless, the Warren–Averbach method is a well established procedure in a variety of applications and is particularly useful for monitoring the changes in diffraction effects due to differences in the preparation or treatment of a sample, or to different experimental conditions.

Scardi, Kothari and Guzman (1991) used both the Warren–Averbach and Vogel–Haase–Hosemann methods to study microstructural disorder in TiN_x thin films on Si substrates, prepared by reactive ion-beam assisted deposition and with different nitrogen content. All films exhibited [111] orientation, with small crystallites (< 100 Å) and large microstrains ($\langle e^2 \rangle^{1/2} \sim 10^{-2}$). The crystallite size diminished and the strain increased with increasing nitrogen concentration, the former being generally observed in non-equilibrium ion-beam techniques. The large microstrain was thought to be due to fluctuations in the lattice parameter introduced by ion bombardment. In another application of the adaptation by Enzo *et al* (1988) of the Warren–Averbach method, Scardi, Lutterotti and Di Maggio (1991) showed that, by obtaining size distributions from the Fourier coefficients, there is a critical size of 300 Å below which tetragonal zirconia will not transform to the monoclinic phase.

10.2.3. Model-based methods. Line-profile analysis by using Fourier series is greatly simplified if lattice distortion is negligible, as is the case if the A_n versus n curves for different orders of a reflection superimpose, or as can be ascertained from a Williamson–Hall plot (section 10.3). This frequently occurs for ceramics and other materials prepared at high temperatures. A typical example is the study by Louër *et al* (1983) of powder ZnO obtained by thermal decomposition of a $Zn(OH)_4(NO_3)_2$ precursor. Electron micrographs suggested that the crystallites were irregular hexagonal prisms and a cylindrical model was used to interpret the variation of line breadth with lattice direction. By this means, the average diameter (120 Å) and height (250 Å) of the crystallites (figure 11) and the

distribution of size were obtained. The direction-dependence of data for ZnO prepared from the same material, but under different conditions, indicated that a right hexagonal prism, with edge length 90 Å and height 210 Å, was a more appropriate model than a cylinder (Vargas, Louër and Langford 1983).

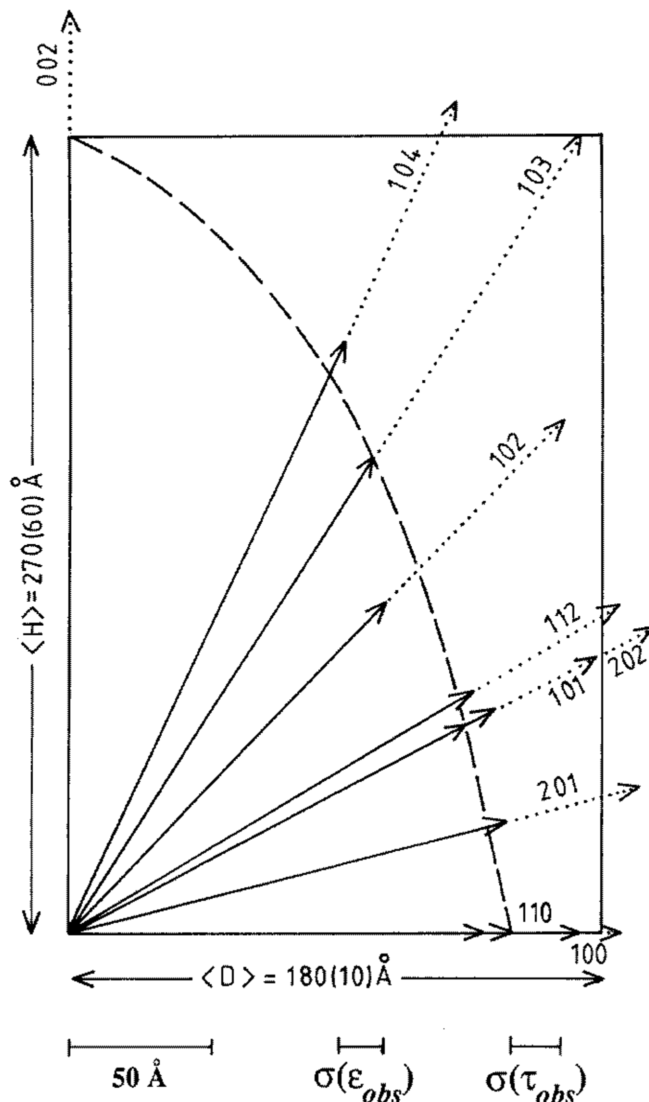

Figure 11. 'Average' form of crystallites in powder ZnO modelled by means of a cylinder with $\langle H \rangle = 270$ (60) Å and $\langle D \rangle = 180$ (10) Å. ——ε_{obs}; – – –ε_{cal}; $\cdots\cdots\tau_{obs}$ (Langford 1992).

Cabañas *et al* (1995) obtained the mean dimensions of crystallites in samples of barium hexaferrite ($BaFe_{12-2x}Co_xTi_xO_{19}$), prepared under different thermal conditions by the co-precipitation method and the liquid-mix technique. The variation of line breadths with lattice direction suggested that the crystallites had the form of platelets and a cylindrical model was again used. There was a marked correlation between the mean diameter $\langle D \rangle$,

height $\langle H\rangle$ and the ratio $\langle D\rangle/\langle H\rangle$ with the method of preparation and these quantities varied systematically with x, the weight fraction of Co and Ti. For a sample with $x = 0.5$, the diameters obtained from X-ray data were of the same order as those observed from TEM images, indicating that the particles were in fact single crystals in this particular case.

An example of a comparison of calculated and observed line profiles is the study of boehmite (AlOOH) by Grébille and Bérar (1985). An indication of the morphology and mean size of crystallites was obtained from TEM images and the form was modelled on the basis of convex polyhedra (section 2.4.2) having the same shape, but a distribution of size, to obtain $f_{\rm cal}(x)$. This was convoluted with g(x) to give $h_{\rm cal}(x)$, which was compared with $h_{\rm obs}(x)$ by a least-squares procedure. The quantities refined were dimensions of the polyhedra and parameters defining the distribution of size and remarkably good agreement between theory and experiment was achieved. Andreev and Lundström (1994) used a similar procedure to determine the crystallite size in boron nitride, which has a turbostratic graphite-like structure. They used a starting model for $f(x)$ based on that given by Warren and Bodenstein (1966) for graphite-like layers.

A determination of the crystallite-size distribution is of paramount importance in studies of chemical reactivity, particularly the behaviour of catalysts, e.g. α-Fe_2O_3 supported by silica gel (Amelse *et al* 1981) and Pt dispered on activated carbon (Polizzi *et al* 1987). Louër and de Guibert (1985) used Bertaut's method, after incorporating the regularization procedure discussed in section 10.2.1, to investigate the electrochemical properties of mechanically-activated nickel hydroxide nitrate. The Fourier coefficients for the 001 and 002 reflections were identical, indicating that lattice distortion was negligible, and the crystallite-size distributions were obtained for samples which had been milled for different lengths of time. The results were compared with specific area measurements, obtained by the BET method, and with the response of electrodes produced from nickel hydroxide nitrate. Another example of the determination of crystallite-size distributions is a study of acicular hematite, by using X-ray diffraction and electron microscopy, by Duvigneaud and Derie (1980). The needle-like habit was quantified by obtaining size distributions in three different crystallographic directions and it was found that the long dimension was perpendicular to the c axis. These are particularly good examples of the detailed information on crystallite size and shape which can be obtained if size effects are the main source of diffraction broadening.

In a neutron and X-ray structural study of the ε, γ and θ transitional phases of alumina, Zhou and Snyder (1991) used line widths to establish the nature of the phases. The transition aluminas occur when the various hydroxides of aluminium are heated. The ε and γ phases have a broadened spinel-type powder diffraction pattern with the unusual feature of a very broad 111 reflection, corresponding to a crystallite size of 20 Å, whereas the 222 reflection is relatively sharp, indicating a size of about 200 Å. These observations can be explained by noting that the structure factor for the 222 reflection is dominated by oxygen scattering and the size of the oxygen sublattice is thus reflected in the *FWHM* of the 222 reflection. A tablet size of 200 Å was also observed by means of TEM. The aluminium ions in the spinel tetrahedral sublattice dominate the structure factor for the 220 reflection, for which the *FWHM* indicates a coherent-domain size of 16 Å for ε alumina and 19 Å for the γ phase. The difference Fourier plot, after refinement of the structure by the Rietveld method, showed that 13% of the Al ions are in 3-fold coordination for the case of ε alumina, which corresponds exactly to the number of Al ions on the surface of 16 Å crystallites. Thus, by means of powder diffraction and ordering domain-length analysis, a model for the catalytic activity of these high surface area catalysts could be devised. The 3-fold coordinated Al ions locked on the crystallite surfaces are obvious Lewis acid sites which bind reacting

molecules to the surfaces, permitting heterogeneous catalysis.

If it is demonstrated that the sample exhibits measurable lattice distortion, then the analysis is less straightforward. There is no single model which accounts for all cases of deformed materials and the one selected in a particular application can be based on the nature, origin and treatment of the sample. Hitherto, the cause of lattice distortion which has received most attention is the presence of dislocations. Indeed, the determination of the nature and density of dislocations is one of the more important applications of line-profile analysis. The first attempt to model line broadening due to strain fields around dislocations was made by Wilson (1952). The theory was developed further by Krivoglas and Ryaboshapka (1963), with subsequent contributions by Wilkens (1970) and Ungár *et al* (1984) which embody different assumptions regarding the random nature of dislocations. The underlying concept is the superposition of the displacement fields of single dislocations in an infinite medium, to model various dislocation configurations. The dislocation density and the 'effective outer cut-off radius' are obtained, together with information on any dipolar nature of the dislocations and on spatial fluctuations in their density (Groma, Ungár and Wilkens 1988). By using high resolution data, Ungár, Groma and Wilkens (1989) obtained these parameters for plastically deformed Cu. Although single crystals were used in this work, the technique is equally applicable to individual grains embedded in polycrystalline samples (Langford *et al* 1992). The procedure for studying dislocations by means of diffraction data has been reviewed by van Berkum *et al* (1994), who also applied the technique to plastically deformed copper and ball-milled tungsten.

An interesting recent development in the model-based approach is the analysis by van Berkum *et al* (1992) of the line broadening due to local elastic distortions induced by finely dispersed misfitting inclusions. These were modelled by considering spherical particles in an elastically distorted matrix. The corresponding diffraction line profiles $f_{\mathrm{cal}}(x)$ were simulated for the case of Al–Si alloys and convoluted with instrumental functions $g(x)$ to obtain $h_{\mathrm{cal}}(x)$. These were then compared with the experimental data $h_{\mathrm{obs}}(x)$. Simulations, based on a 'misfit' parameter which is related to the strain induced by inclusions, were carried out for alloys having between 2 and 18% (by volume) of Si after precipitation. Good agreement between theory and experiment was obtained and the stored energy density of the aluminium matrix was found to be $4.5\,\mathrm{kJ\,m^{-3}}$ per vol. %Si.

10.3. Integral-breadth methods

Improved algorithms and software for pattern decomposition and the availability of good quality data from high resolution diffractometers have resulted in a revival of interest in the use of the integral breadth β in microstructural analysis. An advantage over the Warren–Averbach approach is that, in principle, methods based on β can be applied to data for any crystal system, but in practice the results can be inaccurate for materials with low symmetry and large unit cells. This is due to the problem of obtaining meaningful line-profile parameters for severely overlapped reflections, but the situation may well change as maximum entropy and other statistical methods are applied to the 'unscrambling' of diffraction maxima. A feature of the integral-breadth method is that only average values of microstructural parameters are obtained, which may be a disadvantage in some applications. Also, the analysis requires that an analytical function be ascribed to each reflection. Such a function (a) must clearly model the observed data as precisely as possible, (b) should allow for the breadths of convoluted functions to be readily separated and (c), ideally should have a physical significance. The line profile due to size effects is often assumed to be Lorentzian, which satisfies criterion (b), but not (a) and, in general, (c). The form of the

'strain profile' is frequently taken as Gaussian, which again does not necessarily accord with (a) or (c). Such assumptions can lead to the introduction of appreciable systematic errors and a more flexible function is the Voigtian, the convolution of Lorentzian and Gaussian functions, which was introduced into line-profile analysis by Langford (1978). It has been found in practice that most, though by no means all, symmetrical experimental line profiles can be modelled adequately by this function. It is then a straightforward matter to obtain the corresponding Lorentzian and Gaussian components and their d^* dependence. A detailed account of this procedure has been given by Langford (1992).

After removing instrumental contributions from the observed integral breadths, β_f^* (expressed in reciprocal units) can be interpreted in terms of structural imperfections. A useful overview of the nature of the microstructure of the sample is given by the Williamson–Hall plot (Williamson and Hall 1953; see also Langford 1992), β_f^* versus d^*, with the addition of *hkl* for each reflection. It is immediately apparent from this plot if there are both d^*-independent and d^*-dependent contributions to line breadths, since for the former β_f^* is the same for all orders of a reflection. It is also evident, from the scatter in β_f^*, whether or not there is a direction- or *hkl*-dependence. This can be due to the effects of domain shape, to lattice 'mistakes' or to anisotropy of elastic constants. The interpretation of Williamson–Hall plots has been discussed by Langford (1992) and their main purpose is to determine a strategy for further analysis of the data in terms of microstructural properties.

A straightforward application of the integral-breadth method, by using Voigt function, is the study by Guillou, Auffrédic and Louër (1994) of CeO_2 obtained from the oxide nitrate hydrate. From a Williamson–Hall plot, β_f^* was found to increase linearly with d^*, with little scatter, and the approximation introduced by Halder and Wagner (1966) [see also equation (A.11)] was used to obtain the Lorentzian and Gaussian components of line-profile breadths. Parameters for 16 reflections were used in the analysis and it was demonstrated that on average the crystallites were spherical, with a mean diameter of 276 (7) Å, and that there was small, but significant distortion of the lattice, equivalent to a root-mean square strain of 2.78 (7) $\times 10^{-4}$. The precision of these results, amounting to a few percent, is typical of analyses based on the integral breadth, if data from a large number of reflections are available.

In a study, by using neutron diffraction, of pre-reaction microstructural changes occurring in $Ca(OD)_2$ during heating, Chaix-Pluchéry *et al* (1983) used Williamson–Hall plots, based on different orders of $h00$, $h0h$ and $00l$ reflections, to demonstrate the presence of anisotropic microstrains. With increasing temperature, a sudden decrease of strain in $00l$ planes was observed. This selective effect was interpreted as being due to the formation of water molecules and to slight structural changes prior to decomposition into CaO. An example of the complementary use of X-ray and neutron diffraction is the study by Percheron-Guégan *et al* (1980) of $LaNi_5$ with partial replacement of Ni by Al or Mn, to form intermetallic compounds used for hydrogen storage. Neutron data obtained at the Institut Laue-Langevin, Grenoble, provided structural information and high resolution X-ray data were used to investigate microstructural properties. A large number of samples were studied and Williamson–Hall plots provided an ideal means of displaying the trends in microstructural changes due to different Al or Mn dopant concentrations. In general, significant size and strain effects with marked direction dependence were observed, but for some concentrations the broadening due to imperfections was found to be 'isotropic'.

A different use of the method was the investigation by Langford *et al* (1993) of the microstructure of ZnO powder obtained by thermal decomposition of the oxalate hydrate $ZnC_2O_4.2H_2O$. From a Williamson–Hall plot the dependence of breadth on d^* and *hkl* indicated that the line broadening was due to a combination of crystallite size and stacking

faults, which had not been reported previously for ZnO. By using line-profile data for 27 reflections it was ascertained that the crystallites were prismatic, with a mean height $\langle H \rangle$ of 351 (9) Å and diameter $\langle D \rangle$ of 404 (7) Å, and that the stacking-fault probability was 0.011 (3), corresponding to between one and two fault planes per crystallite, on average. The variation of the microstructure of ex-oxalate ZnO with temperature of formation was also studied (Auffrédic *et al* 1995) and it was found that $\langle H \rangle$ and $\langle D \rangle$ both increased significantly with temperature, whereas there was little change in the ratio $\langle D \rangle / \langle H \rangle$. The corresponding specific surface areas, of importance when ZnO is used as a catalyst, were compared with values obtained by the nitrogen-absorption (BET) method.

Diffraction broadening due to lattice distortion is negligible in the above examples; the treatment of cold-worked tungsten, for which 'strain' broadening is appreciable and 'isotropic' (does not vary with lattice direction), has been considered by Langford (1992). The Williamson–Hall plot for this sample is linear, with negligible scatter and a small intercept. The shape of the diffracting domains is thus spherical, on average, with an average diameter of about 850 (100) Å, and the rms strain was found to be $3.0\,(1) \times 10^{-3}$. These effects are probably due to dislocations, when the dislocation density would be $\sim 4 \times 10^{13} m^{-2}$, but a more detailed analysis of the data is not possible by means of the integral breadth method. An interesting result of this study is that, by using a Voigt function to model $f(x)$, the line profiles due to domain size are predominantly Gaussian and those due to lattice distortion tend to be Lorentzian, the reverse of the customary assumptions for these effects. In cases where line broadening due to lattice distortion is not approximately 'isotropic', data for two or more orders of several reflections are required in order to ascertain the direction dependence of microstrain (e.g. Langford *et al* 1986).

Fiévet *et al* (1979) used X-ray diffraction and electron microscopy to examine in detail the microstructure of samples of non-stoichiometric nickel oxide ($Ni_{1-x}O$) prepared at temperatures in the range 200 to 400°C. For the purpose of comparing the behaviour of different samples, values of *FWHM* were used for Williamson–Hall plots, rather than integral breadths, to give an indication of crystallite size and microstrain. It was found that the cell dimension differed from that of bulk NiO by an amount which varied as the inverse of the crystallite size, but which was insensitive to the degree of non-stoichiometry. A marked inverse correlation between the estimated size and microstrain was also observed.

11. Dynamic and non-ambient diffraction

11.1. Time- and temperature-dependent powder diffraction

The applications discussed in sections 5 to 10 have mainly been concerned with experiments carried out under constant ambient conditions and on stable phases, but the availability of high power radiation sources and the development of position sensitive detectors (PSDs), combined with efficient data storage, have resulted in powder diffraction being used increasingly to investigate changes occurring in crystal structure and microstructure due to some external perturbation. The choice of radiation depends on the speed and nature of the reaction or process of interest. In general, changes in all the diffraction line-profile parameters in equation 2.1 and defined in section 2.1 can be of interest in studies of dynamical phenomena and applications to a wide variety of materials have been reported, including dynamic studies of biological substances.

Due to the possibility of using diffraction techniques to identify materials arising from thermal- or time-dependent events, temperature- and time-resolved diffractometry

offer several advantages over conventional techniques for thermal analysis. These include differential scanning calorimetry (DSC) and thermogravimetric analysis (TG), which are used to measure the energy and weight changes involved in chemical and structural modifications as a function of temperature, time dependence and heating rates. Due to their complementarity, these and other analytical techniques are in fact often combined with powder diffraction. For example, Fawcett *et al* (1985) reported simultaneous analyses of *in situ* reactions, by combining DSC, mass spectrometry (MS) and X-ray powder diffraction to characterize materials heated in controlled atmospheres. The capability of identifying solid phases as they are formed in a reaction chamber can contribute to an understanding of reaction processes. Additionally, structural and microstructural changes during phase transformations can be monitored, if the data are of sufficiently high quality. This has been demonstrated by the repetitive application of the Rietveld method to neutron data from a sample of La_2NiO_4, collected at intervals of 3 minutes as the temperature was increased from 3 to 275 K at a rate of 0.33 K min^{-1}, in order to explain an 'anomalous' change in sample microstrain (Rodriguez-Carvajal, Martinez and Pannetier 1988). With the very narrow instrument function available with synchrotron sources, Rodriguez *et al* (1990) observed the tails of $h00$ reflections from $YBa_2Cu_3O_7$ to have an asymmetry towards higher angles, whereas the $0k0$ reflections had a corresponding asymmetry towards lower angles. This effect corresponds to martensitic strain energy in the crystal structure, resulting in a phase transiton near 580°C which causes (110) twinning. An important feature of diffractometry is that experimental Bragg intensities are related to the diffracting volume of the sample (equation 2.1) and they can therefore be used for obtaining kinetic data, provided that the data acquisition times are short enough compared to the time required to complete the reaction or transformation. For rapid reaction kinetics, shorter acquisition times are required and experiments in 'real' time must be carried out. Considerable use has been made of these developments; powder diffraction studies on a timescale of milliseconds, by using synchrotron sources, have been described by Pennartz *et al* (1992) and time- and temperature-resolved experiments have been reported extensively with neutron diffraction (Pannetier, 1986a, b). Neutron scattering has the advantage of low absorption cross-sections for most elements and a sample can be enclosed in a controlled environment (furnace, cryostat, reaction chamber or pressure cell) with little loss of intensity. Similarly, the high flux 'white-beam' X-rays from synchrotron sources can be used to advantage in energy-dispersive diffraction (EDD) (e.g. Clark *et al* 1994).

11.1.1. Time-dependent diffractometry with conventional X-ray sources. The use of 'real-time' powder diffraction for understanding dynamical processes in solids is well established. For relatively slow processes, conventional X-ray sources and detectors can be used, e.g. the transformation of nickel hydroxide nitrate to nickel hydroxide by hydrolysis has been studied by line-profile analysis, to obtain microstructural data (Le Bail and Louër 1980). Changes in crystallite-size distributions (section 10.2.1) for both the initial and final phases revealed interesting features of the phase transformation and of crystallite growth in $Ni(OH)_2$. An increase in the mean of the distribution, and hence the average crystallite size, occurred in the initial stage, due to removal of the smaller crystallites. Very small crystallites of the hydroxide ($\sim$ 30Å) were formed simultaneously and, by obtaining the size distribution for the final phase, their growth due to coalescence was determined as a function of time. Diffusion during desorption processes in microporous materials has been studied by sequential powder diffraction, with data collection times varying from 100 minutes to 6 days (Mentzen 1988), and the formation of hydrides has been investigated *in situ* by

Notten *et al* (1994). For this purpose a cell was designed for monitoring the absorption or desorption of hydrogen and at the same time obtaining the powder diffraction patterns for hydrided or dehydrided intermetallic compounds. The cell was used to study hydride formation based on $LaNi_5$ over a pressure range up to 10 bar and under both dynamic and steady-state conditions. Dynamic diffraction using a PSD has also been used to characterize reaction kinetics and to obtain sequential powder diffraction patterns for biological systems which had been subjected to external stimulations (electrical, chemical, etc.). For example, the stability of the myelin lattice following nerve stimulation was monitored by means of changes in the intensity of different orders of a reflection in the low-angle scattering region (Padrón, Mateu and Requena 1980; Morán and Mateu 1983), by using the PSD described by Gabriel and Dupond (1972). PSDs have also been used for determining the kinetic behaviour of solid-state reactions under isothermal conditions, e.g. the transformation at room temperature of β-Cs_2CdI_4 to the stable α-phase (Plévert *et al* 1989). In this study, the dramatic influence of preferred orientation on the quantitative interpretation of the reaction process clearly demonstrated that care must be taken to avoid this effect. (See section 4.5.1.) The technique has also been applied to following solid-state reactions, such as the formation of $YBa_2Cu_3O_6$ at 710°C from a mixture of $BaCO_3CuO$ and Y_2O_3 (Forster *et al* 1994). An interesting use of rapid *in situ* analysis to study the phenomenon of melt-texturing of high-T_c superconductors was reported by Snyder (1994). Powder diffraction patterns were collecting by using a PSD capable of collecting data over a range of 10° in one second. In addition, an optical-microscopy hot stage was used to observe the formation of microstructures, which was monitored with a video camera. By means of this system, the mechanism and kinetics of texturing, as well as the dynamics of the formation of the textured microstructure, were established.

A number of *in situ* dynamical studies of the thermal behaviour of materials by means of conventional X-ray sources and position sensitive detectors have been reported. A linear PSD with data collection over an angular range of 15° was used by Chayka and Göbel (1983) for a dynamical study of the γ–δ phase transformation in $NaAlO_2$ and of recrystallization phenomena in $TaSi_2$ thin films at high temperatures. The development of the linear PSD has led to the recording of diffraction data over a range of up to 10° in times down to a few milliseconds when studying oscillatory phenomena. An elegant application of this rate of data collection was demonstrated by Zorn, Wersing and Göbel (1985), where a reflection from piezoelectric PZT was recorded dynamically as a function of an applied electric field. This oscillated at 100 Hz and the powder patterns for various values of field were stored in different channels of a multi-channel analyser. The resulting plot of peak position versus the magnitude of the field led to the complete determination of the electrostriction tensor. X-ray diffraction studies of pharmaceutical materials, by collecting data with a PSD at 5°C intervals while continuously heating the sample at 1°C min^{-1} (Fawcett *et al* 1886) and for the investigation of the melting and crystallization behaviour of polyethylene at 2°C intervals (Crowder *et al* 1986) have also been reported. Isothermal and non-isothermal experiments on drugs were carried out by Anwar and Barnes (1992). A curved position sensitive detector with an angular aperture of 120° (section 4.3.3) was used in a dynamical study of the thermal behaviour of cadmium hydroxide nitrate (Auffrédic, Plévert and Louër 1990) and of the transformation of zirconium hydroxide nitrate into the amorphous and tetragonal forms of zirconia (Bénard, Auffrédic and Louër 1993). In order to improve counting statistics, diffraction data for the latter were collected for 1000 sec at a heating rate of 10°C h^{-1}. Similarly, a conventional X-ray source was used for the study of the thermal decomposition of amorphous hydrous zirconia (Mamott *et al* 1988) and for the crystallization process occurring in thin amorphous films having the composition $CrSi_{2.57}$

(Pitschke *et al* 1994). Phase transitions in NH_4NO_3 have been studied from polycrystalline transmission samples by collecting diffraction data in a few minutes by means of a curved PSD (Wölfel 1983). The power of sequential thermo-diffractometry was also demonstrated by the detection of a subtle phase transition in copper hydroxide nitrate (Guillou, Louër and Louër 1994) and the technique played a major rôle in revealing an unexpected double valence change in cerium during the thermal decomposition of $CeK_2(NO_3)_6$ (Guillou, Auffrédic and Louër 1995). Structure refinement by the Rietveld method during *in situ* diffraction experiments was applied to a study of nickel-exchanged zeolite-Y catalysts by Thomas, Williams and Rayment (1988) and to the dehydration process of the zeolite thomsonite by Ståhl and Thomasson (1992). An improvement in time and temperature resolution with *in situ* X-ray diffraction was obtained by Engler *et al* (1988) in the case of continuously programmed heating. By using a 12 kW rotating-anode X-ray source and a 5 cm linear PSD, the data acquisition time was reduced to 10–30 s in a study of the thermal decomposition of dolomite, $CaMg(CO_3)_2$.

11.1.2. Dynamic diffraction with synchrotron sources. Many important chemical, physical and biological phenomena take place on a time-scale of nanoseconds or picoseconds, and the brightness of synchrotron sources may well bring such time resolution within the scope of X-ray diffraction studies. Already powder diffraction experiments with a time-cale of 2.5 ms have been described, by using a synthesized multilayered material to select the desired wavelength instead a standard crystal monochromator (Pennartz *et al* 1992). Powder diffraction patterns have in fact been obtained in less than a nanosecond by using X-rays emitted from a laser-produced plasma (Woolsey, Wark and Riley 1990). Noteworthy applications of time-resolved synchrotron data to the study of solid combustion reactions have been reported by Wong *et al* (1990). Phase transformations of highly exothermic, fast and self-propagating solid combustion reactions on a subsecond time-scale down to 100 ms, and in some instances to 10 ms, were studied for Ti, C and Ni systems.

An analysis of time-dependent line-profile shapes from CdO samples, obtained from the thermal decomposition of $CdCO_3$ powder, was carried out by means of the variance-range method (see Wilson 1962b) and by using a counting time of 1 to 2 s per step (Schoonover and Lin 1988). Rapid *in situ* EDD was used by Turrillas *et al* (1993) to obtain direct information on the kinetics of the tetragonal-to-monoclinic transformation in zirconia which had been synthesized by heating the hydroxides to 1300°C. The kinetics of the intercalation of cations in crystals of $MnPS_3$ in water by using real-time *in situ* X-ray diffraction was reported by Evans and O'Hare (1994). The reactions were monitored from ambient temperature to 60°C and the diffraction pattern was recorded over a d-spacing range of 20 to 4 Å in as little as 10 sec, allowing the direct observation of changes in the host lattice and the growth of the product phase. Synchrotron powder diffraction studies, based on the Rietveld method, of dehydration processes in the natural zeolites scolecite and mesolite have been reported, by using the INEL curved PSD for collecting data accumulated in 5 minutes (Ståhl and Hanson 1994). This detector was also used for on-line experiments, with data recorded at 5 minute intervals and at temperatures up to 100°C, to study chemical reactions occurring in wet pastes which had been made from a mixture of MgO and $MgCl_2$ aqueous solutions (Christensen, Norby and Hanson 1995). The crystalline reaction products observed were magnesium hydroxide and the basic hydroxide-chloride, and the reaction rates of these heterogeneous systems were found to be strongly dependent on the solution concentrations. *In situ* studies of the kinetics of the crystallization of metallic glasses on time-scales varying from minutes to milliseconds have also been made (Sutton 1994, Fischer *et al* 1994).

For *in situ* experiments there are clearly advantages in bringing together techniques which can be applied simultaneously. Dual measurements with synchrotron radiation involving powder diffraction and XAFS were made by Couves *et al* (1991) to follow the dehydration and reduction of the layered mineral aurichalcite, $Cu_{5-x}Zn_x(OH)_6(CO_3)_2$, when heated in air. This material is converted to a mixture of CuO and ZnO, the precursor of an active catalyst consisting of highly dispersed particles of copper supported by ZnO. There is little change in the structure of the CuK absorption spectrum as aurichalcite is calcined, in contrast to the powder diffraction pattern, which alters dramatically as the oxides of Cu and Zn are formed. Reduction, on the other hand, affects Cu rather than Zn and this metallization was seen vividly in the XAFS data. A differential scanning calorimeter with a temperature range of 77 to 873 K has also been developed for use in combination with either time-resolved X-ray scattering or high-resolution energy-dispersive powder diffraction studies (Bras *et al* 1995).

11.1.3. Dynamic diffraction with neutron sources. Although neutron powder diffraction does not have a temporal resolution comparable to that available with synchrotron sources, the specific properties of the neutron make it a unique tool for investigating phase changes in solids. The potential for combining time-resolved powder diffraction and neutron scattering in materials science are numerous (see, for example, Pannetier 1986a). Diffraction patterns can often be recorded in a few minutes. Examples of earlier studies are intercalation of gaseous ND_3 and liquid pyridine in TaS_2 (Riekel and Schöllhorn 1976; Riekel and Fischer 1979), the replacement of NH_3 by ND_3 in TaS_2 (Riekel 1978), cathodic reduction of TaS_2 in K_2SO_4/D_2O solution (Riekel, Reznik and Schöllhorn 1979) and hydrothermal crystallization of amorphous iron(III) hydroxide (Christensen, Convert and Lehmann 1980). Polymorphic phase transformations and ranges of stability in lithium iodate have been thoroughly investigated by Crettez *et al* (1987). Since single crystals twin, crack and assume a whitish colour due to decrepitation at the transition, powder samples were used in neutron-diffraction experiments and transition temperatures were found to be strongly dependent on particle size. The behaviour of the intermetallic hydride $LaNi_{4.5}Al_{0.5}D_x$ was studied by *in situ* neutron powder diffraction throughout an electrochemical deuterium charge–discharge cycle (Latroche *et al* 1992), when unexpected phases with non-equilibrium cell parameters related to the discharge rate were detected. The evolution of neutron diffraction patterns, obtained at 10 minute intervals, for γ-MnO_2 during discharge in an alkaline electrolyte (figure 12), has been described by Chabre and Pannetier (1995). Superimposed on the high background arising from the silica vessel and the KOD liquid electrolyte, new Bragg reflections from pyrochroite $Mn(OH)_2$ in the final stage of reduction were observed for samples containing structural-defect concentrations, indicating a partial breakdown of the γ-MnO_2 lattice. This work demonstrated that the rechargeability of alkaline MnO_2 batteries is limited by the presence of structural imperfections. The hydration reaction of the hemi-hydrate $CaSO_4.\frac{1}{2}H_2O$ to form gypsum $CaSO_4.2H_2O$ was also followed by neutron diffraction at different temperatures (Christensen, Lehmann and Pannetier 1985). Analysis of the data supported the view that hydration passes through the formation of an intermediate gel phase. The effect of the additives $CaCl_2$ and $CaBr_2$ on the reaction between $Ca_{12}Al_{14}O_{33}$ and water was also investigated by the same technique (Christensen, Fjellvåg and Lehmann 1988). Real-time neutron diffraction measurements during the formation of superconducting phases of the Bi(Pb)-Sr-Ca-Cu-O system were reported by Aldica *et al* (1993). Patterns were recorded every 3 minutes and multiphase Rietveld refinements were applied. The power of neutron diffraction in the investigation of hydration/dehydration of solids has thus been

clearly demonstrated. The high incoherent background arising from hydrogeneous samples provides a straightforward measure of the proton content of the material being investigated. It is then possible to measure simultaneously the composition and structural features of the samples. This property of neutron diffraction has been used in a number of studies e.g. the dehydration of $WO_3.\frac{1}{2}H_2O$ (Pannetier 1986a) and $Fe_2F_5(H_2O)_2$ (Pannetier 1986b), the dehydroxylation of kaolinite in the range 440–600°C and the initial stages of mullite formation at 950–1000°C (Collins, Fitch and Catlow 1991) and the thermal decomposition of cobalt acetate tetrahydrate (Grimes and Fitch 1991).

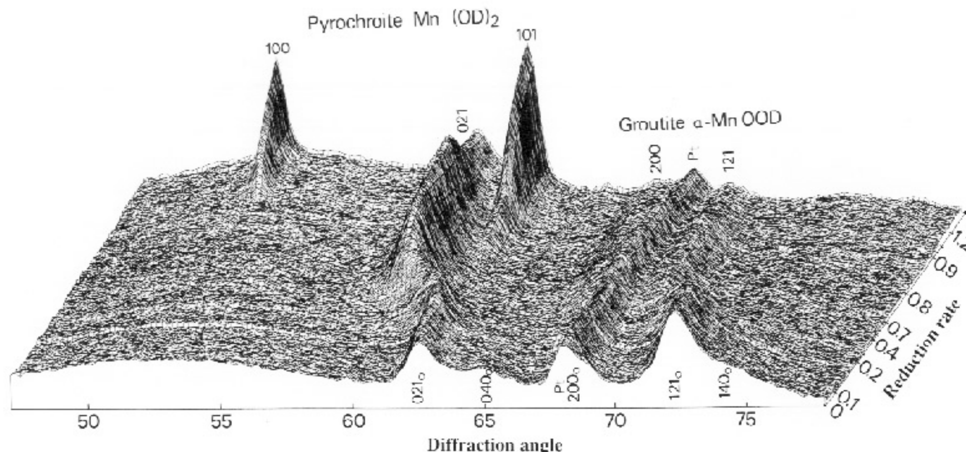

Figure 12. Evolution of neutron powder diffraction pattern for a commercial γ-MnO_2 sample during *in situ* electrochemical reduction ($\lambda = 2.51$ Å; recording time of 10 minutes for each pattern) (Chabre and Pannetier 1995).

11.2. High pressure diffraction

Materials subjected to high pressure undergo a variety of structural changes which can give rise to dramatic changes in their physical properties. The determination of crystal structures, the study of phase transitions and the measurement of compressibility and other properties at high pressure are thus of considerable interest in materials science. High-pressure experiments are carried out with single crystals (e.g. Sowa *et al* 1990), but these are limited by experimental considerations and by pulverizing phase transitions to pressures of about 10–20 GPa (100–200 kbar). The study of the behaviour of materials at non-ambient pressure by means of powder diffraction, on the other hand, has been a growth area since the late 1970s. This has largely been due to the availability of 'dedicated' synchrotron sources, with a corresponding improvement in instrument resolution (e.g. Bourdillon *et al* 1978), and to advances in the design of detectors (section 4.3) and pressure cells (section 4.4.3).

As noted in section 4.4.3, studies at non-ambient pressure can be classified as low, medium or high, depending on the pressure cell used. An example of a low-pressure experiment using a gas-driven cell is the study by Hamaya *et al* (1986) of nucleation and growth processes in a pressure-induced first-order NaCl/CsCl-type phase transition in RbI. Neutron diffraction data were obtained at the Brookhaven National Laboratory reactor and the transformation was found to occur at a critical pressure of 0.35 GPa. The time

dependence of the intensity of selected reflections was monitored after a sudden increase or decrease of pressure relative to the critical value, to establish that the behaviour of RbI accords with the standard model for nucleation and growth. In the medium-pressure range, Häusermann, Daghoogli and Sherman (1990) used energy-dispersive diffraction (EDD) at the Daresbury Laboratory SRS to compare the performance of Bridgman, Drickamer and belt-type cells by measuring the compressibility of Cu at pressures up to 10 GPa. These authors later (1992) used a modified Drickamer cell to measure the compressibility of potassium at pressures to 6.1 GPa. The behaviour of alkali metals is of particular interest, since it is close to that of 'ideal metals', and the value of the bulk modulus obtained for potassium was in good agreement with that derived from the anharmonic theory of crystalline lattices.

The cubic-anvil cell SAM-85 at the NSLS, Brookhaven, (section 4.4.3) has been used extensively to study the behaviour of perovskites and other minerals at temperatures and pressures which are typical of conditions in the Earth's lower mantle. By laboratory simulation of this environment to study phase transitions, equations of state and other quantities, an evaluation of the properties of mantle minerals, particularly the bulk and shear moduli and density, can be undertaken. Also, complementary data to those derived from discontinuities in seismic wave velocity at transition zones in the mantle can be obtained. Minerals in the lower mantle are known to be dominated by $(Mg, Fe)SiO_3$ perovskites, which undergo a series of phase transitions with increasing pressure and temperature, these being associated with dramatic changes in physical properties. By using EDD, Wang *et al* (1991) demonstrated that $MgSiO_3$ transforms to another orthorhombic perovskite at 7.3 GPa and 327°C and obtained the variation of unit-cell dimensions and volumetric expansion with temperature to 980°C. The implications of these results for studies of the Earth's lower mantle, and in relation to the work of others in this field, are discussed by Weidner and Zhao (1992). A similar study by Wang and Weidner (1994) of the thermoelasticity of the $CaSiO_3$ perovskite to about 12 GPa provided evidence for a chemically homogeneous mantle, but subsequent measurements of the unit-cell volume of the more representative mineral $Mg_{1-x}Fe_xO_3$ ($x = 0.0$ and 0.1) indicated that it is unlikely that the lower mantle has a perovskite stoichiometry (Wang *et al* 1994). These EDD experiments provided information on changes in unit cell dimensions, and hence volume, with pressure and temperature. An extension of this work, by using fixed-wavelength radiation and the angle-dispersive mode with the MAX-80 cubic-anvil press (section 4.4.3) at the Tsukuba synchrotron source the 'Photon Factory', was an investigation of the structure of neighborite, $NaMgF_3$, at ambient and under high-pressure conditions (Zhao *et al* 1994). Detailed information on the structural behaviour of this perovskite at high pressure, obtained by the Rietveld method, demonstrated the power of angle-dispersive methods (see below) and also that analyses based solely on changes in unit-cell parameters should be interpreted with caution.

Other minerals studied under high-pressure and high-temperature conditions, by using the SAM-85 cubic-anvil press at the NSLS, include the α (olivine), β and γ (spinel) phases of Mg_2SiO_4, also of relevance in interpreting mantle discontinuities (Meng *et al* 1993). Diffraction studies in the medium-pressure regime were amongst the earliest applications of the time-of-flight technique with pulsed neutral sources (Jorgensen 1990). Recent examples using the LANSCE source (section 4.1.3) are pressure-induced phase transitions in Ca/Al-doped cristobalite (Parise *et al* 1994a) and hydrogen bonding in brucite, $Mg(OD)_2$ (Parise *et al* 1994b). In both cases, structures were refined by means of the Rietveld method. Also, by using the modified Bridgman cell discussed in section 4.4.3 and the ISIS spallation source, Nelmes *et al* (1993, 1995) have extended the pressure range to 10 GPa or more. Precise measurements were made of the dependence on pressure of the structures of deuterated ice

VIII and boron carbide.

Typical of the numerous EDD experiments in the high-pressure régime is the study by Olsen, Gerward and Benedict (1985), carried out at the HASYLAB synchrotron source, Hamburg, of a phase transition in cubic UN, one of the actinide pnictide compounds, whose magnetic properties have been studied extensively. A maximum pressure of 34 GPa was achieved and the characteristics of a new rhombohedral phase, UN III, which appeared at 29 GPa, were obtained. ThN, another actinide pnictide, was studied at pressures up to 47 GPa (Gerward *et al* 1985), but no phase transition was observed, even though this compound is related both structurally and chemically to UN. By using a DAC phase transitions in W and Mo were observed by Ruoff (1992) at pressures in the range 200–300 GPa and a maximum pressure of at least 438 GPa was obtained, well in excess of the calculated static pressure at the centre of the Earth.

Until the early 1990s, EDD had been used for the greater part of high-pressure work. The use of a fixed scattering angle makes it easier to design and accommodate pressure cells and the intense 'white beam' from synchrotron sources in particular compensates for small sample volumes. Data collection can then be rapid and kinetic studies at high pressure are feasible, but the resolution attainable with EDD is relatively low and most experiments have been confined to the measurement of cell dimensions or to classifying the phases present. However, some refinements of crystal structure have been undertaken. For example, Yamanaka and Ogata (1991) used synchrotron radiation at the Photon Factory and a diamond anvil cell (DAC) to obtain the structures of the hexagonal and tetragonal polymorphs of GeO_2 at temperatures up to 580°C and pressures to 10 GPa. Line-profile parameters were obtained by means of pattern decomposition, by fitting pseudo-Voigt functions to the experimental data. In addition to structure refinement based on integrated intensities, cell dimensions were used to establish the pressure dependence of compressibility and thermal expansion coefficients. Yamanaka, Sugiyama and Ogata (1992) then used EDD to carry out a detailed investigation of the hexagonal-tetragonal transformation which GeO_2 undergoes at 3.0 GPa. For this purpose, spectra were recorded at 15 minute intervals, with temperatures in the range 220 to 380°C. Pseudo-Voigt functions were again used to model line profiles and, from the integrated intensities, the transition rate for the transformation and the activation energy were obtained.

It was the introduction of the image-plate 2-dimensional detector (Fujii *et al* 1988), with a dynamic intensity range of $\sim 10^5$, which transformed high-pressure research; high-resolution angle-dispersive experiments could then be carried out with synchrotron radiation, since the problem of small sample volume, inherent with DACs, is then overcome by recording and integrating the intensity around a substantial part of each Debye–Scherrer ring. Software for analysing image-plate data was developed at the Daresbury Laboratory SRS (section 4.3.4) and one of the first materials to be investigated there by using this technique was InSb (Nelmes *et al* 1993a), a III-V semiconductor which had previously been studied extensively by EDD at high pressures (e.g. Vanderborgh, Vohra and Ruoff 1989). A short wavelength (0.4445 Å) was used to minimize the harmonic content of the diffraction pattern, to give a high peak-to-background ratio and to confine the pattern to relatively low angles (figure (5(a)). Three phases were detected at pressures above 2 GPa and their structures were refined by means of the multiphase Rietveld method. One of these phases, InSb-IV, was subsequently shown to have a site-ordered orthorhombic superlattice which is stable over a wide range of pressure and temperature (Nelmes and McMahon 1995), a remarkable phenomenon for a semiconductor of this type. One of the strongest superlattice reflections from the *Cmcm* superstructure of InSb-IV, the (112), can clearly be seen in figure 5(b), for which the data were obtained at 5.1 GPa. Three weaker superlattice reflections, (110),

(111) and (113), with intensities $< 0.1\%$ of the strongest lines, are just visible in the pattern collected for 8 hr near the In K-edge, where the difference in scattering between In and Sb is enhanced by resonant scattering (anomalous dispersion; section 8). These reflections are no longer detectable away from the K-edge and the intensity of the (112) is also reduced significantly. The changes in intensity show the structure to be site-ordered and the detection of the (110) proved to be crucial in determining the correct space group. This work was part of a systematic study of the dependence of structure on pressure for numerous II-VI, III-V and group IV semiconductors. The ability to detect very weak reflections, the acquisition of data of sufficient quality to carry out structure refinement routinely and the use of resonant scattering experiments led to the discovery of several new phases for these materials and to a substantial revision of phase diagrams reported previously. For example, the well-known transition in CdTe from the zincblende to the NaCl phase was found to involve two closely-spaced transitions, from the zincblende to the cinnabar structure at ~ 2.7 GPa and then from cinnabar to NaCl at ~ 3.7 GPa (Nelmes *et al* 1993b). Previously, the structure of cinnabar (HgS) had been regarded as only occurring in mercury chalcogenides. Similarly, new orthorhombic phases were observed for Si between 13.2 GPa and 15.6 GPa (McMahon and Nelmes 1993) and also for GaSb at ~ 7 GPa (McMahon *et al* 1994), rather than the β-tin structure reported previously. McMahon and Nelmes (1995) have summarized the results of these and other structural studies of tetrahedrally-coordinated semiconductors at high pressure. The use of synchrotron radiation for high pressure research in general is reviewed in Nelmes and Häusermann (1992).

Recent examples of the innumerable high-pressure experiments carried out by means of conventional X-ray sources and a DAC are studies of TiO_2 (anatase) (Haines and Léger 1993) and cotunnite-type ZrO_2 (zirconia) (Haines, Léger and Atouf 1995) up to a pressure of 49 GPa. A transition from anatase to the orthorhombic α-PbO_2 structure at pressures greater than 5.4 GPa was observed for the former, which transformed to a monoclinic phase above 10 GPa. Only the cell dimensions were obtained in this experiment and the direction dependence of compressibility and the pressure-volume relationship (equation of state) were obtained for all three phases. In the second experiment, the structure of ZrO_2 was refined *in situ*, by using the Rietveld method, at different pressures for both heated and unheated samples. For the former, an irreversible transition to the cotunnite phase began above 25 GPa and this phase was found to be stable over a large pressure-temperature domain. This was the first reported refinement of a cotunnite-type oxide and the results resolved discrepancies in the literature concerning the behaviour of heated and unheated zirconia at high pressure.

11.3. Magnetic X-ray powder diffraction

Although X-ray diffraction is being used increasingly to study antiferromagnetism in single crystals, measurements on powder samples have, until recently, been restricted to neutron scattering. This is due to the relative weakness of magnetic diffraction peaks compared with fluorescence and electronic scattering. However, by using synchrotron radiation and a high energy discrimination, Collins *et al* (1995) exploited the strong uranium M_4 resonance in UO_2 to detect the magnetic 102 reflection at a temperature $T \sim 23$ K, well below the Néel point T_N. The peak disappeared after transformation to the paramagnetic phase ($T > T_N$), the energy distribution of the magnetic scattering exhibited a sharp resonance and the magnetic scattering cross-section at resonance agreed well with the predicted value, thus confirming the magnetic origin of the observed peak. This first observation of magnetic scattering from a powder sample was based on low resolution data with a poor signal-to-

noise ratio, obtained from an unfocused beam and a simple bending magnet at the Daresbury SRS. Fluxes from undulators at other machines will in future be some three to five orders-of-magnitude greater and it is likely that X-ray powder diffraction will, at least for actinide compounds, be a valuable technique in magnetic studies.

12. Concluding remarks

It will be clear from the foregoing that progress in powder diffraction during the past twenty years or so has been substantial. The main reason for its current status as one of the most versatile and widely used techniques available to material scientists is the advance in procedures for recovering 3-dimensional information on the structure and microstructure of materials from 1-dimensional powder diffraction data. The development of high resolution instruments and the advent of high-intensity sources of radiation have contributed to this development and, in common with most branches of science, powder diffraction has benefited considerably from the revolution in computing facilities during the period reviewed. However, if any one event can be singled out as the cause of the veritable renaissance in powder diffraction during the 1970s, this has to be the introduction of the Rietveld method for refining crystal structures. The Rietveld method was a milestone in the quest to deal with line-profile overlap, but it also had the effect of attracting scientists of international standing in other fields, whose contribution to powder diffraction has since been incalculable. Indeed, the door has been opened to solving crystal structures *ab initio* from powder data and over a hundred examples have been reported in the literature to date. Further impetus was acquired by the discovery and development of new materials, such as high T_c ceramics, in which powder diffraction played a key rôle. In addition to the introduction of new investigative tehniques, there has been progressive enhancement of earlier 'traditional' applications. As a result, the type and quality of information obtained have advanced considerably in all branches of powder diffraction.

What of the future? Most of the techniques discussed in this review are becoming increasingly accessible through public-domain programs and commercial software marketed by manufacturers of diffraction systems. There is an on-going program for instructing powder diffractionists world-wide in modern methods and practices, notably by the ICDD, the Commission on Powder Diffraction (CPD) of the IUCr and the European Community. As a consequence of these developments, there should be a general improvement in the quality of both the routine characterization of materials and fundamental research. Additionally, there will continue to be significant progress in *ab initio* structure analysis. The impact of this important tool for studying the structures of materials which are only available in powder form may well parallel that of structure solution by means of single-crystal data from the 1950s onwards. However, the most significant advances in furthering basic science are likely to involve existing and new-generation high-intensity synchrotron sources. Increasing use will be made of diffraction methods in non-ambient diffraction, in order to follow structural changes and study materials at higher pressures and on shorter time-scales. In so far as structural and microstructural studies are concerned, the main thrust will doubtless be in the 'unscrambling' of overlapping peaks by means of maximum entropy and other methods. For the latter, future work will certainly involve the simulation of diffraction patterns due to various combinations of structural imperfections. Perhaps the most radical development will be in measurements made on individual grains of a polycrystalline sample, thus bringing together the techniques of single-crystal and powder diffraction.

This review was made possible through support from the Engineering & Physical

Science Research Council, formerly the Science & Engineering Research Council, in the form of a Senior Visiting Fellowship (DL), and from the University of Rennes (Visiting Professorship; JIL). We express our grateful thanks to these bodies. We are also indebted to Professor R L Snyder for his constructive comments on the review and for his critical reading of the text. Figure 7 and table 2 are published by courtesy of the International Centre for Diffraction Data (publishers of the Powder Diffraction File), 12 Campus Boulevard, Newtown Square, Pennsylvania, USA, and we are indebted to the Oxford University Press for permission to reproduce figure 10.

Appendix. Analytical functions commonly used to model powder diffraction line profiles

x	Distance from position of maximum intensity; $2\theta - 2\theta_0$ in the angle-dispersive case, $E - E_0$, $d - d_0$, etc., for energy-dispersive experiments.
$\Phi(0)$	Maximum intensity of line-less-background
$2w$	Full width at half maximum intensity (*FWHM*)
β	Integral breadth (area/maximum intensity)
ϕ	Shape factor ($2w/\beta$)
L	Lorentzian function, given by

$$\Phi(x) = \Phi(0)\frac{w^2}{w^2 + x^2} \tag{A.1}$$

with

$$\beta = \pi w \qquad \text{and} \qquad \phi = 2/\pi \tag{A.2}$$

G Gaussian function, given by

$$\Phi(x) = \Phi(0)\exp(-\pi x^2/\beta^2) \tag{A.3}$$

with

$$w = (Ln2/\pi)^{1/2}\beta \qquad \text{and} \qquad \phi = 2(Ln2/\pi)^{1/2}. \tag{A.4}$$

(a) Pearson VII function (Hall *et al* 1977)

The Pearson VII function is simply L^m, where m is the Pearson VII index. The function is easy to compute, but has the disadvantage that the convolution of two such functions is not a Pearson VII unless $m = 1$ or $m = \infty$.

$$\Phi(x) = \Phi(0)\frac{1}{(1 + Cx^2)^m} \tag{A.5}$$

where

$$C = \frac{2^{1/m} - 1}{w^2} \qquad \beta = \frac{\pi 2^{2(1-m)}\Gamma(2m-1)w}{(2^{1/m}-1)[\Gamma(m)]^2} \tag{A.6}$$

and Γ is the gamma function.

(A.5) reduces to a Lorentzian for $m = 1$ and tends to a Gaussian as $m \to \infty$. (For $m = 5$ the area of the Pearson VII is about 5% less than for a Gaussian with the same $I(0)$ and the integral breadths differ by the same amount.) Line profiles with $m < 1$ are regarded as being 'super-Lorentzian' (Wertheim *et al* 1974). m is normally refined in an application which involves modelling of line profiles, but sometimes it is arbitrarily fixed. For example, the case of $m = 2$ is known as a 'modified Lorentzian' and $m = 1.5$ as an 'intermediate Lorentzian'.

(b) Voigt function (Langford 1978)

The Voigt function is the convolution of one or more Lorentzian and Gaussian functions and the convolution of Voigt functions is also Voigtian.

$$\Phi(x) = \Phi(0)\beta\beta_G^{-1}\,\mathrm{Re}\{w(z)\} \tag{A.7}$$

with

$$z = \frac{\sqrt{\pi}x}{\beta_G} + \mathrm{i}k \tag{A.8}$$

and

$$k = \frac{\beta_L}{\sqrt{\pi}\beta_G} \tag{A.9}$$

where k is the Voigt parameter, β_L and β_G are the integral breadths of the Lorentzian and Gaussian components and $\mathrm{Re}\{w(z)\}$ is the real part of the complex error function. [Langford (1992) gives an algorithm for computing $w(z)$.] β_G is given by

$$\beta_G = \beta\exp(k^2)[1 - \mathrm{erf}(k)] \tag{A.10}$$

and β_L can then be obtained from (A.9). Halder and Wagner (1966) introduced the following approximate relation between the integral breadths:

$$\beta^2 \sim \beta_L\beta + \beta_G^2. \tag{A.11}$$

Values of β from (A.11) are accurate to within about 5%, β being less than the true value for a given k (Langford 1978). Ahtee *et al* (1984) have shown that

$$\phi = \frac{E(1 + Ak + Bk^2)}{(1 + Ck + DK^2)} \tag{A.12}$$

where $A = 0.9039645$, $B = 0.7699548$, $C = 1.364216$, $D = 1.136195$ and $E = 2(Ln2/\pi)^{1/2} = 0.9394372$. (A.12) is an approximation, but the maximum difference from the exact value is only 0.16% (at $k = 0.15$). When modelling line profiles, the observed quantities are β and ϕ. k can then be obtained from the inversion of (A.12).

Lorentzian and Gaussian functions are clearly limiting cases of the Voigtian. From (A.2) and (A.4), the Voigt function can only be used to model diffraction line profiles if ϕ is in the range

$$0.6366 \leqslant \phi \leqslant 0.9394. \tag{A.13}$$

(c) Pseudo-Voigt function (Wertheim *et al* 1974)
The pseudo-Voigt function is the sum of a Lorentzian and a Gaussian in the ratio $\eta/(1-\eta)$,where η is the pseudo-Voigt mixing parameter. It is simpler to calculate than the true Voigt, since it does not involve the complex error function, but it again has the disadvantage that the convolution of pseudo-Voigt functions is not a pseudo-Voigt.

$$\Phi(x) = \Phi(0)[\eta L - (1-\eta)G] \tag{A.14}$$

and

$$\begin{aligned}\beta &= \eta\beta_L + (1-\eta)\beta_G \\ &= \eta\pi w_L + (1-\eta)(\pi Ln2)^{1/2} w_G.\end{aligned} \tag{A.15}$$

When modelling line profiles w_L and w_G are usually made equal, but there is no reason

a priori why they should not have different values. The pseudo-Voigt also includes the Lorentzian ($\eta = 1$) and Gaussian ($\eta = 0$) functions as limiting cases. Again, line profiles with $\eta > 1$ are regarded as being 'super-Lorentzian'.

References

Adler T and Houska C R 1979 *J. Appl. Phys.* **50** 3282–7

Ahtee M, Nurmela M, Suortti P and Järvinen M 1989 *J. Appl. Cryst.* **22** 261–8

Ahtee M, Unonius L, Nurmela M and Suortti P 1984 *J. Appl. Cryst.* **17** 352–7

Aldica G, Mironova G M, Popa N C, Stoica A D and Stoica M G 1993 *J. Superconduct.* **6** 273–8

Allen F H, Bergerhoff G and Sievers R 1987 (eds) *Crystallographic Databases* (Chester: IUCr)

Altomare A, Burla M C, Cascarano G, Giacovazzo C, Guagliardi A, Molterni A G G and Polidori G 1995 *J. Appl. Cryst.* **28** 738–44

Altomare A, Cascarano G, Giacovazzo C and Guagliardi A 1994 *J. Appl. Cryst.* **27** 1045–50

Amelse J A, Arcuri K B, Butt J B, Matyl R J, Schwartz L H and Shapiro
A 1981 *J. Phys. Chem.* **85** 708–11

Amemiya Y 1995 *J. Synchr. Rad.* **2** 13–21

Andreev Y D 1994 *J. Appl. Cryst.* **27** 288–97

Andreev Y G and Lundström L 1994 *J. Appl. Cryst.* **27** 767–71

Antoniadis A, Berruyer J and Filhol A 1990 *Acta Cryst.* A **46** 692–711

Anwar J and Barnes P 1992 *Phase Transitions* **39** 3–11

Arndt U W 1992 *International Tables for Crystallography Vol. C, Mathematical, Physical and Chemical Tables* ed A J C Wilson (Dordrecht: IUCr/Kluwer) pp 543–52

Arnold H, Bartl H, Fuess H, Ihringer J, Kosten K, Löchner U, Pennartz P U, Prandl W and Wroblewski T 1989 *Rev. Sci. Instrum.* **60** 2380–1
Attfield J P 1990 *Nature (London)* **343** 46–9
—— 1992 *Accuracy in Powder Diffraction II* ed E Prince and J K Stalick *NIST Spec. Pub. No. 846* (Gaithersburg, MA: US Dept Commerce) pp 175–82
Attfield J P, Sleight A W and Cheetham A K 1986 *Nature* **322** 620–2
Auffrédic J P, Boultif A, Langford J I and Louër D 1995 *J. Amer. Ceram. Soc.* **78** 323–8
Auffrédic J P, Plévert J and Louër D 1990 *J. Solid State Chem.* **84** 58–70
Baerlocher C 1982 *XRS-82 The X-ray Rietveld system*, Inst. fur Krist., ETH, Zurich
—— 1984 *Proc. 6th Int. Zeolite Conf*, Reno, USA, 823–33
—— 1995 *The Rietveld Method* ed R A Young (Oxford: OUP/IUCr) pp 186–96
Ballon J, Comparat V and Pouxe J 1983 *Nucl. Instrum. Methods* **217** 213–16
Balzar D 1992 *J. Appl. Cryst.* **25** 559–70
Balzar D and Ledbetter H 1992 *J. Mat. Sci. Lett.* **11** 1419–20
—— 1993 *J. Appl. Cryst.* **26** 97–103
Balzar D, Ledbetter H and Roshko A 1993 *Powder Diffr.* **8** 2–6
Begum R, Hart M, Lea K R and Siddons D P 1986 *Acta Cryst.* A **42** 456–64
Bell A M T, Henderson C M B, Redfern S A T, Cernik R J, Champness P E, Fitch A N and Kohn S C 1994 *Acta Cryst.* B **50** 31–41
Bénard P, Auffrédic J P and Louër D 1993 *Powder Diffr.* **8** 39–46
Bénard P, Louër D, Dacheux N, Brandel V and Genet M 1994 *Chem. Mater.* **6** 1049–58
Bénard P, Louër M and Louër D 1991a *J. Solid State Chem.* **94** 27–35
—— 1991b *Powder Diffr.* **6** 10–15
Bénard P, Nord A G, Werner P E and Westdahl M 1992 *J. Solid State Chem.* **99** 290–6
Bendall P J, Fitch A N and Bender B E F 1983 *J. Appl. Cryst.* **16** 164–70
Benedetti A, Fagherazzi G, Enzo S and Battagliarin M 1988 *J. Appl. Cryst.* **21** 543–9
Bérar J F and Baldinozzi G 1993 *J. Appl. Cryst.* **6** 128–9
Bérar J F and Lelann P 1991 *J. Appl. Cryst.* **24** 1–5
Berg J E and Werner P E 1977 *Zeits. Krist.* **145** 310–20
Bergerhoff G and Brown I D 1987 *In Crystallographic Databases* ed F H Allen, G Bergerhoff and R Sievers (Chester: IUCr) pp 77–95
Bertaut E F 1949 *C.R. Acad. Sci. Paris* **228** 187–9, 492–4
—— 1950 *Acta Cryst.* **3** 14–18
Berti G 1993 *Powder Diffr.* **8** 89–97
Besson J M, Hamel G, Grima T, Nelmes R J, Loveday J S, Hull S and Häusermann D 1992 *High Press. Res.* **8** 625–30
Bish D L 1992 *Accuracy in Powder Diffraction II* ed E Prince and J K Stalick *NIST Spec. Pub. No. 846* (Gaithersburg MA: US Dept of Commerce) pp 154–64
Bish D L and Chipera S J 1988 *Adv. X-ray anal.* **31** 295–308
—— 1989 *Powder Diff.* **4** 137–43
Bish D L and Howard S A 1988 *J. Appl. Cryst.* **21** 86–91
Bish D L and Post J E 1993 *Amer. Miner.* **78** 932–40
Bish D L and Von Dreele R B 1989 *Clays and Clay Minerals* **37** 289–96
Blanton T N, Huang T C, Toraya H, Hubbard C R, Robie S B, Louër D, Göbel H E, Will G, Gilles R and Raftery T 1995 *Powder Diff.* **10** 91–5
Bley F, Calvayrac Y and Fayard M 1974 *J. Appl. Cryst.* **7** 493–7
Bonse U and Hartmann-Losch I 1984 *Nucl. Instrum. Methods* **222** 185–8
Boutif A and Louër D 1991 *J. Appl. Cryst.* **24** 987–93
Bourdillon A J, Glazer A M, Hidaka M and Bordas I 1978 *J. Appl. Cryst.* **11** 684–7
Bras W, Derbyshire G E, Devine A, Clark S M, Cooke J, Komanschek B E and Ryan A J 1995 *J. Appl. Cryst.* **28** 26–32
Bricogne G 1984 *Acta Cryst.* A **40** 410–45
—— 1991 *Acta Cryst.* A **47** 803–29
Brown A and Edmonds J W 1980 *Adv. X-ray Anal.* **23** 361–74
Cabañas M V, Germi P, González-Calbet J M, Pernet M and Vallet-Regí M 1995 *J. Solid State Chem.* **114** 534–8
Caglioti G, Paoletti A and Ricci F P 1958 *Nucl. Instrum. Methods* **35** 223–8
Carpenter J M 1977 *Nucl. Instrum. Methods* **145** 91–113
Cascarano G, Favia L and Giacovazzo C 1992 *J. Appl. Cryst.* **25** 310–7

Caussin P, Nusinovici J and Beard D W 1988 *Adv. X-ray Anal.* **31** 423–30
—— 1989 *Adv. X-ray Anal.* **32** 531–8
Cernansky M 1983 *J. Appl. Cryst.* **16** 103–12
Cernik R J, Cheetham A K, Prout C K, Watkin D J, Wilkinson A P and Willis B T M 1991 *J. Appl. Cryst.* **24** 222–6
Cernik R J and Louër D 1992 *J. Appl. Cryst.* **26** 277–80
Cerny R, Valvoda V and Chladek M 1995 *J. Appl. Cryst.* **28** 247–53
Chabre Y and Pannetier J 1995 *Prog. Solid State Chem.* **23** 1–130
Chaix-Pluchéry O, Bouillot J, Ciosmak D, Niepce J C and Freund F 1983 *J. Solid State Chem.* **50** 247–55
Chayka P V and Göbel H E 1983 *Adv. X-ray Anal.* **27** 157–65
Cheary R W and Cline J P 1994 *Adv. X-ray Anal.* **38** 75–82
Cheary R W and Coelho A 1992 *J. Appl. Cryst.* **25** 109–21
—— 1994 *J. Appl. Cryst.* **27** 673–81
Cheetham A K 1995 *The Rietveld Method* ed R A Young (Oxford: IUCr/OUP) pp 276–92
Cheetham A K, David W I F, Eddy M M, Jakeman R J B, Johnson M W and Torardi CC 1986 *Nature* **320** 46–8
Cherukuri C and Snyder R L 1983 *Adv. X-ray Anal.* **26** 99–104
Chipera S J and Bish D L 1995 *Powder Diffr.* **10** 47–55
Christensen A N, Convert P and Lehmann M S 1980 *Acta Chem. Scand. Ser. A* **34** 771–6
Christensen A N, Cox D E and Lehmann M S 1989 *Acta Chem. Scand.* **43** 19–25
Christensen A N, Fjellvåg H and Lehmann M S 1988 *Acta Chem. Scand. Ser. A* **42** 117–23
Christensen A N and Hewat A W 1990 *Acta Chem. Scand.* **44** 388–691
Christensen A N, Lehmann M S and Pannetier J 1985 *J. Appl. Cryst.* **18** 170–2
Christensen A N, Norby P and Hanson J C 1995 *J. Solid State Chem.* **114** 556–9
Chung F H 1974a *J. Appl. Cryst.* **7** 519–25
—— 1974b *J. Appl. Cryst.* **7** 526–31
Cirujeda J, Ochando L E, Amigó J M, Rovira C, Rius J and Veciana J 1995 *Angew. Chem. Int. Ed. Engl.* **34** 55–7
Clark S M, Evans J S O, O'Hare D, Nuttall C J and Wong H-V 1994 *Chem. Soc. Chem. Commun.* 809–10
Cline J P and Snyder R L 1983 *Adv. X-ray Anal.* **26** 111–17
—— 1985 *Advances in Materials Characterization* II ed R L Snyder, R A Condrate and P F Johnson (New York: Plenum) pp 131–44
—— 1987 *Adv. X-ray Anal.* **30** 447–56
Cole M, Fitch A N and Prince E 1993 *J. Mater. Chem.* **3** 519–22
Collins D R, Fitch A N and Catlow C R A 1991 *J. Mater. Chem.* **1** 965–70
Collins S P, Laundy D, Tang C C and Cernik R J 1995 *J. Phys.: Condens. Matter* **7** L223–9
Cooper M J, Rouse K D and Sakata M 1981 *Zeits. Krist.* **157** 101–17
Copley J R D, David W I F and Neuman D A 1993 *Neutron News* **4** 20–8
Cosier J and Glazer A M 1986 *J. Appl. Cryst.* **19** 105–7
Couves J W, Thomas J M, Waller D, Jones R H, Dent A J, Derbyshire G E and Greaves G N 1991 *Nature* **354** 465–8
Cox D E, Hastings J B, Thomlinson W and Prewitt C T 1993 *Nucl. Instrum. Methods* **208** 573–8
Crettez J M, Coquet E, Michaux B, Pannetier J, Bouillot J, Orland P, Nonat A and Mutin J C 1987 *Physica* B **144** 277–91
Crist B and Cohen J B 1977 *J. Polym. Sci., Polym. Phys. Ed.* **17** 1001–10
Croche R and Gatineau L 1977 *J. Appl. Cryst.* **10** 479–85
Crowder C E, Wood S, Landes B G, Newman R A, Blazy J A and Bubeck R A 1986 *Adv. X-ray Anal.* **29** 315–22
David W I F 1987 *J. Appl. Cryst.* **20** 316–19
—— 1990 *Nature* **346** 731–4
David W I F, Ibberson R M, Matthewman J C, Prasides K, Dennis T J S, Hare J P, Kroto H W, Taylor R and Walton D R M 1991 *Nature* **353** 147–9
David W I F and Jorgensen J D 1995 *The Rietveld Method* ed R A Young (Oxford: IUCr/OUP) pp 197–226
David W I F and Matthewman J C 1985 *J. Appl. Cryst.* **18** 461–6
Davis B L 1992 *Accuracy in Powder Diffraction II* ed Prince and J K Stalick *NIST Spec. Publ. No. 846* (Gaithersburg MA: US Dept of Commerce) pp 7–16
Davis B L and Smith D K 1988 *Powder Diffr.* **3** 205–8
Davis B L, Smith D K and Holomany M A 1989 *Powder Diffr.* **4** 201–5
de Bergevin F and Germi P 1972 *J. Appl. Cryst.* **5** 416–20
de Courville-Brenasin J, Joyez G and Tchoubar D 1981 *J. Appl. Cryst.* **14** 17–23
de Keijser T H, Mittemeijer E J and Rozendaal H J C 1983 *J. Appl. Cryst.* **16** 309–16

de Wolff P M 1957 *Acta Cryst.* **10** 590–5
—— 1961 *Acta Cryst.* **14** 579–82
—— 1968 *J. Appl. Cryst.* **1** 108–13
de Wolff P M and Visser J W 1988 *Powder Diffr.* **3** 202–4
Deboer B G, Sakthivel A, Cagle J R and Young R A 1991 *Acta Cryst.* B **47** 683–92
Debye P and Scherrer P 1916 *Physik. Z.* **17** 277–83
Deem M W and Newsam J M 1989 *Nature* **342** 260–2
Delhez R, de Keijser T H, Langford J I, Louër D, Mittemeijer E J and Sonneveld E J 1995 *The Rietveld Method* ed R A Young (Oxford: IUCr/OUP) pp 132–66
Delhez R, de Keijser T H and Mittemeijer E J 1980 *Accuracy in Powder Diffraction* ed S Block and C R Hubbard *NBS Spec. Pub. No 567* (Gaithersburg MA: US Dept of Commerce) pp 213–53
—— 1982 *Fresenius Z. Anal. Chem.* **312** 1–16
Delhez R, de Keijser T H, Mittemeijer E J and Langford J I 1986 *J. Appl. Cryst.* **19** 459–66
Delhez R and Mittemeijer E J 1975 *J. Appl. Cryst.* **8** 609–11
Deslattes R D and Henins A 1973 *Phys. Rev. Lett.* **31** 972–5
Dollase W A 1986 *J. Appl. Cryst.* **19** 267–272
Duvigneaud P H and Derie R 1980 *J. Solid State Chem.* **34** 323–33
Dzyabchenko A V, Belsky V K and Zorkii P M 1979 *Kristallografiya* **24** 221–6
Elsenhans O 1990 *J. Appl. Cryst.* **23** 73–6
Engler P, Santana M W, Mittleman M L and Balazs D 1988 *Thermochim. Acta* **130** 309–18
Enzo S, Fagherazzi G, Benedetti A and Polizzi S 1988 *J. Appl. Cryst.* **21** 536–42
Ergun S 1968 *J. Appl. Cryst.* **1** 19–23
Eriksson L, Louër D and Werner P E 1989 *J. Solid State Chem.* **81** 9–20
Espinat D, Thevenot F, Grimoud J and El Malki K 1993 *J. Appl. Cryst.* **26** 368–83
Estermann M A and Gramlich V 1993 *J. Appl. Cryst.* **26** 396–404
Estermann M A, McCusker L B and Baerlocher C 1992 *J. Appl. Cryst.* **25** 539–43
Evans J S O and O'Hare D 1994 *Adv. Mater.* **6** 646–48
Fawcett T G *et al* 1988 *Powder Diffr.* **3** 209–18
Fawcett T G, Crowder C E, Whiting L F, Tou J C, Scott W F, Newman R A, Harris W C, Knoll F J and Caldecourt V J 1985 *Adv. X-ray Anal.* **28** 227–32
Fawcett T G, Martin E J, Crowder C E, Kincaid P J, Strandjord A J, Blazy J A, Armentrout D N and Newman R A 1986 *Adv. X-ray Anal.* **29** 323–32
Fiala J 1980 *Anal. Chem.* **52** 1300–4
Fiévet F, Germi P, de Bergevin F and Figlarz M 1979 *J. Appl. Cryst.* **12** 387–94
Finger L W, Cox D E and Jephcoat A P 1994 *J. Appl. Cryst.* **27** 892–900
Fischer H E, Brauer S, Zaluska A, Sutton M, Strom-Olsen J O and Stephenson G B 1994 *Mater. Science Engin.* **A179/A180** 396–400
Fitch A N, Wright A F and Fender B E F 1982 *Acta Cryst.* B **38** 2546–54
Forano C, Slade R C T, Krogh Andersen E, Krogh Andersen I G and Prince E 1989 *J. Solid State Chem.* **82** 95–102
Forster K M, Formica J P, Richardson J T and Luss D 1994 *J. Solid State Chem.* **108** 152–7
Frevel L K 1965 *Anal. Chem.* **37** 471–82
Fujii Y, Hose K, Ohishi Y, Fujihisa H, Hamaya N, Takemura K, Shimomura O, Kikegawa T, Amemiya Y and Matsushita T 1988 *Phys. Rev. Lett.* **63** 536–9
Fyfe C A, Feng Y, Grondey G T, Kokotailo G T and Gies H 1991 *Chem. Rev.* **91** 1525–43
Fyfe C A, Gies H, Kokotailo G T, Marler B and Cox D E 1990 *J. Phys. Chem.* **94** 3718–21
Gabriel A and Dupond Y 1972 *Rev. Sci. Instrum.* **43** 1600–2
García-Martínez O, Rojas R M, Vila E and Martín de Vidales J L 1993 *Solid State Ionics* **63–65** 442–9
Gerward L, Olsen J S, Benedict U, Itié J P and Spirlet J C 1985 *J. Appl. Cryst.* **18** 339–41
Gies H and Rius J 1995 *Zeits. Krist.* **210** 475–80
Gilmore C J, Henderson K and Bricogne G 1991 *Acta Cryst.* A **47** 830–41
Göbel H 1981 *Adv. X-ray Anal.* **24** 123–38
Goehner R P and Garbauskas M F 1983 *Adv. X-ray Anal.* **26** 81–6
—— 1984 *X-ray Spectr.* **13** 172–9
Gorter S and Smith D K 1995 *World Directory of Powder Diffraction Programs* Release 2.2 (1995) (Leiden Univ: CPD)
Greaves C 1985 *J. Appl. Cryst.* **18** 48–50
Grébille D and Bérar J F 1985 *J. Appl. Cryst.* **18** 301–7

Grimes R W and Fitch A N 1991 *J. Mater. Chem.* **1** 461–8
Groma I, Ungár T and Wilkens M 1988 *J. Appl. Cryst.* **21** 47–53
Guillou N, Auffrédic J P and Louër D 1994 *J. Solid State Chem.* **112** 45–52
—— 1995b *J. Solid State Chem.* **115** 295–8
Guillou N, Louër M and Louër D 1994 *J. Solid State Chem.* **109** 307–14
Guinier A 1963 *X-ray Diffraction* (San Francisco: Freeman)
Guinier A and Dexter D L 1963 *X-ray Studies of Materials* (New York: Interscience)
Haines J and Léger J M 1993 *Physica* B **192** 233–7
Haines J, Léger J M and Atouf A 1995 *J. Amer. Ceram. Soc.* **78** 445–8
Halder N C and Wagner C N J 1966 *Acta Cryst.* **20** 312–3
Hall M M, Veeraraghavan V G, Rubin H and Winchell P G 1977 *J. Appl. Cryst.* **10** 66–8
Hall S R, Allen F H and Brown I D 1991 *Acta Cryst.* A **47** 655–85
Hamaya N, Yamada Y, Axe J D, Belanger D P and Shapiro D M 1986 *Phys. Rev.* B **33** 7770–6
Hanawalt J D, Rinn H W and Frevel L K 1938 *Indust. Chem. Anal. Ed.* **10** 457–512
Harding M M and Kariuki B M 1994 *Acta Cryst.* C **50** 852–4
Harding M M, Kariuki B M, Cernik R J and Cressey G 1994 *Acta Cryst.* B **50** 673–6
Harris D K M, Tremayne M, Lightfoot P and Bruce P G 1994 *J. Am. Chem. Soc.* **116** 3543–7
Harris K, Hill R J and Rand D A J 1984 *J. Electrochem. Soc.* **131** 474–82
Hasnain S S, Heliwell J R and Kamitsubo H 1994 *J. Synchr. Rad.* **1** 1–4
Hastings J B, Thomlinson W and Cox D E 1984 *J. Appl. Cryst.* **17** 85–95
Hathaway B J and Hewat A W 1984 *J. Solid State Chem.* **51** 364–75
Häusermann D, Daghoogli M R and Sherman W F 1990 *High Press. Res.* **4** 414–16
—— 1992 *High Press. Res.* **10** 472–5
Hayakawa M and Oka M 1981 *J. Appl. Cryst.* **14** 145–8
Hepp A and Baerlocher C 1988 *Austr. J. Phys.* **41** 229–36
Hermann H and Ermrich M 1989 *Powder Diffr.* **4** 189–95
Hewat A W 1986 *Chem. Scripta* **26A** 119–30
—— 1990 *Neutron News* **1** 28–34
Hill R J 1991 *Powder Diffr.* **6** 74–7
—— 1992 *J. Appl. Cryst.* **25** 589–610
Hill R J and Cranswick L M D 1994 *J. Appl. Cryst.* **27** 802–44
Hill R J and Fischer R X 1990 *J. Appl. Cryst.* **23** 462–8
Hill R J and Flack H D 1987 *J. Appl. Cryst.* **20** 356–61
Hill R J and Howard C J 1986 *Austral. Atomic Energy Comm. Rep. No. M112* (Lucas Heights Res. Lab., NSW: ANSTO)
—— 1987 *J. Appl. Cryst.* **20** 467–74
Hill R J and Madsen I C 1987 *Powder Diffr.* **2** 146–62
Hill R J and Reichert B E 1990 *J. Am. Ceram. Soc.* **73** 2822–7
Hossfeld F and Oel H J 1966 *Z. Angew. Phys.* **20** 493–8
Howard C J, Kisi E H, Roberts R B and Hill R J 1990 *J. Am. Ceram. Soc.* **73** 2828–33
Howard S A and Snyder R L 1983 *Adv. X-ray Anal.* **26** 73–81
—— 1985 *Advances in Materials Characterization II* ed R L Snyder, R A Condrate and P F Johnson (New York: Plenum) pp 43–56
—— 1989 *J. Appl. Cryst.* **22** 238–43
Howland R S, Geballe P H, Laderman S S, Fischer-Colbrie A, Scott M, Tarascon J M and Barroux P 1989 *Phys. Rev.* B **39** 9017–27
Hoyt J J, de Fontaine D and Warburton W K 1984 *J. Appl. Cryst.* **17** 344–51
Huang T C and Parrish W 1975 *Appl. Phys. Lett.* **27** 123–4
Huang T C, Toraya H, Blanton T N and Wu Y 1993 *J. Appl. Cryst.* **26** 180–4
Hubbard C R, Evans E H and Smith D K 1976 *J. Appl. Cryst.* **9** 169–74
Hubbard C R and Snyder R L 1988 *Powder Diffr.* **3** 74–78
Hull A W 1917 *Phys. Rev.* **9** 83–7, **10** 661–96
Iannelli P 1994 *J. Appl. Cryst.* **27** 1055–60
Immirzi A and Iannelli P 1988 *Macromolecules* **21** 768–73
Inouye H, Karthigasan J and Kirschner D A 1989 *Biophys. J.* **56** 129–37
Ishibashi H, Shimomoto K and Nakahigashi 1994 *J. Phys. Chem. Solids* **55** 809–14
Iwasa Y *et al* 1994 *Science* **264** 1570–2
Izumi F 1995 *The Rietveld method* ed R A Young (Oxford: IUCr/OUP) pp 236–53

Izumi F, Takayama-Muromachi E, Fujimori A, Kamiyama T, Asano H, Akimitsu J and Sawa H 1989 *Physica* C **158** 440–8
Jansen E, Schäfer W and Will G 1988 *J. Appl. Cryst.* **21** 228–39
—— 1994 *J. Appl. Cryst.* **27** 492–6
Jansen J, Peschar R and Schenk H 1992 *J. Appl. Cryst.* **25** 237–43
Jarayaman A 1983 *Rev. Mod. Phys.* **55** 65–108
Järvinen M 1993 *J. Appl. Cryst.* **26** 525–31
Jenkins R 1989a *(ed) Methods & Practices in X-ray Powder Diffraction* (Newtown Square PA: ICDD)
—— 1989b *Modern Powder Diffraction* ed D L Bish and J E Post *Rev. Mineral.* **20** 19–71
—— 1994 *Adv. X-ray Anal.* **37** 117–21
Jenkins R, Fawcett T G, Smith D K, Visser J W, Morris M C and Frevel L K 1986 *Powder Diffr.* **1** 51–63
Jenkins R and Holomany M A 1987 *Powder Diffr.* **2** 215–19
Jenkins R and Schreiner W N 1986 *Powder Diffr.* **1** 305–19
Johnson Jr G G and Vand V 1967 *Indust. Eng. Chem.* **59** 19–31
Jones A F and Misell D L 1970 *J. Phys.* A **3** 462–72
Jorgensen J D 1990 *High Press. Res.* **4** 441–3
Jorgensen J D *et al* 1987 *Phys. Rev.* B **36** 3608–16
Jorgensen J D and Rotella F J 1982 *J. Appl. Cryst.* **15** 27–34
Kalceff W, Armstrong N and Cline J P 1994 *Adv. X-ray Anal.* **38** 387–95
Kauzlarich S M, Stanton J L, Faber J and Averill B A 1986 *J. Am. Chem. Soc.* **108** 7946–51
Kidron A and De Angelis R J 1971 *Acta Cryst.* A **27** 596–9
Kikegawa T 1992 *High Press. Res.* **8** 631–7
Kitaigorodskii A I 1973 *Molecular Crystals and Molecules* (London: Academic)
Klug H P and Alexander L E 1974 *X-ray Diffraction Procedures for Polycrystalline and Amorphous Materials* 2nd ed (New York: Wiley)
Kogan V A and Kupriyanov M F 1992 *J. Appl. Cryst.* **25** 16–25
Kohlbeck F and Hörl E M 1976 *J. Appl. Cryst.* **9** 28–33
Kojdecki M A 1991 *Int. J. Appl. Electromag. Mat.* **2** 147–159
Krivoglas M A and Ryaboshapka K P 1963 *Phys. Met. Metall.* **15** 14–26
Kusuhara H, Yamanaka A, Sakuma H and Hashizume H 1989 *Jap. J. Appl. Phys.* **28** 678–84
Kwei G H, Von Dreele R B, Williams A, Goldstone J A, Lawson II A C and Warburton W K 1990 *J. Mol. Structure* **223** 383–406
Ladell J. Zagofsky A and Pearlman S 1970 *J. Appl. Cryst.* **8** 499–506
Lager G A, Ross F K, Rotella F J and Jorgensen J D 1981 *J. Appl. Cryst.* **14** 137–9
Langford J I 1978 *J. Appl. Cryst.* **11** 10–14
—— 1980 *Accuracy in Powder Diffraction* ed S Block and C R Hubbard *NBS Spec. Pub. No. 457* (Gaithersburg MA: US Dept of Commerce) pp 255–69
—— 1981 *Acta Cryst.* A **37** C2–C3
—— 1987 *Prog. Cryst. Growth and Charact.* **14** 185–211
—— 1992 *Accuracy in Powder Diffraction II* ed E Prince and J K Stalick, *NIST Spec. Pub. No. 846* (Gaithersburg MA: US Dept of Commerce) pp 110–26
Langford J I, Boultif A, Auffrédic J P and Louër D 1993 *J. Appl. Cryst.* **26** 22–33
Langford J I, Cernik R J and Louër D 1991 *J. Appl. Cryst.* **24** 913–9
Langford J I, Delhez R, de Keijser T H and Mittemeijer E J 1988 *Austr. J. Phys.* **41** 173–87
Langford J I and Louër D 1982 *J. Appl. Cryst.* **15** 20–6
Langford J I, Louër D, Sonneveld E J and Visser J W 1986 *Powder Diffr.* **1** 211–21
Langford J I, Ungár T, Vorös G and Cernik R J 1992 *Synchrotron Radiation* Daresbury Laboratory Annual Report 1991/1992 p 302
Larson A C and Von Dreele R B 1987 *Los Alamos Nat. Lab. Report* No LA-UR-86-748
Lartigue C, Le Bail A and Percheron-Guégan A 1987 *J. Less Com. Met.* **129** 65–76
Latroche M, Percheron-Guégan A, Chabre Y, Poinsignon C and Pannetier J 1992 *J. Alloys Comp.* **189** 59–65
Le Bail A 1985 *Proc. 10th Colloque Rayons X* pp 45–58, Siemens, Grenoble
—— 1992 *Accuracy in Powder Diffraction II* ed E Prince and J K Stalick *NIST Spec. Pub. No. 846* (Gaithersburg MA: US Dept of Commerce) p 213
Le Bail A, Duroy H and Fourquet J L 1988 *Mater. Res. Bull.* **23** 447–52
Le Bail A and Louër D 1976 *Bull. Soc. Francé. Minér. Crist.* **96** 340–5
—— 1978 *J. Appl. Cryst.* **11** 50–5
—— 1980 *Rev. Chimie Minér.* **17** 530–40

Lehman M S, Christensen A N, Fjellvag H, Feidenhans'l R and Nielsen M 1987 *J. Appl. Cryst.* **20** 123–9
Lightfoot P, Glidewell C and Bruce P G 1992 *J. Mater. Chem.* **2** 361–2
Liu L and Bassett W A 1986 *Elements, Oxides, Silicates: High Pressure Phases with Implications for the Earth's Interior* (Oxford: OUP)
Louër D 1992 *Accuracy in Powder Diffraction II* ed E Prince and J K Stalick *NIST Spec. Pub. No. 846* (Gaithersburg MA: US Dept of Commerce) pp 92–104
—— 1994 *Adv. X-ray Anal.* **37** 27–35
Louër D, Auffrédic J P, Langford J I, Ciosmak D and Niepce J C 1983 *J. Appl. Cryst.* **16** 183–91
Louër D, Coupé R and Le Bail A 1984 *J. Appl. Cryst.* **17** 131–3
Louër D and de Guibert A 1985 *J. Mater. Sci.* **20** 3729–34
Louër D and Langford J I 1988 *J. Appl. Cryst.* **21** 430–7
Louër D and Louër M 1972 *J. Appl. Cryst.* **5** 271–5
—— 1987 *J. Solid State Chem.* **68** 292–9
Louër D, Louër M and Touboul M 1992 *J. Appl. Cryst.* **25** 617–23
Louër D, Louër M, Dzyabchenko V A, Agafonov V and Ceolin R 1995 *Acta Cryst.* B **51** 182–7
Louër D, Weigel D and Louboutin R 1969 *Acta Cryst.* A **25** 335–8
Louër M and Louër D 1994 *Adv. X-ray Anal.* **37** 21–5
Louër M, Plévert J and Louër D 1988 *Acta Cryst.* B **44** 463–7
Lutterotti L and Scardi P 1990 *J. Appl. Cryst.* **23** 246–52
Lutterotti L, Scardi P and Maistrelli P 1992 *J. Appl. Cryst.* **25** 459–62
Mack M and Parrish W 1967 *Acta Cryst.* **23** 693–700
Madden R P and Codling K 1963 *Phys. Rev. Lett.* **10** 516–18
Madsen I C and Hill R J 1990 *Powder Diffr.* **5** 195–9
—— 1992 *Adv. X-ray Anal.* **35** 39–47
—— 1994 *J. Appl. Cryst.* **27** 385–92
Maichle J K, Ihringer J and Prandl W 1988 *J. Appl. Cryst.* **21** 22–7
Mallory C L and Snyder R L 1979 *Adv. X-ray Anal.* **22** 121–32
Malmros G and Thomas J O 1977 *J. Appl. Cryst.* **10** 7–11
Mamott G T, Barnes P, Tarling S E, Janes S L and Norman C J 1988 *Powder Diffr.* **3** 234–9
March A 1932 *Zeits. Krist.* **81** 285–97
Mårdalen J, Riekel C and Müller H 1994 *J. Appl. Cryst.* **27** 192–5
Marezio M, Cox D E, Rossel C and Maple M B 1988 *Solid State Comm.* **67** 831–5
Marler B, Deroche C, Gies, H, Fyfe C A, Grondey H, Kokotailo G T, Feng Y, Ernst S, Weitkamp J and Cox D E 1993 *J. Appl. Cryst.* **26** 636–44
Matheis D P and Snyder R L 1994 *Powder Diffr.* **9** 28–37
McCusker L B 1988 *J. Appl. Cryst.* **21** 305–10
—— 1991 *Acta Cryst.* A **47** 297–313
—— 1992 *Accuracy in Powder Diffraction II* ed E Prince and J K Stalick *NIST Spec. Pub. No. 846* (Gaithersburg MA: US Dept of Commerce) pp 75–9
McCusker L B, Baerlocher C, Jahn E and Bülow M 1991 *Zeolites* **11** 308–13
McCusker L B, Baerlocher C and Nawaz R 1985 *Zeits. Krist.* **171** 281–9
McKinstry H A 1970 *J. Appl. Phys.* **41** 5074–9
McMahon M I and Nelmes R J 1993 *Phys. Rev.* B **47** 8337–40
—— 1995 *J. Phys. Chem. Solids* **56** 485–90
McMahon M I, Nelmes R J, Wright M I and Allan D R 1994 *Phys. Rev.* B **50** 13047–50
Meng Y, Weidner D J and Fei Y 1993 *Geophys. Res. Lett.* **20** 1147–50
Meng Y, Weidner D J, Gwanmesia G D, Liebermann R C, Vaughan M T, Wang Y, Leinenweber K, Pacalo R E, Yeganeh-Haeri A and Zhao Y 1993 *J. Geophys. Res.* **98** 22199–207
Mentzen B F 1988 *J. Appl. Cryst.* **21** 266–71
Mighell A D, Hubbard C R and Stalick 1980 NBS ∗ AIDS80: *A Fortran Program for Crystallographic Data Evaluation. NBS Tech. Note No 1141* (Gaithersburg MA: US Dept of Commerce) [NBS ∗ AIDS83 is an expanded version of NBS ∗ AIDS80.]
Mighell A D and Santoro A 1975 *J. Appl. Cryst.* **8** 372–4
Mignot J and Rondot D 1975 *Acta Metall.* **23** 1321–4
—— 1977 *Acta Cryst.* A **33** 327–33
Moggeridge G D, Rayment T and Lambert R M 1992 *J. Catal.* **134** 242–52
Morán O and Mateu 1983 *Nature* **304** 344–5
Moraweck B, de Montgolfier P H and Renouprez A J 1977 *J. Appl. Cryst.* **10** 184–90, 191–6

Moroney L M, Thompson P and Cox D E 1988 *J. Appl. Cryst.* **21** 206–8
Morris R E, Harrison W T A, Nicol J M, Wilkinson A P and Cheetham A K 1992 *Nature* **359** 519–22
Mortier W J and Costenoble M L 1973 *J. Appl. Cryst.* **6** 488–90
Nandi R K, Kuo H K, Schlosberg W, Wissler G, Cohen J B and Crist B 1984 *J. Appl. Cryst.* **17** 22–6
Nelmes R J *et al* 1993 *Phys. Rev. Lett.* **71** 1192–5
Nelmes R J *et al* 1995 *Phys. Rev. Lett.* **74** 2268–71
Nelmes R J and Häusermann D 1992 *(eds Proc. IUCr Workshop on Synchrotron Radiation Instrumentation for High Pressure Crystallography*, SERC Daresbury Laboratory, 20–21 July 1991) High Press. Res. **8** 617–737
Nelmes R J and McMahon M I 1994 *J. Synchr. Rad.* **1** 69–73
—— 1995 *Phys. Rev. Lett.* **74** 106–9
Nelmes R J, McMahon M I, Hatton P D, Crain J and Piltz R O 1993a *Phys. Rev.* B **47** 35–54, 9949–52
Nelmes R J, McMahon M I, Wright N G and Allan D R 1993b *Phys. Rev.* B **48** 1314–17, 16246–51
Newsam J M, Deem M W and Freeman C M 1992 *Accuracy in Powder Diffraction II* ed E Prince and J K Stalick *NIST Spec. Pub. No. 846* (Gaithersburg MA: US Dept of Commerce) pp 80–91
Nichols M C 1966 *A Fortran II Program for the Identification of X-ray Powder Diffraction Patterns* UCRL-70078, Lawrence Livermore Laboratory
Niepce J C and Benabad-Sidky A 1986 *Chemica Scripta* **26A** 11–5
Noläng B I and Tergenius L E 1980 *Acta Chem. Scand.* A **34** 311–2
Nord A G 1986 *Chemica Scripta* **26A** 115–8
Nord A G and Ericsson T 1982 *Amer. Miner.* **67** 826–32
Notten P H L, Daams J L C, De Veirman A E M and Staals A A 1994 *J. Alloys Comp.* **209** 85–91
Nusinovici J and Bertelmann D 1993 *Adv. X-ray Anal.* **36** 327–32
Nusinovici J and Winter M J 1994 *Adv. X-ray Anal.* **37** 59–66
Ohmasa M and Ohsumi K 1995 *Acta Cryst.* A **51** 87–91
Olsen J S, Gerward L and Benedict U 1985 *J. Appl. Phys.* **18** 37–41
Ortendahl D, Perez-Mendez V, Stoker J and Beyermann W 1978 *Nucl. Instrum. Methods* **156** 53–6
Ozerin A N, Ivanov S A, Chvalun S N and Zubov Y A 1986 *Zavods. Laborat.* **52** 20–3
Padrón R, Mateu L and Requena J 1980 *Biochim. Biophys. Acta* **602** 221–33
Pannetier J 1986a *Chemica Scripta* **26A** 131–9
—— 1986b *Ber. Bunsenges. Phys. Chem.* **90** 634–8
Pannetier J, Bassas-Alsina J, Rodriguez-Carvajal J and Caignaert V 1990 *Nature* **346** 343–5
Parise J B, Yeganeh-Haeri A, Weidner D J, Jorgensen J D and Saltzberg M A 1994a *J. Appl. Phys.* **75** 1361–7
Parise J B, Leinenweber K, Weidner D J, Tan K and Von Dreele R B 1994b *Amer. Mineralog.* **79** 193–6
Parrish W 1992 *International Tables for Crystallography Vol. C, Mathematical, Physical and Chemical Tables* ed A J C Wilson (Dordrecht: IUCr/Kluwer) pp 538–43
Parrish W and Huang T C 1980 *Accuracy in Powder Diffraction* ed S. Block and C R Hubbard *NBS Spec. Pub. No. 457* (Gaithersburg MA: US Dept of Commerce) pp 95–110
Parrish W and Huang T C 1983 *Adv. X-ray Anal.* **26** 35–44
Parrish W, Huang T C and Ayers G L 1976 *Trans. Amer. Cryst. Assoc.* **12** 55–73
Parrish W and Mack M 1967 *Acta Cryst.* **23** 687–92
Parrish W and Wilson A J C 1992 *International Tables for Crystallography Vol. C, Mathematical, Physical and Chemical Tables* ed A J C Wilson (Dordrecht: IUCr/Kluwer) p 424
Paszkowicz W 1987 *J. Appl. Cryst.* **20** 161–5
Pausescu P, Manaila R, Popescu M and Jijovici E 1974 *J. Appl. Cryst.* **7** 281–6
Pawley G A 1981 *J. Appl. Cryst.* **14** 357–61
Pennartz P U, Löchner U, Fuess H and Wroblewski T 1992 *J. Appl. Cryst.* **25** 571–7
Percheron-Guégan A, Lartigue C, Achard J C, Germi P and Tasset F 1980 *J. Less Com. Metals* **74** 1–12
Perkins D A and Attfield J P 1991 *J. Chem. Soc.: Chem. Comm.* 229–31
Pertsin A J and Kitaigorodskii A I 1987 *The Atom–Atom Potential Method* (Berlin: Springer)
Peschar R, Schenk H and Capkova P 1995 *J. Appl. Cryst.* **28** 127–40
Petit S, Coquerel G, Perez G, Louër D and Louër M 1993 *New J. Chem.* **17** 187–92
Petrov K P 1976 *Dokl. Bolg. Akad. Nauk* **29** 1141–4
Phillips D L 1962 *J. Assoc. Comput. Mach.* **9** 84–97
Phillips J C and Hodgson K O 1980 *Acta Cryst.* A **36** 854–64
Pielaszek J, Cohen J B, Burwell R L and Butt J B 1983 *J. Catal.* **80** 479–81
Piltz R O, McMahon M I, Crain J, Hatton P D and Nelmes R J 1992 *Rev. Sci. Instrum.* **63** 700–2
Pitschke W, Koch M, Heinrich A and Schumann J 1994 *Fresenius J. Anal. Chem.* **349** 246–7
Pivan J Y, Achak O, Louër M and Louër D 1994 *Chem. Mater.* **6** 827–30

Platbrood G 1983 *J. Appl. Cryst.* **16** 24–7
Plévert J, Auffrédic J P, Louër M and Louër D 1989 *J. Mater. Sci.* **24** 1913–8
Plévert J and Louër D 1990 *J. Chim. Phys.* **87** 1427–40
Polak E, Munn J, Barnes P, Tarling S E and Ritter C 1990 *J. Appl. Cryst.* **23** 258–62
Polizzi S, Benedetti A, Fagherazzi G, Franceschin S, Goatin C, Talamini G and Toniolo L 1987 *J. Catal.* **106** 483–93
Post J E and Bish D L 1988 *Am. Mineral.* **73** 861–9
Price G L 1982 *J. Appl. Phys.* **53** 4571–8
Prince E 1981 *J. Appl. Cryst.* **14** 157–9
Puxley D C, Squire G D and Bates D R 1994 *J. Appl. Cryst.* **27** 585–94
Pyrros N K and Hubbard C R 1983 *J. Appl. Cryst.* **16** 289–94
Rachinger W A 1948 *J. Sci. Instrum.* **25** 254–5
Riekel C 1978 *Solid State Commun.* **28** 385–7
Riekel C and Fischer C O 1979 *J. Solid State Chem.* **29** 181–90
Riekel C, Reznik H G and Schöllhorn R 1979 *J. Solid State Chem.* **29** 181–90
Riekel C and Schöllhorn R 1976 *Mater. Res. Bull.* **11** 369–76
Rietveld H M 1967 *Acta Cryst.* **22** 151–2
—— 1969 *J. Appl. Cryst.* **2** 65–71
Rius J 1993 *Acta Cryst.* A **49** 406–9
Rius J and Miratvilles C 1988 *J. Appl. Cryst.* **21** 224–7
Rius J, Sañé J, Miratvilles C, Gies H, Marler B and Oberhagemann U 1995 *Acta Cryst.* A **51** 840–5
Rodgers K D and Wood G H 1987 *Crystallographic Databases* ed F H Allen, G Bergerhoff and R Sievers (Chester: IUCr) pp 96–106
Rodriguez-Carvajal J 1990 *Collected Abstracts of Powder Diffraction Meeting* ed J Galy July 1990 Toulouse, France p 127
—— 1993 *Physica* B **192** 55–69
Rodriguez-Carvajal J and Fontcuberta J 1987 *J. Mater. Sci.* **22** 1001–5
Rodriguez-Carvajal J, Martinez J L and Pannetier J 1988 *Phys. Rev.* B **38** 7148–51
Rodriguez M A, Matheis D P, Bayya S S, Simmins J J, Snyder R L and Cox D E 1990 *J. Mater. Res.* **5** 1799–1801
Rudman R 1976 *Low-Temperature X-ray Diffraction: Apparatus and Techniques* (New York: Plenum)
Rudolf P and Clearfield A 1985 *Acta Cryst.* B **41** 418–25
Ruoff A R 1992 *High Press. Res.* **8** 639–45
Sabine T M 1985 *Austr. J. Phys.* **38** 507–18
—— 1988 *Acta Cryst.* A **44** 368–73
Sakata M and Cooper M J 1979 *J. Appl. Cryst.* **12** 554–63
Sakata M, Mori R, Kumazawa S, Takata M and Toraya H 1990 *J. Appl. Cryst.* **23** 526–34
Sakata M, Uno T, Takata M and Howard C J 1993 *J. Appl. Cryst* **26** 159–65
Sarode P R, Ramasesha S, Madhusudan W H and Rao C N R 1979 *J. Phys. C: Solid State Phys.* **12** 2439–45
Scardi P, Kothari D C and Guzman L 1991 *Thin Solid Films* **195** 213–23
Scardi P, Lutterotti L and Di Maggio R 1991 *Powder Diffr.* **6** 20–5
Scardi P, Lutterotti L and Maistrelli P 1994 *Powder Diffr.* **9** 180–6
Schlosberg W and Cohen J B 1983 *J. Appl. Cryst.* **16** 304–8
Schneider J and Schultz H 1993 *Zeits. Krist.* **203** 1–15
Schoonover J R and Lin S H 1988 *J. Solid State Chem.* **76** 143–59
Schuster M and Göbel H 1995 *J. Phys. D: Appl. Phys.* 28 A270–5
Scott H G 1983 *J. Appl. Cryst.* **16** 156–63
Shirley R 1978 *Computing in Crystallography* ed H Schenk, R Oltyof-Hazekamp, H van Koningsveld and G C Bassi (Delft: Delft University Press) pp 221–34
—— 1980 *Accuracy in Powder Diffraction* ed S Block and C R Hubbard *NBS Spec. Pub. No. 567* (Gaithersburg MA: US Dept of Commerce) pp 361–82
Shishiguchi S, Minato I and Hashizume H 1986 *J. Appl. Cryst.* **19** 420–6
Sivia D S and David W I F 1994 *J. Appl. Cryst.* A **50** 703–14
Slade R C T, West B C, Ramanan A, David W I F and Harrison W T A 1989 *Eur. J. Solid State Inorg. Chem.* **26** 15–22
Smith D K, Hoyle S Q and Johnson Jr G G 1993 *Adv. X-ray Anal.* **36** 287–99
—— 1994 *Adv. X-ray Anal.* **37** 67–77
Smith D K, Johnson Jr G G and Hoyle S Q 1991 *Adv. X-ray Anal.* **34** 377–85
Smith G S 1977 *J. Appl. Cryst.* **10** 252–5

Smith G S and Snyder R L 1979 *J. Appl. Cryst.* **12** 60–5
Smith S T, Snyder R L and Brownell W E 1979a *Adv. X-ray Anal.* **22** 181–92
—— 1979b *Adv. X-ray Anal.* **22** 77–87
Smrcok L 1989 *Cryst. Res. Technol.* **24** 607–11
Snyder R L 1981 *Adv. X-ray Anal.* **24** 83–90
—— 1992a *Accuracy in Powder Diffraction II* ed E Prince and J K Stalick *NIST Spec. Pub. No. 846* (Gaithersburg MA: US Dept of Commerce) pp 25–33
—— 1992b *Powder Diffr.* **7** 186–93
—— 1994 *Adv. Mater. Processes* **8** 20–5
—— 1995 *The Rietveld Method* ed R A Young (Oxford: IUCr/OUP) pp 111–31
Snyder R L and Bish D L 1989 *Modern Powder Diffraction* ed D L Bish and J E Post *Reviews in Mineralogy* **20** (Washington: Min. Soc. Am.) pp 101–44
Sonneveld E J and Visser J W 1975 *J. Appl. Cryst.* **8** 1–7
Sowa H, Reithmayer K, Macavei J, Rieck W and Schultz H 1990 *J. Appl. Cryst.* **23** 397–405
Ståhl K and Hanson J 1994 *J. Appl. Cryst.* **27** 543–50
Ståhl K and Thomasson R 1992 *J. Appl. Cryst.* **25** 251–8
Stalick J K and Mighell A D 1986 *Crystal Data, Version 1: Database Specification, NBS Tech. Note 1229* (Gaithersburg MD: NIST)
Stephens P W, Bortel G, Falgel G, Tegze M, Jánossy A, Pekker S, Oszlanyl G and Forró L 1994 *Nature* **370** 636–9
Stokes A R 1948 *Proc. Phys. Soc. Lond.* **61** 382–91
Stokes A R and Wilson A J C 1942 *Proc. Camb. Phil. Soc.* **38** 313–22
—— 1944 *Proc. Phys. Soc. Lond.* **56** 174–81
Sudo N, Hashizume H and Carvalho A M 1995 *Powder Diffr.* **10** 34–9
Suitch P R and Young R A 1983 *Clays and Clay Minerals* **31** 357–66
Suortti P 1995 *The Rietveld Method* ed R A Young (Oxford: IUCr/OUP) pp 167–85
Suortti P, Hastings J P and Cox D E 1985 *Acta Cryst.* A **41** 413–20
Sutton M 1994 *Mater. Science Engin.* A **178** 265–70
Taupin D 1973a *J. Appl. Cryst.* **6** 266–73
—— 1973b *J. Appl. Cryst.* **6** 380–5
—— 1988 *J. Appl. Cryst.* **21** 485–9
Taylor J C 1985 *Austr. J. Phys.* **38** 519–38
—— 1991 *Powder Diffr.* **6** 2–9
Taylor J C and Aldridge L P 1993 *Powder Diffr.* **8** 138–44
Taylor J C and Matulis C E 1991 *J. Appl. Cryst.* **24** 14–7
Taylor J C, Miller S A and Bibby D M 1986 *Zeits. Krist.* **176** 183–92
Terblanche S P 1989 *J. Appl. Cryst.* **22** 283–4
Thomas J M, Williams C and Rayment T 1988 *J. Chem. Soc. Faraday Trans. 1* **84** 2915–31
Thompson P, Cox D E and Hastings J B 1987 *J. Appl. Cryst.* **20** 79–83
Thompson P, Reilley J J and Hastings J B 1987 *J. Less Com. Met.* **129** 105–14
Tikhonov A N 1963 *Dokl. Akad. Nauk. SSSR* **151** 501–4
Toby B H, Harlow R L and Holomany M A 1990 *Powder Diffr.* **5** 2–7
Toby B H, Langford J I and Hall S R 1993 *Acta Cryst.* A **49** 410–1
Toraya H 1985 *J. Appl. Cryst.* **18** 351–8
—— 1986 *J. Appl. Cryst.* **19** 440–7
—— 1990 *J. Appl. Cryst.* **23** 485–91
—— 1995 *The Rietveld Method* ed R A Young (Oxford: IUCr/OUP) pp 254–75
Toraya H, Yoshimura M and Sömiya S 1983 *J. Appl. Cryst.* **16** 653–7
—— 1984 *J. Amer. Ceram. Soc.* C 119–21
Tremayne M, Lightfoot P, Mehta M A, Bruce P G, Harris K D M, Shankland K, Gilmore C J and Bricogne G 1992 *J. Solid State Chem.* **100** 191–6
Turrillas X, Barnes P, Häusermann D, Jones S L and Norman C J 1993 *J. Mater. Res.* **8** 1406–19
Ungár T, Groma I and Wilkens M 1989 *J. Appl. Cryst.* **22** 26–34
Ungár T, Mughrabi H, Rönnpagel D and Wilkens M 1984 *Acta Metall.* **32** 333–42
van Berkum J G M, Delhez R, de Keijser T H and Mittemeijer E J 1992 *Phys. Stat. Sol.* A **134** 335–50
van Berkum J G M, Sprong G J M, de Keijser T H, Delhez R and Sonneveld E J 1995 *Powder Diffr.* **10** 129–39
van Berkum J G M, Vermeulen A C, Delhez R, de Keijser T H and Mittemeijer E J 1994 *J. Appl. Cryst.* **27** 345–57
van Cittert P H 1931 *Z. Phys.* **69** 298–308

Vand V and Johnson G G 1968 *Acta Cryst.* A **24** 543–6
Vanderborgh C A, Vohra Y K and Ruoff A L 1989 *Phys. Rev.* B **40** 12450–6
Vargas R, Louër D and Langford J I 1983 *J. Appl. Cryst.* **16** 512–8
Vermeulen A C, Delhez R, de Keijser Th H and Mittemeijer E J 1991 *Mater. Sci. Forum* **79–82** 119–24
—— 1992 *J. Appl. Phys.* **71** 5303–9
Visser J W 1969 *J. Appl. Cryst.* **2** 89–95
Visser J W and de Wolff P M 1964 *Absolute Intensitie Report* 641.109 Delft Phys. Dienst (The Netherlands)
Vogel W, Haase J and Hosemann R 1974 *Z. Naturforsch.* A **29** 1152–8
Von Dreele R B 1989 *Modern Powder Diffraction ed D L Bish and J E Post Rev. Mineral.* **20** 333–69
—— 1995 *The Rietveld Method* ed R A Young (Oxford: IUCr/OUP) pp 227–53
Wagner C N J 1966 *Local Atomic Arrangements Studied by X-ray Diffraction* ed J B Cohen and J E Hilliard (Reading, MA: Addison-Wesley) p 219
Wang Y and Weidner D J 1994 *Geophys. Res. Lett.* **21** 895–8
Wang Y, Weidner D J, Liebermann R C, Liu X, Ko J, Vaughan M T, Zhao Y, Yeganeh-Haeri A and Pacalo R E G 1991 *Science* **251** 410–3
Wang Y, Weidner D J, Liebermann R C and Zhao Y 1994 *Phys. Earth & Planetary Interiors* **83** 13–40
Warner J K, Cheetham A K and Cox D E 1990 *Synchrotron Radiation* (Daresbury Annual Report 1990/91) p 195
Warren B E 1969 *X-ray Diffraction* (Reading MA: Addison-Wesley)
Warren B E and Averbach B L 1950 *J. Appl. Phys.* **21** 595–9
—— 1952 *J. Appl. Phys.* **23** 497
Warren B E and Bodenstein P 1966 *Acta Cryst.* **20** 602–5
Weidner D J, Vaughan M T, Ko J, Wang Y, Leinenweber K, Liu X, Yeganeh-Haeri A, Pacalo R E and Zhao Y 1992a *High Press. Res.* **8** 617–23
Weidner D J, Vaughan M T, Ko J, Wang Y, Liu X, Yeganeh-Haeri A, Pacalo R E and Zhao Y 1992b *High Press. Res.: Application to Earth and Planetary Sciences* ed Y Syono and M H Manghnani (Washington DC: Am. Geophys. Union) pp 13–7
Weidner D J and Zhao Y 1992 *High Press Res.: Application to Earth and Planetary Sciences* ed Y Syono and M H Manghnani (Washington DC: Am. Geophys. Union) pp 191–6
Werner P E 1964 *Zeits. Krist.* **120** 375–87
—— 1980 *Accuracy in Powder Diffraction* ed S Block and C R Hubbard *NBS Spec. Pub. No. 567* (Gaithersburg MA: US Dept of Commerce) pp 503–9
—— 1986 *Chemica Scripta* **26A** 57–64
—— 1992 *Accuracy in Powder Diffraction II* ed E Prince and J K Stalick *NIST Spec. Pub. No. 846* (Gaithersburg MA: US Dept of Commerce) pp 51–62
Werner P E, Eriksson L and Westdahl M 1985 *J. Appl. Cryst.* **18** 367–70
Werner P E, Salomé S, Malmros G and Thomas J O 1979 *J. Appl. Cryst.* **12** 107–9
Wertheim G K, Butler M A, West K W and Buchanan D N E 1974 *Rev. Sci. Instrum.* **11** 1369–71
Wiedemann K E, Unnam J and Clark R K 1987 *Powder Diff.* **2** 136–45
Wiles D B and Young R A 1981 *J. Appl. Cryst.* **14** 149–51
Wilkens M 1970 *Phys. Stat. Sol.* **2** 359–70
—— 1979 *J. Appl. Cryst.* **12** 119–25
—— 1984 *Microstructural Characterisation of Materials by Non-Microscopical Techniques* ed N H and B N Singh *NBS Sp. Pub. No. 317* (Gaithersburg MA: US Dept of Commerce) pp 153–68
Wilkinson A P and Cheetham A K 1992 *J. Appl. Cryst.* **25** 654–7
Wilkinson A P, Cheetham A K and Cox D E 1991 *Acta Cryst.* B **47** 155–61
Will G 1979 *J. Appl. Cryst.* **12** 483–5
—— 1989 *Zeits. Krist.* **188** 169–86
Will G, Bellotto M, Parrish W and Hart M 1988 *J. Appl. Cryst.* **21** 182–91
Will G, Masciocchi N, Hart M and Parrish W 1987 *Acta Cryst.* A **43** 677–83
Will G, Masciocchi N, Parrish W and Lutz H D 1990 *Zeits. Krist.* **190** 277–85
Will G, Parrish W and Huang T C 1983 *J. Appl. Cryst.* **16** 611–22
Williams A, Kwei G H, Von Dreele R B, Larson A C, Raistrick I D and Bish D L 1988 *Phys. Rev.* B **37** 7960–2
Williamson G K and Hall W H 1953 *Acta Metall.* **1** 22–31
Wilson A J C 1952 *Acta Cryst.* **5** 318–22
—— 1962a *X-ray Optics* 2nd ed (London: Methuen)
—— 1962b *Nature* **193** 568–9
—— 1963 *Mathematical Theory of X-ray Powder Diffractometry* (Eindhoven: Philips)
—— 1967 *Acta Cryst.* **23** 888–98

—— 1970 *Elements of X-ray Crystallography* (Reading, MA: Addison-Wesley)
—— 1992 (ed) *International Tables for Crystallography Vol. C, Mathematical, Physical and Chemical Tables* (Dordrecht: IUCr/Kluwer)
Wilson C C 1989 *Acta Cryst.* A **45** 833–9
Wilson C C and Wadsworth J W 1990 *Acta Cryst.* A **46** 258–62
Wölfel E R 1983 *J. Appl. Cryst.* **16** 341–8
Wong J, Larsen E M, Holt J B, Waide P A, Rupp B and Frahm R 1990 *Science* **249** 1406–9
Wong-Ng W and Hubbard C R 1987 *Powder Diffr.* **2** 242–8
Wood I G and Brown G 1988 *J. Appl. Cryst.* **21** 154–8
Woolsey N C, Wark J S and Riley D 1990 *J. Appl. Cryst.* **23** 441–3
Wu E 1989 *J. Appl. Cryst.* **22** 506–10
Yamamoto A, Onoda M, Takayama-Muromachi E, Izumi F, Ishigaki T and Asano H 1990 *Phys. Rev.* B **42** 4228–39
Yamanaka T and Ogata K 1991 *J. Appl. Cryst.* **24** 111–8
Yamanaka T, Sugiyama K and Ogata K 1992 *J. Appl. Cryst.* **25** 11–5
Young R A 1995 *The Rietveld Method* ed R A Young (Oxford: IUCr/OUP) pp 1–38
Young R A, Gerdes R G and Wilson A J C 1967 *Acta Cryst.* **22** 155–62
Young R A and Hewat A W 1988 *Clays and Clay Minerals* **36** 225–32
Young R A, Mackie P E and Von Dreele R B 1977 *J. Appl. Cryst.* **10** 262–9
Young R A and Sakthivel A 1988 *J. Appl. Cryst.* **21** 416–25
Young R A, Sakthivel A, Moss T S and Paiva-Santos C O 1995 *J. Appl. Cryst.* **28** 366–7
Young R A and Wiles D B 1982 *J. Appl. Cryst.* **15** 430–8
Yvon K, Jeitschko W and Parthe E 1977 *J. Appl. Cryst.* **10** 73–4
Zevin L S and Zevin S L 1989 *Powder Diffr.* **4** 196–200
Zhao Y, Parise J B, Wang Y, Kusaba K, Vaughan M T, Weidner D J, Kikegawa T, Chen J and Shimomura O 1994 *Am. Mineralog.* **79** 615–21
Zhou R S and Snyder R L 1991 *Acta Cryst.* B **47** 617–30
Zorn G, Wersing W and Göbel H 1985 *Japan. J. Appl. Phys.* **24** 721–3